

R761239

C.2

TURBULENT BOUNDARY LAYER CHARACTERISTICS OVER A ROUGH SURFACE IN AN ADVERSE PRESSURE GRADIENT Report 2659



NAVAL SHIP RESEARCH AND DEVELOPMENT CENTER

Washington, D.C. 20007



V393
.R46

PROPERTY OF N. A. & M. E. DEPT
PLANS FILE

TURBULENT BOUNDARY LAYER CHARACTERISTICS
OVER A ROUGH SURFACE IN AN
ADVERSE PRESSURE GRADIENT

by

Victor E. Scottron



This document has been approved for public release
and sale; its distribution is unlimited.

HYDROMECHANICS LABORATORY
RESEARCH AND DEVELOPMENT REPORT

September 1967

Report 2659



TURBULENT BOUNDARY LAYER CHARACTERISTICS
OVER A ROUGH SURFACE IN AN
ADVERSE PRESSURE GRADIENT

by

Victor E. Scottron

REPRINT

of a dissertation submitted to the Johns Hopkins University
in conformity with the requirements for the degree of
Doctor of Engineering

September 1967

ADMINISTRATIVE INFORMATION

This work was performed at the Naval Ship Research and Development
Center under Bureau of Ships Project S-R011 01 01, Task 0401

ABSTRACT

The boundary layers produced on rough surfaces in adverse pressure gradients have been investigated. Experimental data on two pressure gradients are studied and compared with flow over a smooth surface. Experimental data obtained with both pitot tubes and hot wires are carefully analyzed and corrected for the effects of high level turbulence. An improved pitot tube correction is proposed. It is shown that a boundary layer on a rough wall will separate more readily than on a smooth wall.

PREFACE AND ACKNOWLEDGEMENTS

Shortly before World War II, Professor Boris A. Bakhmeteff of Columbia University suggested to me that I might profit academically by translating the papers of Dönch and Nikuradse on flow in divergent channels. Neither of us was aware at the time that he was sparking an interest in a phase of fluid flow which would ultimately result in the research described in this thesis. Not too long after this first exposure to channel flows, it was also my privilege to work with Dr. Karl E. Schoenherr on a great variety of problems in naval hydrodynamics. His interest in the behavior of the turbulent boundary layer has since served as an example. I would be remiss in not pointing out the profound influence of both of these outstanding engineers on my subsequent career.

I should like to express my sincere thanks to Dr. John C. Geyer for his continuing encouragement in this endeavor, to Dr. Stanley Corrsin for a great many years of cheerful academic discussion and for his careful and critical review of this thesis, and to Dr. Francis H. Clauser for his many interesting suggestions.

The research for this dissertation was performed at the David Taylor Model Basin. That this was made possible originally by Dr. Karl E. Schoenherr and, since the retire-

ment of the latter, by Dr. William E. Cummins is deeply appreciated. There have been many suggestions and much thoughtful discussion provided by Dr. Avis Borden and Mr. Paul S. Granville. The author is especially grateful for the assistance of Mr. John L. Power in running the experiments and gratefully acknowledges the help provided by Messrs. Edwin P. Rood and Mark Scher in conducting experimental work and in the reduction of data.

Needless to say, my family has at times been inconvenienced by the scope of this undertaking. I must therefore reserve my warmest thanks for Jan for patience and understanding on a project which has extended over far too long a time.

TABLE OF CONTENTS

Chapter		Page
	TABLE OF ILLUSTRATIONS	vii
	NOTATION	x
1	INTRODUCTION	1
2	INTRODUCTORY ANALYSIS	6
	2.1 THE SKIN FRICTION COEFFICIENT	6
	2.2 ORIGIN OF THE ROUGH WALL	14
	2.3 EVALUATION OF THE MOMENTUM THICKNESS	18
3	EXPERIMENTAL PROGRAM	20
	3.1 APPARATUS	20
	3.2 INSTRUMENTATION	27
4	INSTRUMENTATION ERRORS AND CORRECTIONS	40
	4.1 INTRODUCTION	40
	4.2 ESTIMATES OF v' AND w'	42
	4.3 TURBULENCE CORRECTIONS FOR THE HOT-WIRE	50
	4.4 ERROR IN MEAN VELOCITY MEASUREMENTS DUE TO VELOCITY REVERSALS	53
	4.5 ERROR IN TURBULENCE INTENSITY DUE TO VELOCITY REVERSALS	56
	4.6 HOT-WIRE CORRECTIONS	58
	4.7 MEASUREMENT OF STATIC PRESSURE IN HIGH LEVEL TURBULENCE	63
	4.8 MEASUREMENT OF TOTAL PRESSURE IN HIGH LEVEL TURBULENCE	66

TABLE OF CONTENTS (Continued)

Chapter		Page
	4.9 FURTHER COMMENTS ON THE PITOT TUBE	68
	4.10 CONCLUSIONS	79
5	ANALYSIS OF THE VELOCITY AND SHEAR FIELDS	90
	5.1 THE MEAN VELOCITY FIELD	90
	5.2 COMPUTATION OF ψ AND V	91
	5.3 THE WALL SHEAR STRESS	92
	5.4 SHEAR STRESS DISTRIBUTION	95
6	PRESENTATION OF RESULTS	96
7	COMPARISON WITH THE LAW OF THE WAKE	116
	7.1 THE ROUGH WALL FUNCTION	116
	7.2 COMPARISON OF FUNCTIONS WITH EXPERIMENTAL DATA	120
8	COMPARISON OF ROUGH AND SMOOTH WALL DATA	126
9	CONCLUSIONS	140
10	RECOMMENDATIONS	145
11	BIBLIOGRAPHY	146

TABLE OF ILLUSTRATIONS

Figure No.	Title	Page
1	Logarithmic Portion of Typical Mean Velocity Profiles for Smooth and Rough Surfaces.	13
2	Location of y'	17
3	General Arrangement of Wind Tunnel	21
4	Wind Tunnel Exterior	22
5	Wind Tunnel Interior with Instrumentation	25
6	Small Pitot Tube	29
7	Small Pitot Tube Mounting Arrangement	31
8	One-Sixteenth Inch Pitot Tube	32
9	Hot Wire Probe Mounting Arrangement	35
10	Hot Wire and Pitot Tube Mean Velocity Profiles	39
11	Comparison of Normal Turbulence Intensities	44
12	Comparison of Lateral Turbulence Intensities	45
13	Working Values of $(v'/u')^2$ and $(v'/u')^2 + (w'/u')^2$	49
14	Constant Temperature Hot-Wire System	52
15	Normally Distributed Velocity where $u' \rightarrow U$	52
16a	Corrected versus Measured Turbulence Intensity (High Values)	60
16b	Turbulence Intensity Correction (Low Values)	61

TABLE OF ILLUSTRATIONS (Continued)

Figure No.	Title	Page
17	Mean Velocity Correction for Hot-Wire	62
18	Comparisons of Raw and Corrected Data Station 9, Rough Wall, Pressure Gradient 2	85
19	Comparisons of Raw and Corrected Data Station 11, Rough Wall, Pressure Gradient 2	86
20	Hot-Wire and Pitot-Tube Correction Functions, Station 9, Rough Wall, Pressure Gradient 2	87
21	Hot-Wire and Pitot-Tube Correction Functions, Station 11, Rough Wall, Pressure Gradient 2	88
22	Comparison of Pitot-Tube Correction Functions for Smooth and Rough Walls	89
23a	Boundary Layer Characteristics, Rough Wall, Pressure Gradient 1	104
23b	Boundary Layer Characteristics, Rough Wall, Pressure Gradient 2	105
23c	Boundary Layer Characteristics, Smooth Wall, Pressure Gradient 2	106
24a	Streamline Distribution, Rough Wall, Pressure Gradient 1	107
24b	Streamline Distribution, Rough Wall, Pressure Gradient 2	108
24c	Streamline Distribution, Smooth Wall, Pressure Gradient 2	109
25a	Wall Shear Coefficient, Rough Wall Pressure Gradient 1	110

TABLE OF ILLUSTRATIONS (Continued)

Figure No.	Title	Page
25b	Wall Shear Coefficient, Rough Wall Pressure Gradient 2	111
25c	Wall Shear Coefficient, Smooth Wall Pressure Gradient 2	112
26a	Shear Coefficients, Rough Wall Pressure Gradient 1	113
26b	Shear Coefficients, Rough Wall Pressure Gradient 2	114
26c	Shear Coefficients, Smooth Wall Pressure Gradient 2	115
27	Comparison of Rough Coles Function with Experimental Data, $\delta/k = 20$	121
28	Comparison of Rough Coles Function with Experimental Data, $\delta/k = 40$	122
29	Comparison of Smooth Coles Function with Experimental Data, $R_\delta = 4 \times 10^5$	123
30	Comparison of Mean Velocities in Flows Approaching Separation	129
31	Comparison of Turbulent Intensities in Flows Approaching Separation	131
32	Comparison of Turbulent Intensities Based on Local Mean Velocities in Flows Approaching Separation	132
33	Variation of the Pressure Parameter β for a Variety of Pressure Gradients	138

NOTATION

A	Experimentally determined constant
a	Pipe radius
B	Experimentally determined constant
b	Half-width in a two-dimensional conduit
C	Experimentally determined constant
c_f	Skin friction coefficient $c_f = \tau_o / \frac{1}{2} \rho U_1^2$
c_τ	Shear coefficient $c_\tau = \tau / \frac{1}{2} \rho U_1^2$
D	Experimentally determined constant
$f_{1,2,3}$	Turbulence correction functions
F_h	Hot-wire mean velocity function
F_p	Pitot-tube mean velocity function
F_t	Hot-wire turbulence function
G	Experimentally determined constant
H	Shape factor δ^*/θ
I	Electric heating current
K	Experimentally determined constant
k	Wall roughness \equiv two wire diameters or the screen thickness in this report.
p	Pressure
p_m	Measured pressure
p_o	Reference pressure
p_t	Total or impact pressure
R_g	Electric resistance of hot wire at air temperature

NOTATION (Continued)

R_w	Electric resistance of heated wire
R_x	Reynolds number $U_1 k/\nu$
R_{x_0}	Reynolds number $U_0 k/\nu$
R_δ	Reynolds number $U_1 \delta/\nu$
R_θ	Reynolds number $U_1 \theta/\nu$
U	Local mean velocity along wall (Sometimes written \bar{U} for clarity)
U_0	Free stream velocity at station of maximum velocity in pressure gradient tests
U_1	Free stream velocity just outside boundary layer
U_m	Local mean velocity measured by pitot tube
U_s	Sensed instantaneous velocity
U_w	Local mean velocity measured by hot-wire
U_τ	Shear velocity $\sqrt{\frac{\tau_0}{\rho}}$
$\Delta U/U_\tau$	Shift of logarithmic profile caused by roughness
u	Longitudinal turbulence velocity fluctuations
u'	Longitudinal turbulence intensity $\sqrt{u'^2}$
u'_w	Longitudinal turbulence intensity $\sqrt{u'^2}$ measured by hot-wire
V	Mean velocity component normal to wall
v	Turbulence velocity fluctuations normal to the wall
v'	Turbulence intensity $\sqrt{v'^2}$ normal to wall
W	Mean velocity component parallel to wall and normal to longitudinal axis of wind tunnel

NOTATION (Continued)

w	Lateral turbulence velocity fluctuations
w'	Lateral turbulence intensity $\sqrt{\overline{w^2}}$
w(y/δ)	The Coles' "wake function"
x	Distance along the wall
y	Normal distance from wall
y'	Distance from effective origin in rough surface normal to wall
z	Distance parallel to wall and normal to longitudinal axis of test wall
α	Wall shear function $\approx 5.6 \sqrt{\frac{c_f}{2}} = 5.6 U_\tau / U_1$
β	Experimentally determined constant
β	Pressure gradient parameter $\delta^* dp/dx / \tau_o$
δ	Boundary layer thickness
δ*	Displacement thickness $\int_0^\delta \left[1 - \frac{U}{U_1} \right] dy$
ε	Effective displacement of pitot-tube centerline
η	Relative distance from wall, y/δ , y/a , or y/b
η	Variable in error function, $\text{erf}(\eta) = \frac{2}{\pi} \int_0^\eta e^{-x^2} dx$ where $\eta = \frac{U}{\sqrt{2u'}} \text{ or } \frac{U}{\sqrt{2u'^2}}$ when used in turbulence corrections.
θ	Momentum thickness $\int_0^\delta \frac{U}{U_1} \left[1 - \frac{U}{U_1} \right] dy$
ν	Kinematic viscosity of fluid
Π	The Coles' "profile parameter"
ρ	Mass density of fluid

NOTATION (Continued)

τ_0	Wall shear stress
τ	Shear stress, essentially in plane parallel to wall
φ	Angle of yaw
ψ	Stream function

1. INTRODUCTION

In spite of the great many experiments which have been conducted on the behavior of boundary layers in non-uniform flows, the nature of such flows continues to be one of the major unresolved problems of hydraulic engineering. This lack of knowledge is typical of rough boundary layers in pressure gradients; the flows about ship hulls, in settling basins, and in natural watercourses being examples of this type of flow field. Because the greater part of all practical boundary layer flows takes place in pressure gradients with some degree of roughness existing on the wall surface, it seemed highly desirable to initiate experiments which could explore the behavior of such flows. Consequently, the present series of tests was started at the David Taylor Model Basin about 4 years ago to provide basic experimental information on rough boundary layers in pressure gradients. This report presents the results and analyses of these experimental studies.

The regions of experimental research concerned with two-dimensional boundary layer flows of the sort which permit calculation of the frictional resistance of ship hulls and other similar turbulent flows may be classified into four broad categories: smooth or rough wall, with or without pressure gradient. Of these the smooth wall at zero

pressure gradient has received the greatest amount of attention.¹⁻⁶ The roughened wall in a constant pressure flow has also been studied extensively; see References 6-10.

Boundary layer flows in pressure gradients have offered a tremendous challenge both in theory and experiment. In 1954 Clauser¹¹ set the stage by attacking this problem with great breadth and clarity. His concept of "equilibrium" flow provided the impetus for the recent analytic solution by Mellor and Gibson.¹² A continuous attack has been made on the smooth wall case for the last 20 years using both the experimental approach and the analytical approach.¹¹⁻²³

In contrast, the study of roughened boundaries in the presence of pressure gradients has received little attention. Persh and Bailey²⁴ have studied the use of an arbitrary roughness to prevent separation in a wide angle diffuser. Recently, Perry and Joubert²⁵ reported experiments similar to the present tests, but their tests were limited to relatively mild pressure gradients.

The present program has considered the effects of a course roughness produced by a screen mesh of the type used by Hama¹ on his constant pressure tests. A simple screen having a 1/2 inch mesh and a 0.105 inch diameter wire has been applied to a flat wall to provide a roughness of known

¹⁻⁶ Note: Superscripts denote reference numbers.

and duplicable type. Tests have been run in a constant mean pressure condition to provide a comparison with Hama's¹ work and also with that of Moore⁷ who used different type of roughness. Also, two finite pressure conditions have been studied, one at a mild adverse pressure gradient and the other at a pressure gradient that nearly produces separation. For purposes of comparison, and as a check on the peculiarity of the test facility, tests have been run on a smooth wall at constant pressure and also at the same dimensionless pressure distribution which approached separation on the rough wall. When the tests were begun, it was not known whether the wind tunnel test section would tolerate adverse pressure gradients without strong secondary flows and corner separation. It was also noted that no provisions were made for stabilizing flow in the corners by auxiliary flow or bleeding of air locally. Consequently, only simple flow geometries were attempted. The two pressure gradients were obtained by setting the wall opposite the test section at divergence angles of approximately 2.9 and 11.8 deg. The divergence was then faired into the throat section upstream and into the diffuser section downstream.

It was the original intention when this project was started to study boundary layers under the combined influence of wall roughness and pressure gradient. As is the case

with many explorations, some of the details have grown into major factors, but it is hoped that these have not been permitted to obscure the main objectives. The usual boundary layer parameters, such as displacement and momentum thicknesses and shape factors which are dependent on the mean velocity distributions, have been evaluated. Shear stress is interconnected with both mean and turbulent velocity fields and with pressure in a complex fashion. The wall shear and the shear stress distributions have been studied.

One of the principal goals of the tests was to obtain data on turbulence intensities. It was anticipated that the local turbulence levels would be high as a consequence of both the wall roughness and adverse pressure gradients. For this reason it was considered advisable to take all mean velocity measurements by both pitot tubes and hot-wire probes in order to be able to correct for the effect of turbulence on the mean measurements. The measurements of the longitudinal turbulence intensities have been used to establish the order of magnitude of these corrections.

Finally, a number of special projects or comparisons have been undertaken. Velocity fields have been worked out for the severely adverse pressure gradient for both the mean and longitudinal turbulent velocities. The Coles¹⁹ "Law of

the Wake" has been investigated for the Hama¹ roughness and comparisons have been made with mean velocity distributions. Boundary layer parameters and behavior have been investigated for the same severely adverse pressure gradient over rough and smooth surfaces. A discussion of this comparison is presented.

2. INTRODUCTORY ANALYSIS

The discussion which follows is intended to set the stage for presentation of the experimental results. The relationships which are given or developed are required merely to evaluate the usual boundary layer parameters. The mean velocity profiles and turbulence intensities were obtained directly from measurements and have then been corrected by the methods which are given in Chapter 4. The displacement and momentum thicknesses were obtained by integration of these corrected velocity profiles.

2.1 EVALUATION OF THE SKIN FRICTION COEFFICIENT

The skin friction coefficient, c_f , may be determined either by direct measurement under proper circumstances or by the two analytical methods which follow. Experimental techniques for measuring the wall shear and the skin-friction coefficient have been used in many investigations. For the smooth-wall case, it is possible to use small floating elements in the wall,²⁶ hot film elements¹⁵ similar to hot-wires which are set flush with the wall surface, or a variety of impact tubes^{27,28} in contact with the wall. The small floating element can not generally be used with pressure gradients because the pressure change affects its readings more seriously than the shear stress which it is intended to

measure. These have been used for moderately rough surfaces in constant pressure boundary layers. Both the hot-film elements and the small impact tubes have given satisfactory results on smooth walls with pressure gradients. None of these methods is believed to be presently acceptable with rough surfaces in pressure gradients.

As an alternative to direct measurement of c_f , the distribution of mean velocity in the boundary layer may be applied either to a momentum equation or to the logarithmic velocity law near the wall to provide a solution by direct calculation.

MOMENTUM EQUATION

The momentum equation in terms of c_f for a two-dimensional incompressible boundary layer may be written (see Equation 4.5 and Table 5 of Reference 6)

$$c_f = 2 \frac{d\theta}{dx} + 2(H + 2) \frac{\theta}{U_1} \frac{dU_1}{dx} - \frac{2}{U_1^2} \frac{d}{dx} \int_0^{\delta} (u'^2 - v'^2) dy \quad (1)$$

where $H = \frac{\delta^*}{\theta}$, shape factor (2)

$$\delta^* = \int_0^{\delta} \left(1 - \frac{U}{U_1}\right) dy, \text{ displacement thickness} \quad (3)$$

$$\theta = \int_0^{\delta} \frac{U}{U_1} \left(1 - \frac{U}{U_1}\right) dy, \text{ momentum thickness,} \quad (4)$$

representing the mean-flow momentum loss^{*}

- δ is the nominal boundary layer thickness
- U is the local longitudinal mean velocity
- $U_1(x)$ is the free stream velocity just outside the boundary layer
- x is the longitudinal distance along wall
- y is the normal distance from wall
- u' is the longitudinal turbulent intensity $\sqrt{u'^2}$
- v' is the turbulent intensity $\sqrt{v'^2}$, normal to wall
- u is the turbulence velocity fluctuation in longitudinal direction
- v is the turbulence velocity fluctuation normal to wall

When U_1 is constant, as in the constant pressure case, only the first term on the right-hand side of Equation (1) is significant (see Reference 11, p. 107). This permits evaluation of c_f by graphical differentiation of the momentum thickness $\theta(x)$. This method was used to determine c_f for the constant pressure runs. When pressure gradients

*Note: For convenience while running tests, the mean-flow form of the momentum thickness was used as given here. Later in Chapter 6, the turbulent normal stress terms were included in the calculation of c_f .

exist, however, this method is no longer valid. Under these conditions the second and third terms on the right-hand side of Equation (1) become significant. The significance of the third term, which is often omitted in the usual linearization, is discussed in Reference 29. In addition, the effects of three-dimensionality in the flow which occur near separation can add additional terms to Equation (1) (see Reference 11, p. 108). When these factors are not considered, significant errors in the calculated values of c_f can result. See Wieghardt and Tillmann, Figures 2-6 of Reference 30, for examples of unreliable shear coefficients obtained from flows with pressure gradients, using only the first and second terms on the right-hand side of Equation (1). An alternative method for estimating c_f by making use of the logarithmic velocity law is described in the following section.

LOGARITHMIC VELOCITY LAW

Clauser^{11,20} and Hama¹ have demonstrated that an equation of the following form may be used to describe the mean velocity distribution of the "inner" region of the turbulent flow near a rough boundary in a constant pressure field.

$$\frac{U}{U_\tau} = \frac{1}{K} \ln \frac{yU_\tau}{\nu} + A - \frac{\Delta U}{U_\tau} \quad (5)$$

where

$U_\tau = \tau_o/\rho$ is the shear velocity

τ_o is the wall shear stress

ρ is the mass density of fluid

K is an experimentally determined constant

A is an experimentally determined constant

ΔU is a defect velocity, such that $\Delta U/U_\tau$ represents the shift of the logarithmic profile caused by roughness Reynolds number, $R_k = kU_\tau/\nu$, where k is the nominal wall roughness (in this case taken arbitrarily to be twice the screen wire diameter)

ν is the kinematic viscosity of fluid

This relationship applies over distances from the magnitude of k to about 10 to 20 percent of the boundary layer thickness in boundary layers where the free stream pressure is held constant.* The extent of the linear-logarithmic portion of the boundary layer is a complicated function of both yU_τ/ν and the local Reynolds number. For example, see Figure 10 of Reference 20. Local wall disturbances affect both the pressure and velocity to a distance of about

*The effect of a pressure gradient on the "inner" region is discussed later.

2 wire diameters from the wall and cause departure from the logarithmic form in this portion of the boundary layer. Beyond the linear-logarithmic part of the boundary layer thickness the "law of the wake" produces further deviation from the logarithmic form. This "outer" layer, or "wake" region, is amply described and illustrated by Coles¹⁹ and by Perry and Joubert.²⁵

Clauser¹¹ presents Equation (5) as follows

$$\frac{U}{U_{\tau}} = 5.6 \log_{10} \frac{yU_{\tau}}{\nu} + 4.9 - \frac{\Delta U}{U_{\tau}} \quad (6)$$

To use Equation (6) to obtain c_f we first obtain an alternate expression for U_{τ} . The definitions of U_{τ} and c_f are

$$U_{\tau}^2 = \frac{\tau_o}{\rho} \quad \text{and} \quad c_f = \frac{\tau_o}{1/2\rho U_1^2}$$

Combining these expressions, we get

$$U_{\tau} = \sqrt{\frac{c_f}{2}} U_1 \quad (7)$$

Substituting (7) into (6), we obtain

$$\frac{U}{U_1} = \sqrt{c_f} \left[3.96 \log_{10} \frac{yU_1}{\nu} + 1.98 \log_{10} c_f + 2.87 - \frac{1}{2} \frac{\Delta U}{U_{\tau}} \right] \quad (8)$$

If Equation (8) is plotted on semilogarithmic paper with y as the abscissa, U/U_1 as the ordinate, and with fixed values of c_f , solutions will appear as a series of straight lines with slopes equal to $3.96 \sqrt{c_f}$. The term $\frac{\Delta U}{U_{\tau}}$ is a

function of the roughness and shifts the plots vertically but does not change the slopes. Values of $\frac{\Delta U}{U_\tau}$ as a function of the roughness have been collected by Hama¹ and are presented by Clauser in Figure 11 of Reference 20. For the smooth wall case $\frac{\Delta U}{U_\tau}$ is zero. Where $\frac{kU_\tau}{\nu} > 70$, an equation of the type

$$\frac{\Delta U}{U_\tau} = 5.6 \log_{10} \frac{kU_\tau}{\nu} + D \quad (9)$$

may be used (see Reference 20, Equation 2.12). The flow conditions at the wall are said to be "fully rough" when Equation (9) may be applied with a constant value of D . If we use a value of $D = -1.2$, obtained from Hama's¹ experiments, and substitute (9) into (8), the relation for the fully rough wall case becomes

$$\frac{U}{U_1} = \sqrt{c_f} \left[3.96 \log_{10} \frac{y}{k} + 4.30 \right] \quad (10)$$

This equation demonstrates that for the fully rough case the influence of viscosity has ceased to exist. Sample plots of Equation (8) for the smooth wall $\frac{\Delta U}{U_\tau} = 0$ with $c_f = 0.002$ and 0.004 , and Equation (10) for the fully rough wall with $c_f = 0.0001, 0.001, 0.002, 0.005,$ and 0.010 , are presented in Figure 1. A value of 2 wire diameters (0.21 in.) was used for k .

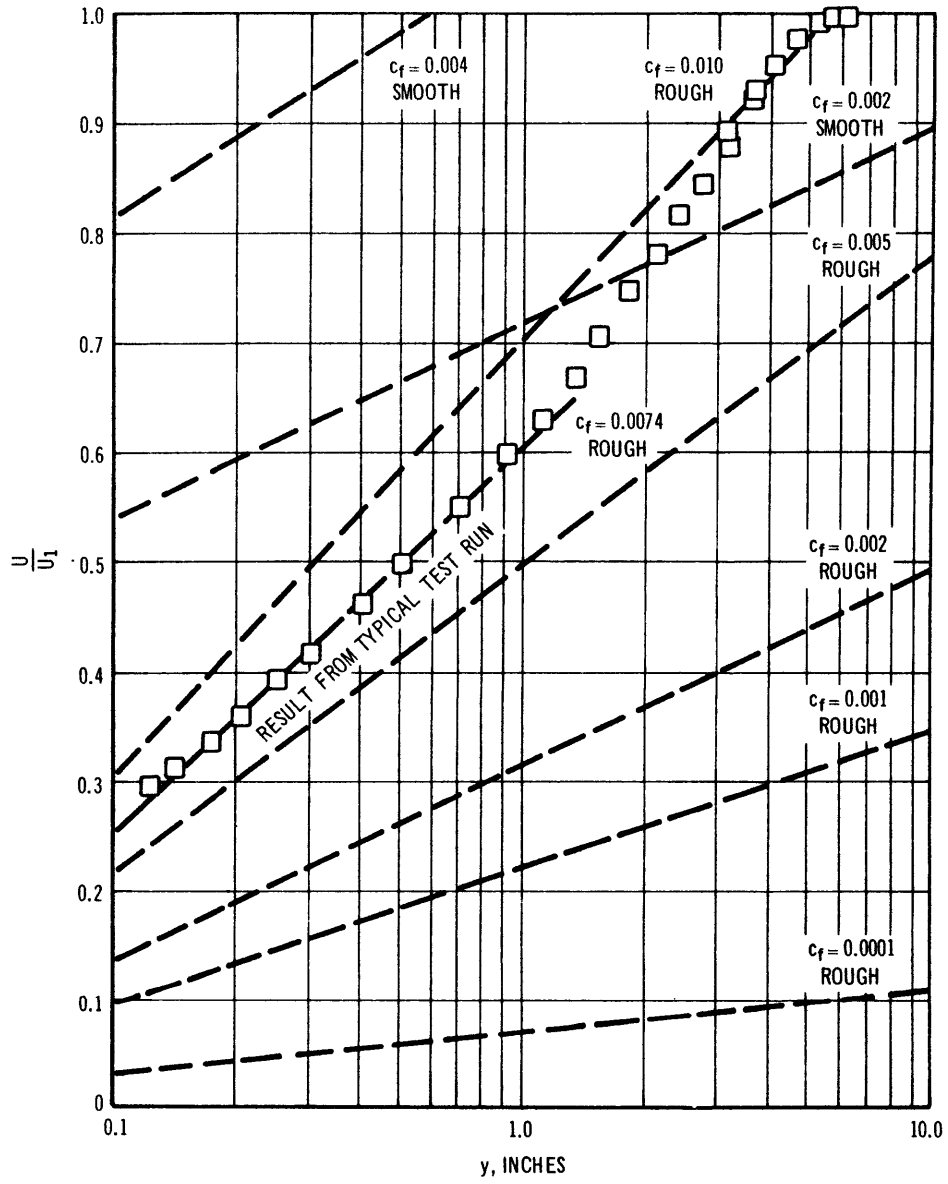


FIGURE 1—Logarithmic Portion of Typical Mean Velocity Profiles for Smooth and Rough Surfaces and for a DTMB Run

Essentially, if the logarithmic portion of a boundary layer velocity profile (U/U_1 versus y) is plotted on semilogarithmic paper, it will appear as a straight line with c_f as a simple function of the slope. The values of c_f for the two pressure gradient cases in the present experiments were determined by this method. A typical set of data from a constant pressure traverse is shown plotted in Figure 1. By plotting the complete velocity profile it was possible to establish the logarithmic portion of the experimental curves.

2.2 ORIGIN OF ROUGH WALL

The presentation of the rough wall data is seriously complicated by the fact that the origin of y is undefined because of the presence of roughness elements. The evaluation of such an "effective" origin is dependent on a knowledge of the mean velocity distribution. Clauser²⁰ presents the generally accepted argument which permits such evaluation. His first point is that experiments^{14,15,30} have amply demonstrated the existence of a logarithmic region for flows over smooth boundaries in a variety of pressure gradients. The second point assumes the validity of a velocity defect relationship or correlation scheme for the outer portion of the boundary layer. This is illustrated by

by Figure 5 of Reference 20 which cites data from References 1, 3, and 7 among others. Unfortunately, the rough wall data must be plotted against an "effective" y which minimizes the scatter of the experimental points in the process of providing a logarithmic velocity distribution near the wall. The assumption of the velocity defect relationship for rough walls appears to be justified largely on the basis of the large number of experiments which have served to verify this hypothesis.

Once the existence of a logarithmic region near the wall is accepted, it is possible to locate an "effective" origin. A very workable method for determining the "effective" location of the wall is described by Perry and Joubert.²⁵ Their scheme consisted essentially of adjustment of the y origin until a best-fitting straight line could be drawn for the U/U_1 versus y points on a semilogarithmic plot, for data taken at the constant and mildly adverse pressure gradients. A similar method applied to the present research located the effective origin approximately one screen wire diameter below the outer wire mesh surface. Since the screen wire diameter is 0.105 in., apparently the fluid "sees" the wall at about one-half the roughness depth for this type of roughness. Intuitively, one would expect the origin to lie somewhere between the trough and crest of any

roughness. This has proved to be the case in a variety of experiments.^{7,25,37} For the remainder of the report, unless otherwise noted, y' will be used to designate the normal distance from the effective origin and y the distance from a surface defined by the outer extremity of the wire mesh as shown in Figure 2.

When the adverse pressure gradient increases in magnitude, the length of the inner or logarithmic portion of the velocity profile becomes shorter. Thus it is not possible to use this "best fit" method to define an origin as the boundary layer approaches separation. In fact Stratford^{21,22} and Mellor and Gibson¹² have concluded that for smooth walls at incipient separation, $\tau_o = 0$, the inner law disappears completely. This is also borne out by Coles,¹⁹ Figures 10 through 16, where with rising pressure gradient, the linear portions of the plots gradually shorten and vanish at separation. Therefore, for the large pressure gradient of this experiment, it was assumed that an origin might be selected to be the same as for zero and mild pressure gradients.

The location of an effective origin may be presumed to be associated with the generation of turbulence at the wall. In the case of the solid smooth wall, it is well known³¹ that the turbulent eddies appear very close to the wall, but must

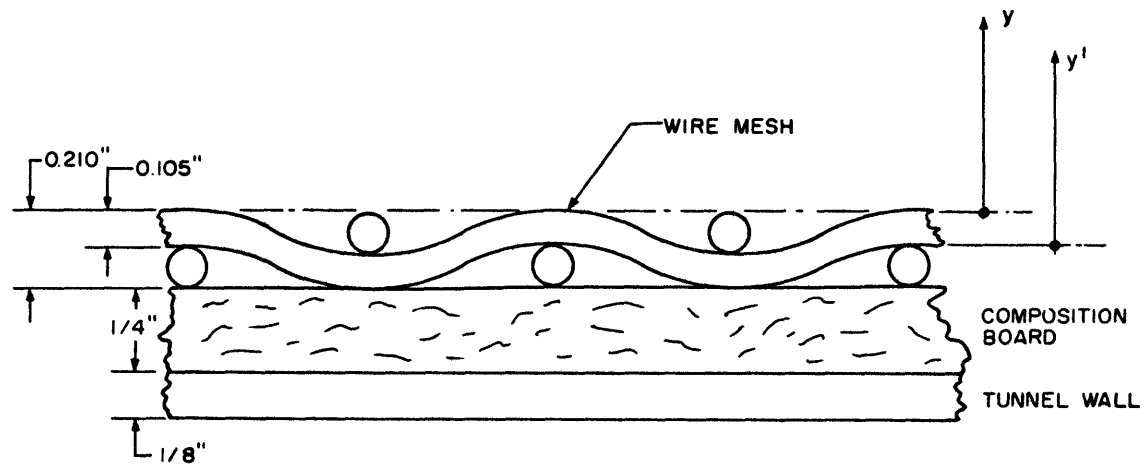


Figure 2 - Location of y'

cease right at the wall ($y = 0$) because of the restriction provided by the wall itself. The rough wall supplies high level turbulence about the discreet roughnesses by an eddy-shedding process. Presumably these perturbed flows can exist down to the bottoms of the troughs between the roughnesses but they would also be limited in their intensity by the presence of the solid boundary. If the location of an effective origin is tied to the eddy-shedding process, its position must be dependent on roughness geometry and the local roughness Reynolds number, Uk/ν . The latter condition implies that the origin would gradually change its position as separation is approached, but there is no evidence on which to base a choice of direction for this migration. The best that may be concluded, in an intuitive fashion, is that the effective origin will still be located between the crests and troughs of the roughness elements.

2.3 EVALUATION OF THE MOMENTUM THICKNESS

Evaluation of the momentum thickness from Equation [4] posed the problem of attempting to project the integrand of this function back to the "effective" wall since there was obviously a certain amount of flow passing through the interstices of the screen mesh. A variety of calculations were made, and it was decided that the contribution to θ within

and immediately adjacent to the roughness elements was not very meaningful because of the uncertainties of mean velocity measurements in this region. The momentum thickness was therefore originally calculated from the unadjusted values of mean velocities taken by both Pitot tube and hot wire from the plane of the screen out to the free stream. Since the integral is relatively insensitive to small differences in mean velocity measurement, the values obtained by the two instruments were quite close. In fact, during the experimental tests large differences in the value of θ obtained from the two sets of unadjusted readings tended to single out erroneous velocity profiles.

The momentum thicknesses presented in Chapter 6 have been recomputed from corrected data using the same approach as that discussed in the preceding paragraph.

3. EXPERIMENTAL PROGRAM

3.1 APPARATUS

WIND TUNNEL

The low turbulence wind tunnel facility,³² Figure 3, is an open return type having an adjustable test section about 15 ft long with a 2-ft by 4-ft cross section at both ends, a contraction ratio of 12.5:1, and a 3:1 rectangular diffuser followed by two 90-deg turns. Although the maximum speed of the tunnel is 150 fps, the desired data for the present test configuration was obtainable at speeds between 30 and 100 fps.

For simplicity in mounting and locating the probes which passed through the rough wall, it was considered desirable to hold this wall as close to a plane as possible. All pressure adjustments were made by varying the shape of the opposite smooth wall by means of the jack screws installed for this purpose. Figure 4 shows this wall adjusted to the configuration corresponding to the maximum pressure gradient. Although the smooth wall bore the brunt of the divergence, the boundary layer showed no tendency to separate from it in any of the pressure gradients.

At each pressure condition the flow across the entire width was carefully checked at several positions along the

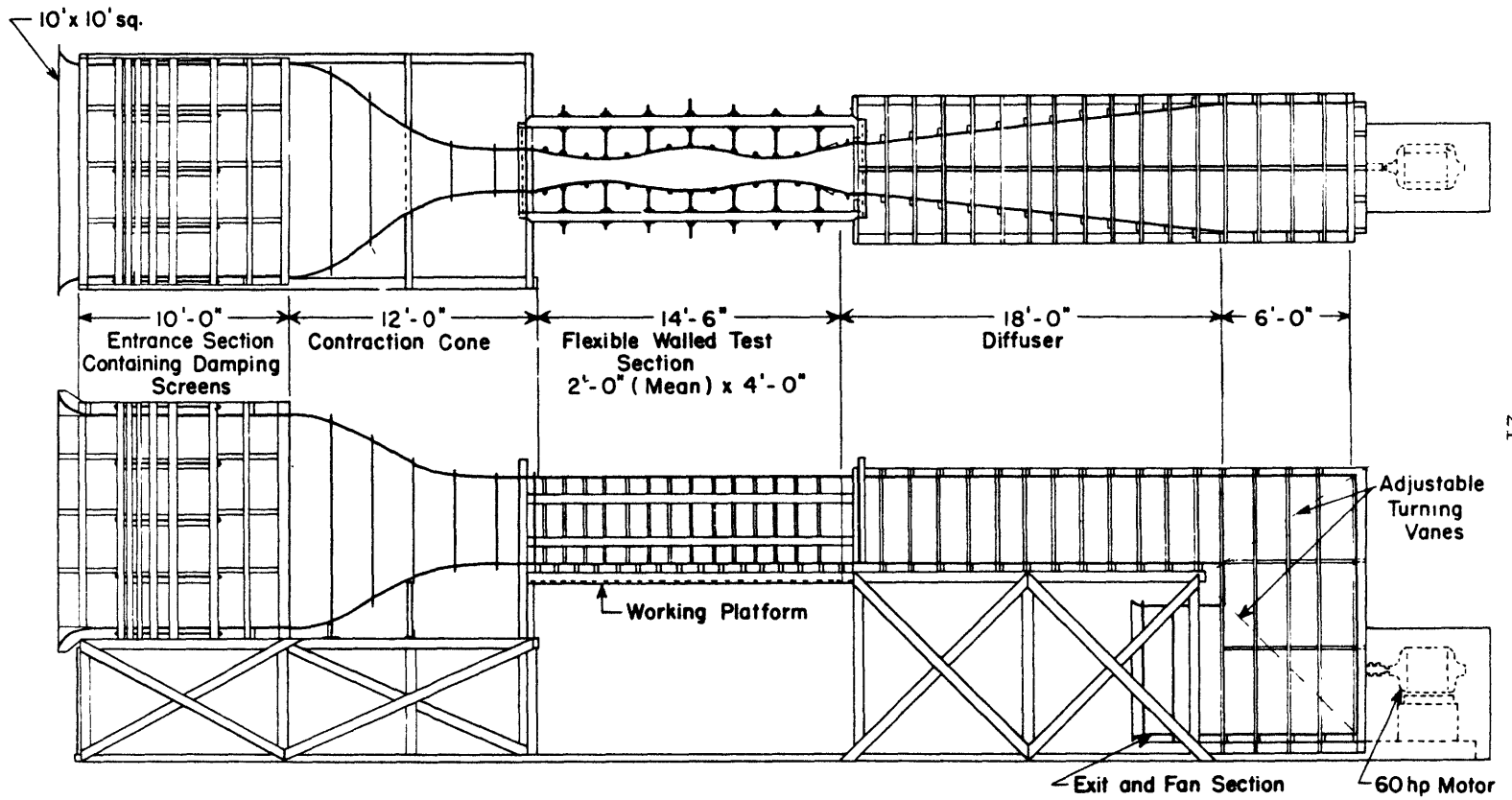


Figure 3 - General Arrangement of Wind Tunnel

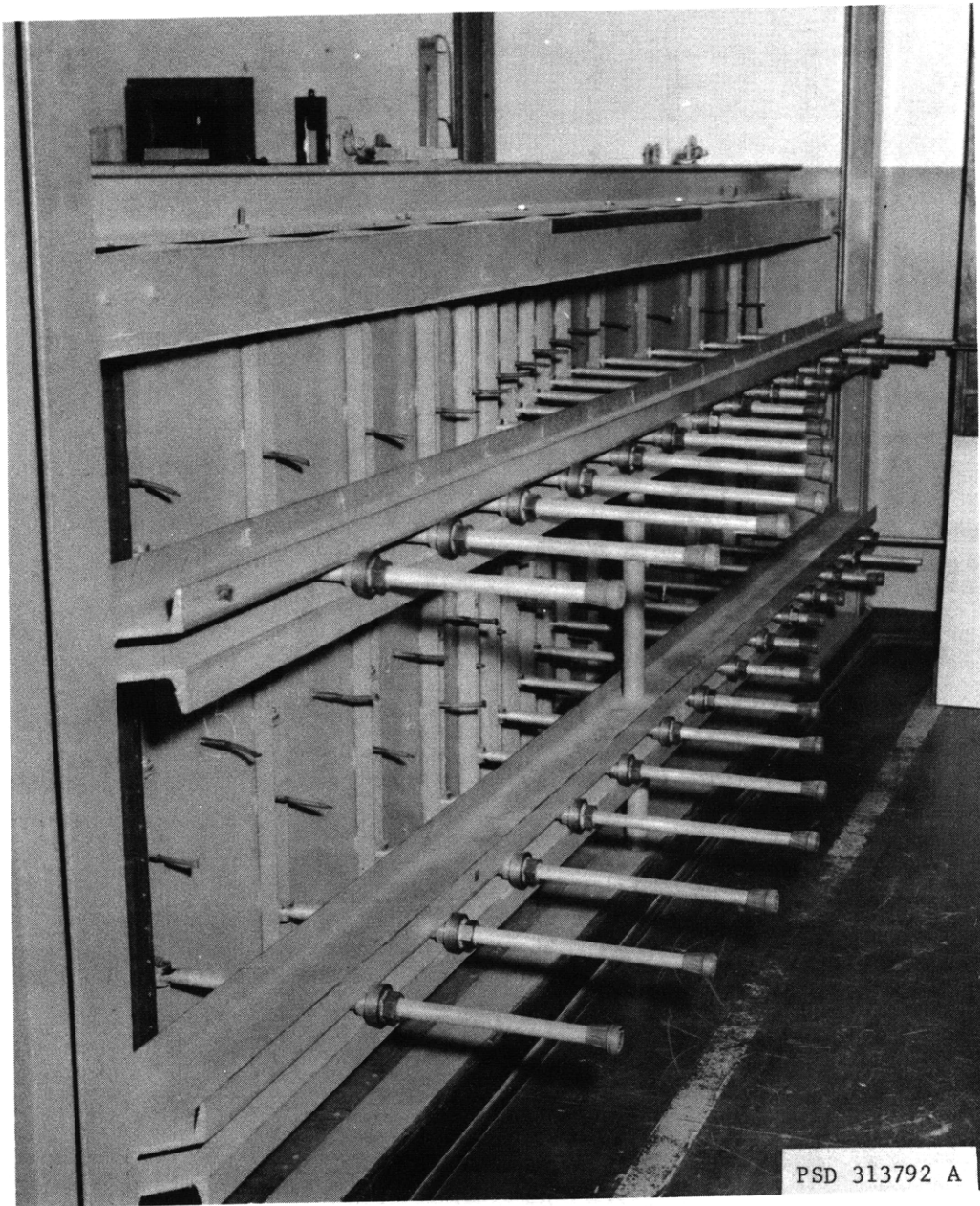


Figure 4 - Wind Tunnel Exterior Showing Contoured Wall and Jack Screws

length of the test section to determine any departure from two-dimensionality and any tendencies toward separation. Pitot tube traverses were taken from wall to wall at positions 8 in. up from the floor, 8 in. down from the top, and on the center line. Hot wire traverses of mean velocity and longitudinal turbulence intensity in the boundary layer were obtained at the same positions from the rough wall into the free stream. Tufts were placed on the smooth wall at corresponding vertical positions and about 2 ft apart longitudinally in order to observe the flow. The flows were reasonably symmetrical with only a slight increase in mean velocity (1 to 2 percent) in the free stream at the top and bottom of the tunnel. Although the boundary layer was quite thick (11 to 12 in. at the maximum pressure gradient) at the downstream end of the test wall, the low turbulence free stream zone remained clearly defined even at the maximum pressure gradient condition. At no time was separation observed at any point in the flow. Previous mean velocity studies³² in this wind tunnel show that the flow in the test section appears to be two-dimensional along the centerlines of the vertical walls at a constant pressure condition in spite of a tendency for the boundary layer to thicken more rapidly on the top surface than on the other three boundaries.

ROUGHNESS ELEMENTS

The test wall, Figures 2 and 5, consisted of a plane surface of 1/4-inch tempered composition board to which the roughness elements were attached. The roughness consisted of a square mesh screening made from 0.105-in.-diameter wire having a mesh 1/2-inch on centers in both directions. This screening, after some preliminary flattening in sheet metal rollers, was secured to the composition board by fine wires spaced every 6 in. on the downstream side of the screen wires. Apparently, these fine wires were in the separated regions within the mesh and did not influence the flow. The rough wall, as installed, had slight undulations of 12 to 30 in. length and not exceeding 0.050 in. amplitude. It was necessary to cut the wall into two sections to fit it into the tunnel. The lead section was 4 ft long by 4 ft high and the trailing section 12 ft long by 4 ft high. The joint was carefully aligned, and subsequent tests indicated negligible disturbance from it in the boundary layer downstream.

With such a rough boundary no extra precautions were needed to ensure turbulence or a thick boundary layer. Measurements taken within 3 ft from the leading edge displayed well-developed high intensity turbulence and a minimum boundary layer thickness of about 4 in.

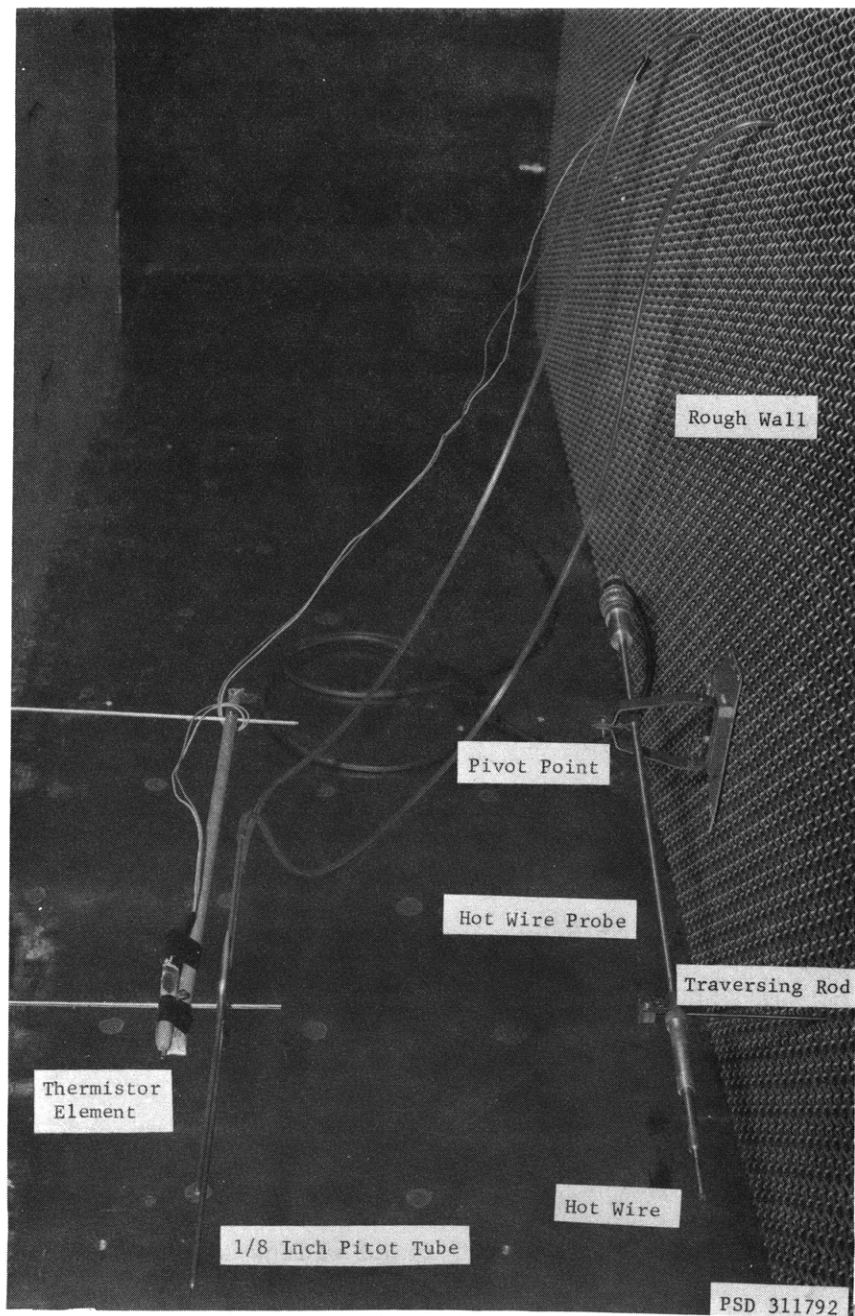


Figure 5 - Wind Tunnel Interior Showing Rough Wall, Mounted Hot Wire, One-Eighth Inch Pitot Tube, and Thermistor Element.

PRESSURE DISTRIBUTIONS

The obtainable pressure distributions were limited by the design of the wind tunnel. Since the smooth wall is fixed at both ends and its lateral adjustment is only a fraction of the mean width of the cross section, only a portion of the wall length may be used to form a diffuser. Some preliminary experimentation with the smooth wall contours led to simple wedge-shaped divergences having carefully faired entrances and exits with included angles of about 2.9 and 11.8 deg. Consequently, these studies do not present results obtained with carefully chosen gradients of the "equilibrium" type and must be considered to be exploratory in nature. However, the high pressure gradient condition provides some very interesting comparisons with the smooth boundary data of Schubauer and Klebanoff¹⁴ in spite of the rather different flow geometries.

For the zero pressure gradient tests the boundary layer growth in the downstream direction required a continuous divergence of the smooth wall to maintain a constant pressure condition. With the 2-ft fixed widths at both ends of the test section it was impossible to obtain this divergence over the whole test section length. As an alternative the wall was adjusted to produce a mildly accelerated flow over the first 6 ft of the roughened wall and a constant pressure

for the remaining distance. This arrangement apparently influences the boundary layer characteristics for some additional distance beyond the first 6 feet of the test wall. However, this configuration gave satisfactory results once the boundary layer had stabilized at the downstream end of the test section.

The smooth wall tests were run under essentially the same conditions as those for the rough wall. However, it was necessary to provide some wall roughness ahead of the test section in order to thicken the boundary layer. The roughness used consisted of two feet of 1/16 inch sandpaper (# 4, 3M Brand) placed near the back of the wind-tunnel convergence. The angles of divergence of the test section were somewhat less for the smooth wall since the boundary layer displaced a smaller amount of flow for a given pressure gradient.

3.2 INSTRUMENTATION

The mean velocity was measured with both pitot tubes and hot wire probes since it was anticipated that the local turbulence levels would be extremely high and it was considered desirable to run a continuous check of one type of instrument against the other. The hot wire systems were carefully linearized to make simultaneous readings of longi-

tudinal turbulence intensities u' and mean velocities. The distances from the wall for both pitot tubes and hot wires were regulated by a traversing mechanism constructed from a standard Hardinge lathe crossfeed. Access to the tunnel during operation was by means of 1/8-in.-diameter ports placed in vertical columns at 1-ft intervals along the tunnel walls. The dimensions and positioning of the hot wires and pitot tubes were such that the measurements were made 6 in. ahead of the entrance ports. Several arrangements of pitot tubes and hot wires were used and are described here. The various pressure and temperature recording instruments and the traversing mechanism are also discussed.

PITOT TUBES

Three pitot tubes were used to make the velocity measurements: All had separate impact and static elements. The small pitot tube had a geometrical construction that permitted measurements near the wall. A picture of this pitot tube is shown in Figure 6. The impact element was hypodermic tubing, 0.025 in. outside diameter and 0.016 in. inside diameter, shaped so that it could be placed tangent to the wall. The static element was 1/16-in.-diameter tubing with four holes of 0.016 inch spaced at 90-degree intervals around the tube at a distance of approximately 10 diameters

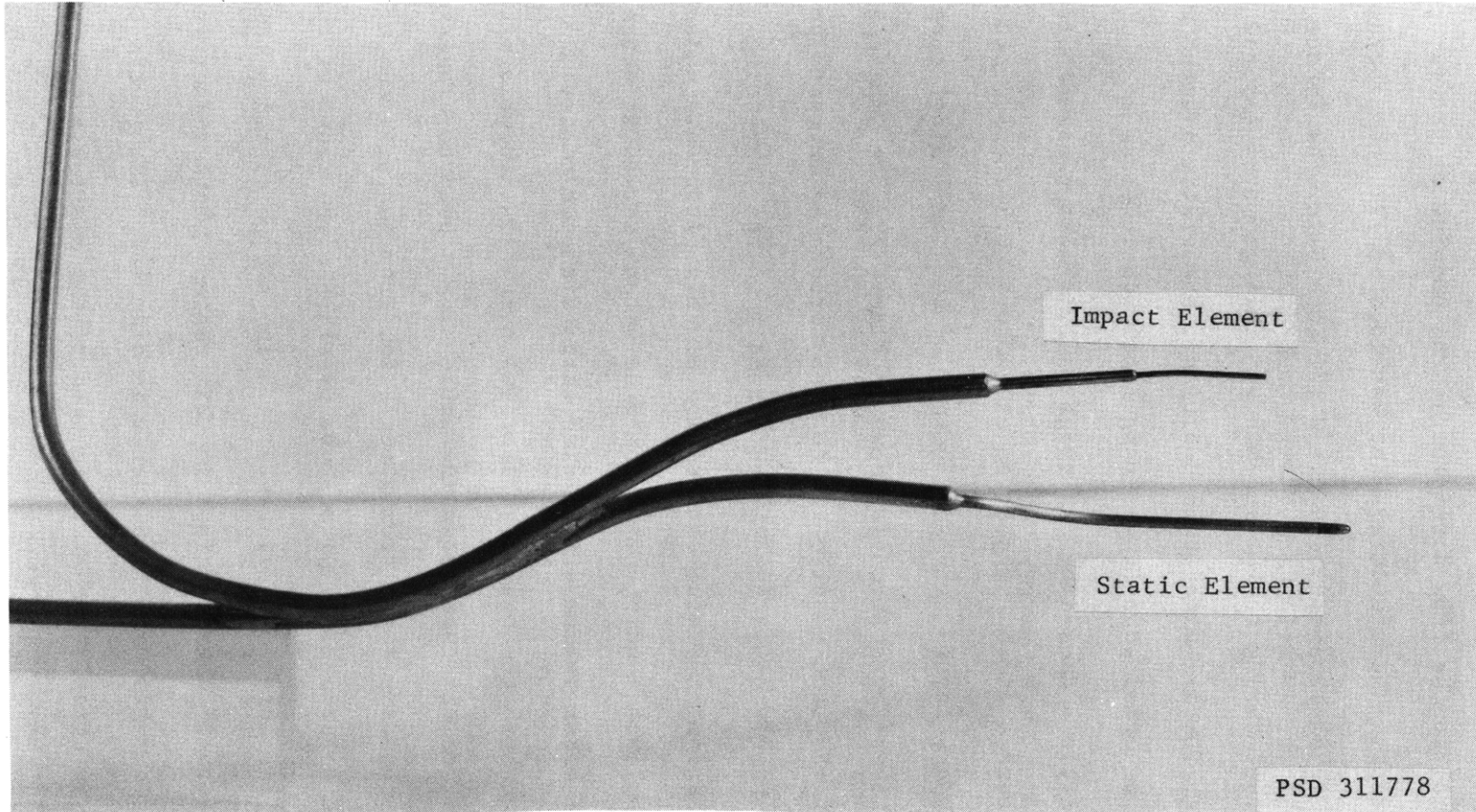


Figure 6 - Small Pitot Tube

from the leading edge. These holes were in the same plane normal to the flow direction as the opening of the impact element. The static element was located 1/2 inch farther out in the boundary layer and 1/2 inch below the impact element during the measurements. This geometry ensured that, for all pitot tube positions, the static element would not be affected by the strong local static pressure variations caused by the rough wall. These pressure disturbances did not appear to extend over 0.3 inches into the boundary layer. The arrangement of the small pitot tube at a traversing station is shown in Figure 7. The impact element was bent to allow it to pass through an entrance port so that it could be clamped directly to the traversing mechanism. Careful calibration of this pitot tube under low turbulence conditions in the free stream showed no appreciable error in comparison with large diameter tubes.

Where the boundary layer was over 7 in. thick a pitot tube, of the type shown in Figure 8, was used to traverse the boundary layer from about 4 in. from the wall out to the free stream. This pitot tube overlapped the range of the smaller tube for a distance of 3 in. and permitted a comparison of data obtained in this region. Both impact and static tubes were 1/16 inches in diameter. The static tube was identical to the static tube of the smaller pitot tube

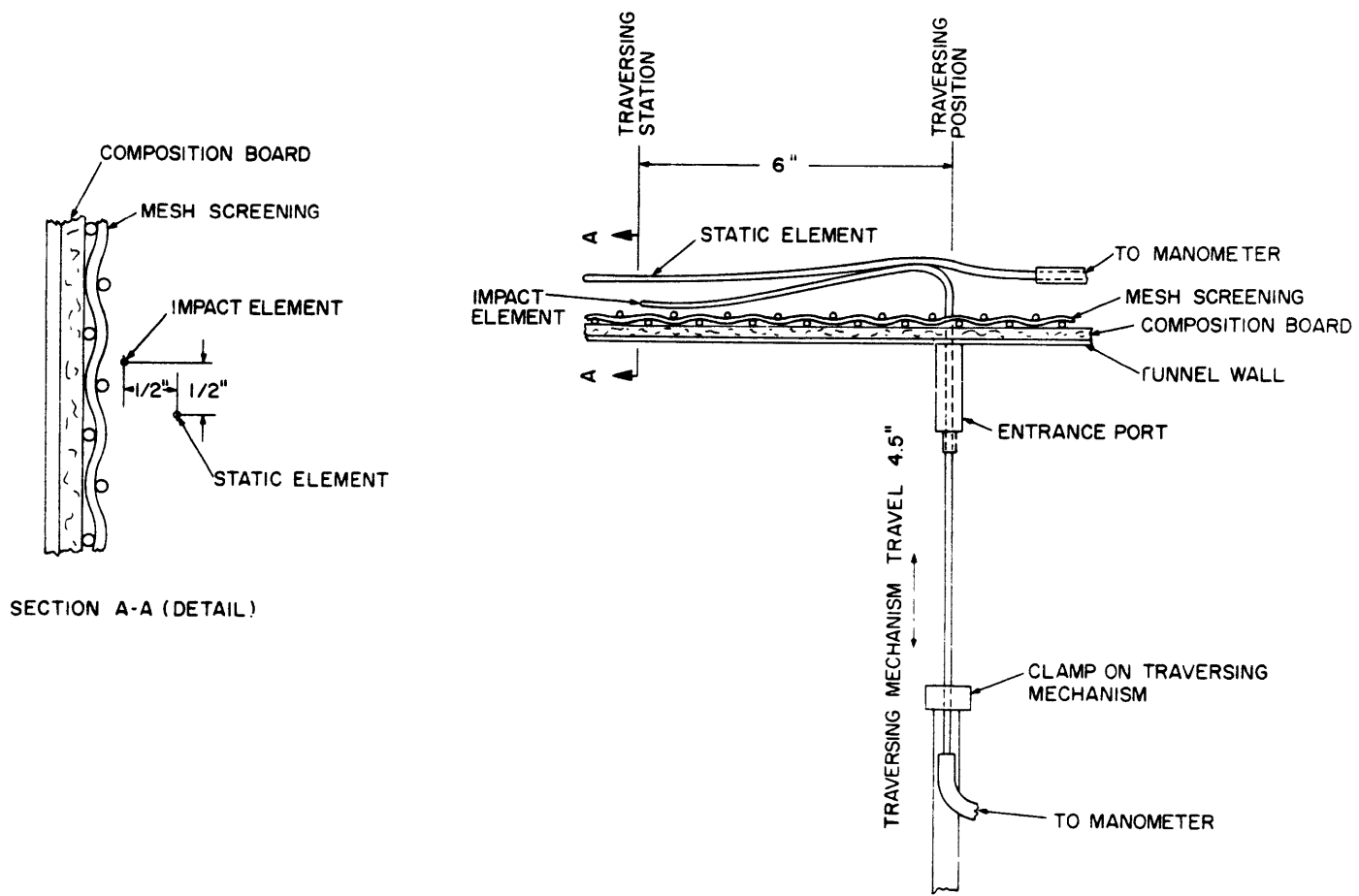


Figure 7 - Diagram of Small Pitot Tube Mounting Arrangement

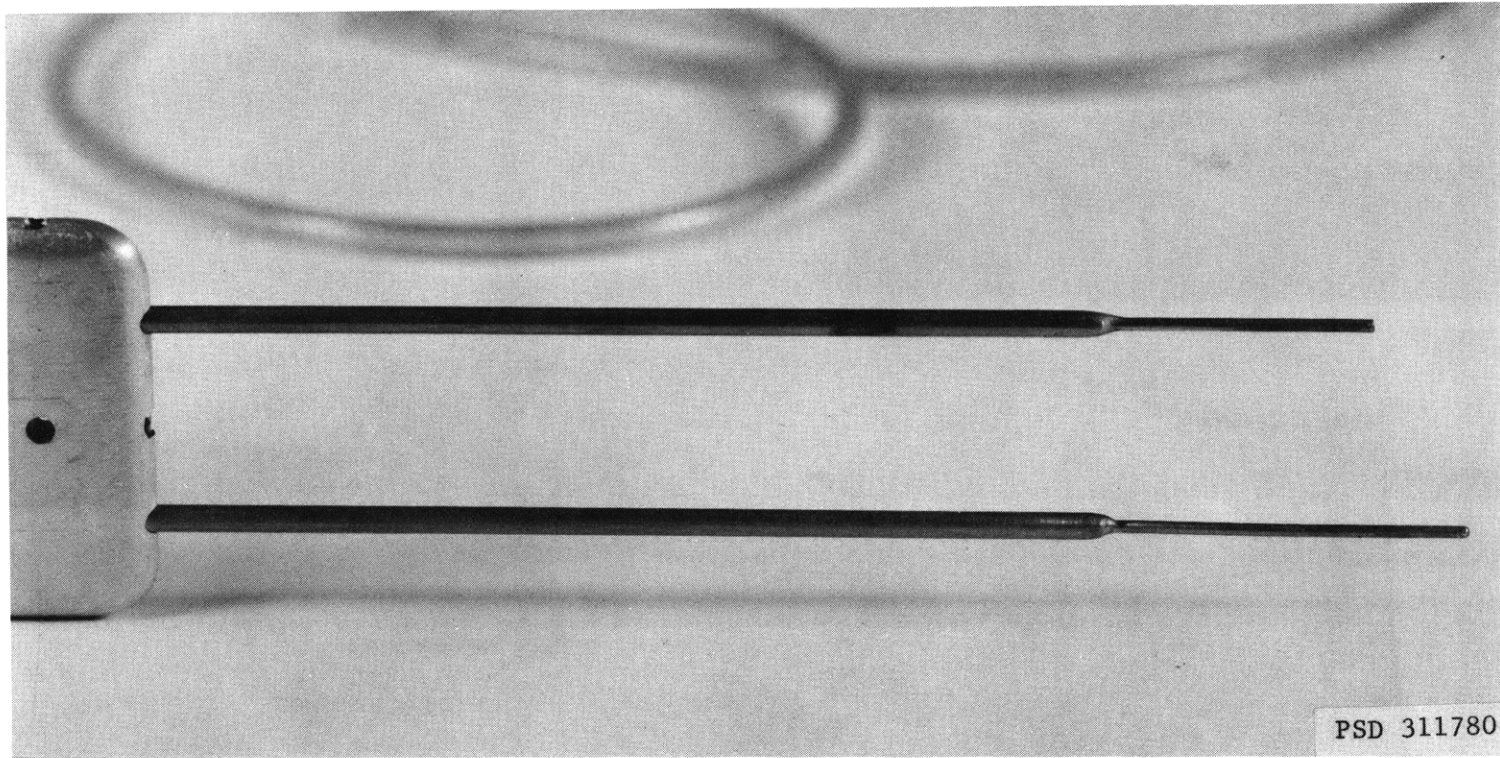


Figure 8 - One-Sixteenth Inch Pitot Tube

and was located 1 in. from the impact tube. The tip of the impact tube had an internal diameter of 0.052 in. This pitot tube was positioned by a 1/8-in.-diameter rod, one end of which was clamped to the pitot tube and the other to the traversing mechanism.

A pitot tube similar to the 1/16-in. probe, but having 1/8-in.-diameter impact and static tubes, was used as a free stream reference and, when it would not disturb the flow at a measuring station, for monitoring the steadiness of the flow. This pitot tube was fixed in position for a given set of measurements. The standard reference velocity for the wind tunnel was obtained by calibrating the pressure difference between a fixed impact tube at the entrance to the tunnel contraction and a static (smooth wall) tap at the beginning of the test section against the pressure differences across the 1/8-in. pitot tube at fixed locations in the free stream.

HOT WIRES

The hot-wire probes were standard Flow Corporation 0.00015-in.-diameter copper-plated tungsten wire having an active length of about 1 mm. These were set with the wire vertical and parallel to the wall at a location 6 in. ahead of the entrance port. The distance from the wall was

controlled by an 1/8-in. rod attached to the traversing mechanism. The body of the probe pivoted about a point 12 in. downstream from the traverse position. This arrangement permitted accurate positioning of the hot wire for a range of about 7 in. for a single setting of the traverse. The hot wire mounted in the tunnel is shown in Figure 5. Figure 9 is a diagram of the mounting arrangement.

The hot wire anemometer used was the Iowa University Mark 3A type.³³ This is a constant temperature type of instrument that provides a linear relation between mean velocity and d-c amperage measurements. Two channels of signal amplification and linearization are available.

TRAVERSING MECHANISM

The traversing mechanism consisted of a standard Hardinge lathe crossfeed suitably adapted to permit clamping and positioning of a 1/8-in.-diameter traversing rod or the stem of the small pitot tube. This lathe crossfeed could be set to within 0.0005 in. but had a limited travel of less than 5 in. This required repositioning the pitot tube or hot wire in the traversing mechanism during the surveys of the thicker boundary layers. Relocating the pitot tubes and hot-wire probes, when repositioning was necessary, was a time-consuming process since the wind tunnel had to be

slowed to idling speed, the probe fitted, and then located with respect to the roughness "face" of the wall. It is doubtful that the accuracy of absolute positioning was any better than ± 0.005 in. in spite of the high accuracy of relative location. The principal advantage of this cross-feed was the ease with which the hot-wire probe could be moved out into the low level turbulence for a calibration check.

PRESSURE MEASUREMENTS

A sensitive micromanometer,³⁴ which could be read to the nearest 0.0002 in., was used to measure pressures at the lower velocities. This gave excellent results in regions of low turbulence but proved overly sensitive and difficult to read in regions of high turbulence. Most of the pressure readings were taken on precision inclined manometers which had slope settings from 1:10 up to 1:4. Reproducibility of readings proved quite satisfactory with these manometers. The manometer fluid for all the units was Dow Corning Silicone 200 (specific gravity of 0.817), which has properties highly suitable for this use.

The distribution of static pressure in the wind tunnel was determined independently by two different means. Pressure taps located at 1-ft intervals in the smooth floor

of the wind tunnel were connected with an electronic data processing system (Datex) having a resolution of about 0.02 in. of water (0.10 lb/ft²). It was also possible to compute the static pressure from the measured velocities at the free stream edge of the boundary layer. Both methods were used and provided a satisfactory check on each other.

TEMPERATURE MEASUREMENTS

To ensure precise measurement of air density the temperature was monitored and recorded during the runs. Figure 5 shows a thermistor element attached to the top of the pitot tube mounting. This was calibrated against a variable resistance bridge, and the resulting measurement had a resolution of 0.1 deg F. Also a mercury thermometer, with graduations of 0.1 deg C was placed in the smooth wall. As the mercury thermometer checked the thermistor readings quite closely and was more convenient to use, it was used exclusively for the temperature measurements in the tunnel for most of the tests.

MEAN VELOCITY MEASUREMENTS

During the tests extremely high levels of turbulence intensity were encountered close to the wall. Here the rms values of u' were from 40 to 50 percent of the local mean velocity. This gave rise to sizeable errors in the

measurement of both mean velocity and turbulent intensity. Figure 10 illustrates a typical comparison of hot wire and pitot tube mean velocity readings. It has been apparent right from the start that the correction of instrument readings would constitute one of the key problems in these tests. This special topic has therefore been placed by itself in the next chapter.

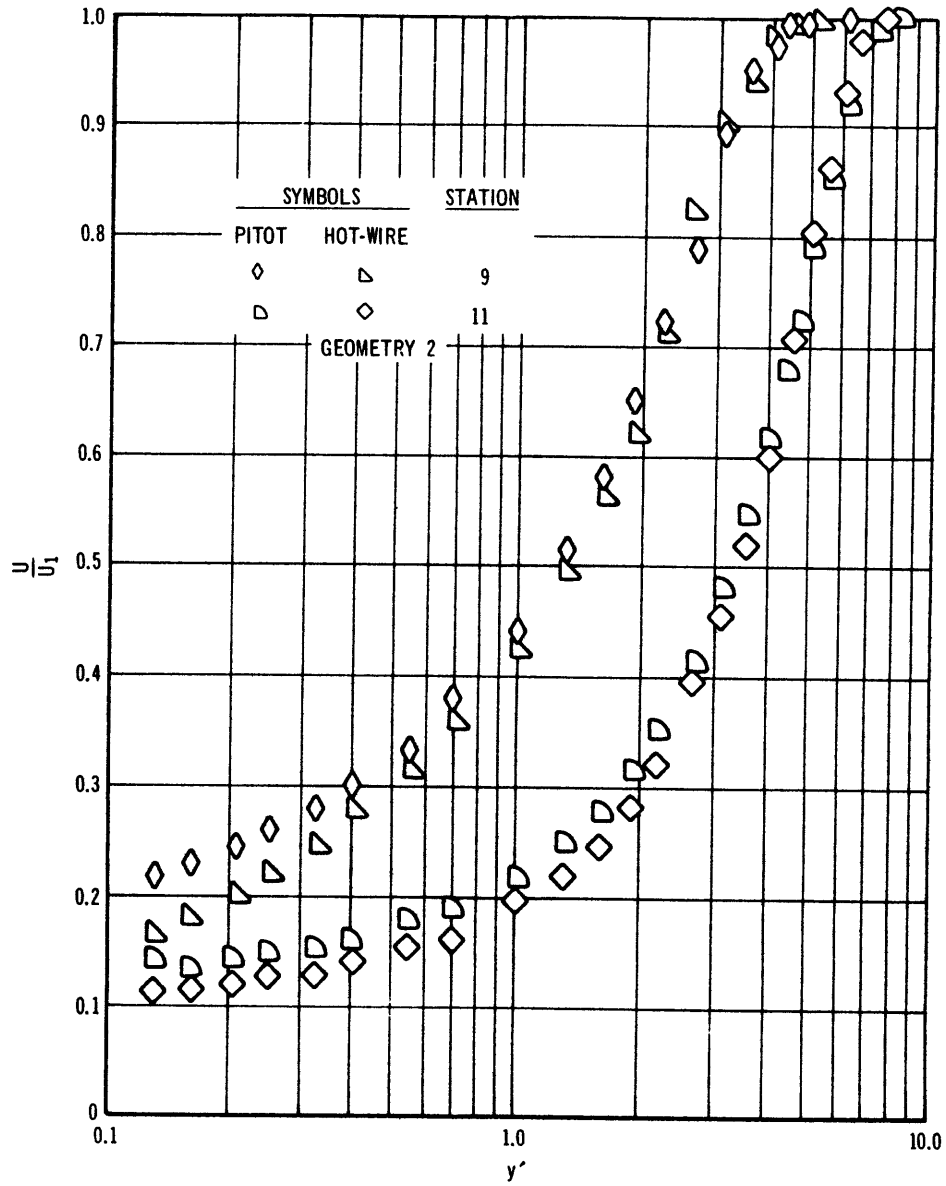


FIGURE 10—Comparison of Hot Wire and Pitot Tube Mean Velocity Profiles

4. INSTRUMENTATION ERRORS AND CORRECTIONS

4.1 INTRODUCTION

At a very early stage in these experiments it became apparent that instrument errors in high level turbulence must be dealt with. As the work progressed and approximate values became available, it was realized that the turbulence levels were higher than had been originally anticipated. The question was raised at one point about the validity of the measured values in such flow fields and whether any of the corrected results could be used.

In order to evaluate the appropriate corrections, some idea of the steps involved is a necessary preliminary. Fortunately, all runs were made with both a hot wire probe and with a small pitot tube having separate impact and static elements so that mean velocity corrections might be checked. The hot wire anemometer was of the constant temperature type and was carefully linearized for all runs. Also, since a low turbulence free-stream core existed outside of the boundary layer near the center of the test section, it was possible to maintain a constant check on the mean velocity reference level of the hot wire.

The primary quantities being measured were the mean velocity, U , and the longitudinal turbulence intensity, u' . Since both the normal, v' , and lateral, w' ,

turbulence intensities enter into the corrections to varying degrees, it has been necessary to estimate these from the work of others. So that it will be clear how the latter information is obtained, the discussion of these estimates will be given first.

The arrangement of articles in this chapter will then be as follows:

4.2 Estimation of values of v' and w' from existing data.

4.3 Basic errors in mean velocity and longitudinal turbulence measurements due to instantaneous velocity reversal at high turbulence levels using a linearized constant temperature hot-wire anemometer.

4.4 Estimate of the displacement of mean velocity U as the turbulence level u' approaches measured U in size.

4.5 Estimate of distortion of u' as u' approaches U in size.

4.6 Combined correction factors for u'/U and U/U_1 based on the preceding analyses.

4.7 Analysis of the static probe in a turbulent field.

4.8 Analysis of the impact tube in a turbulent field including Reynolds number and wall effects.

4.9 Corrections of the mean velocity values obtained with a pitot tube in high level turbulence.

4.10 Comparison of corrected values of mean velocity for the hot-wire and pitot probes.

4.2 ESTIMATES OF v' AND w'

In this series of tests, no attempt has been made so far to measure either v' or w' in the presence of the rough wall. It was known from the beginning of this program that respectable estimates of v'/U_1 and w'/U_1 would be needed in order to correct data from both the hot wire and the pitot tube. However, it is apparent from the analysis by Parthasarathy and Tritton³⁵ that errors of a very high order of magnitude are to be anticipated in such measurements. Even measurements which have been made in a strongly adverse pressure gradient near a smooth wall in this test series have proved to be very unsatisfactory.

An alternate approach has been used. Published data taken under a wide variety of conditions have been compared. These have been reduced to non-dimensional form, v'/u' and w'/u' , so that they may be multiplied by measured values of u'/U_1 in order to be applied to the rough-wall test data. At best, these are crude estimates, since careful study reveals unresolved inconsistencies in much of the data. This is particularly noticeable where the boundary layer is carried to separation as in the Schubauer and Klebanoff¹⁴

and Newman²⁴ experiments. The results from the former were expressed in terms of $(v'/u')^2$ and $(w'/u')^2$ versus y/δ , then averaged for the stations within the adverse pressure field upstream from separation. The justification for this is largely intuitive and based upon careful study of plots of the test data. Adjacent stations exhibited a high degree of random scatter about the calculated mean lines for the whole set of stations. The Newman data were rejected since they exhibited a consistent error in the form of negative values of $(v'/u')^2$ near the wall.

Figures 11 and 12 show plots of $(v'/u')^2$ versus η and $(w'/u')^2$ versus η , $\eta = y/\delta$, y/a , or y/b

where δ = boundary layer thickness

a = pipe radius

b = half width in a two-dimensional conduit

estimated from the following wide range of published test results:

1. Smooth wall, constant pressure, boundary layer; Klebanoff³¹, NBS.
2. Smooth wall, adverse pressure, boundary layer; Schubauer and Klebanoff¹⁴, NBS.
3. Moderately rough wall, constant pressure, boundary layer; Corrsin and Kistler¹⁰, JHU.
4. Smooth circular pipe, $R = 5 \times 10^5$; Laufer³⁶, CIT.

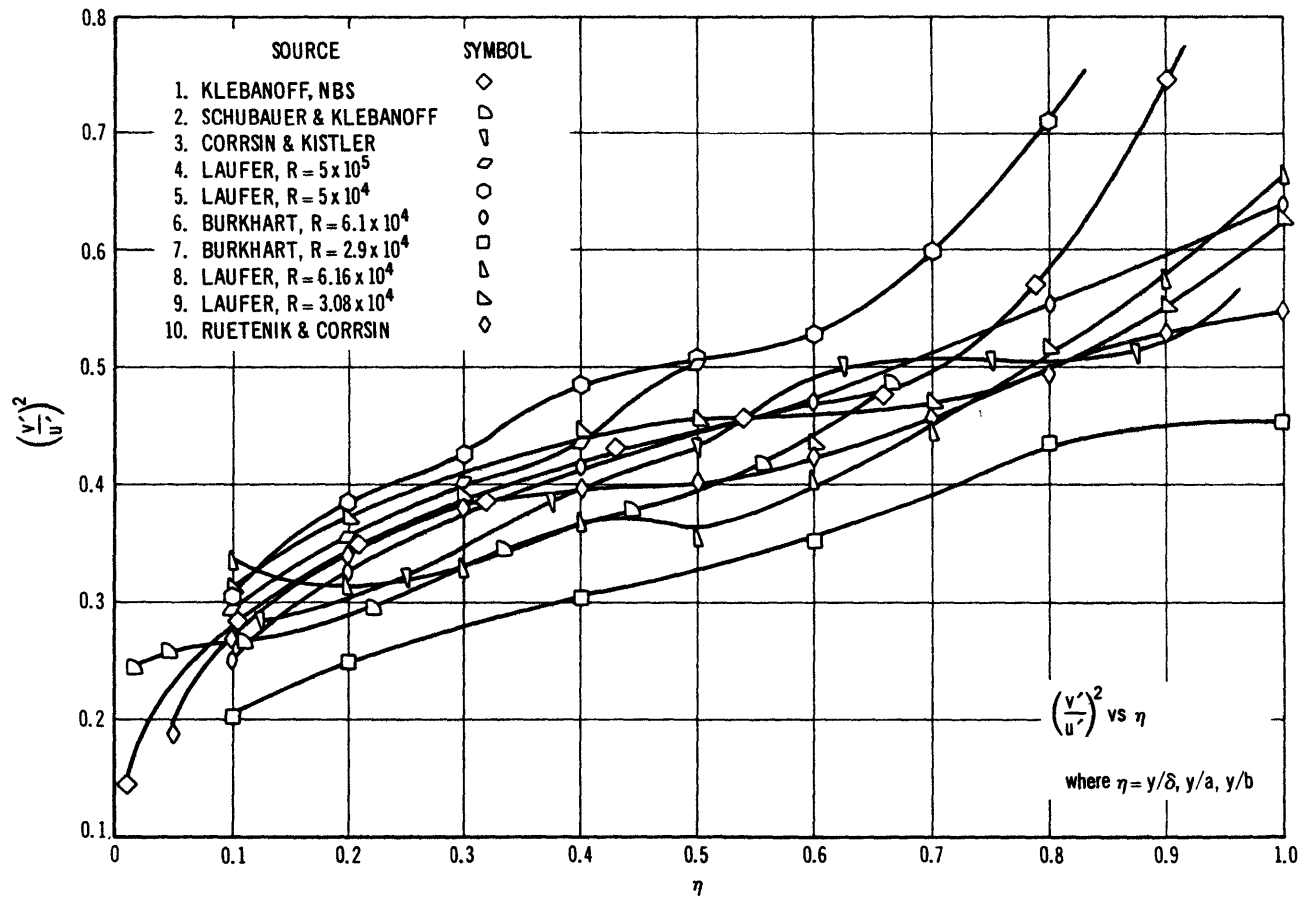


FIGURE 11—Comparison of Normal Turbulence Intensities

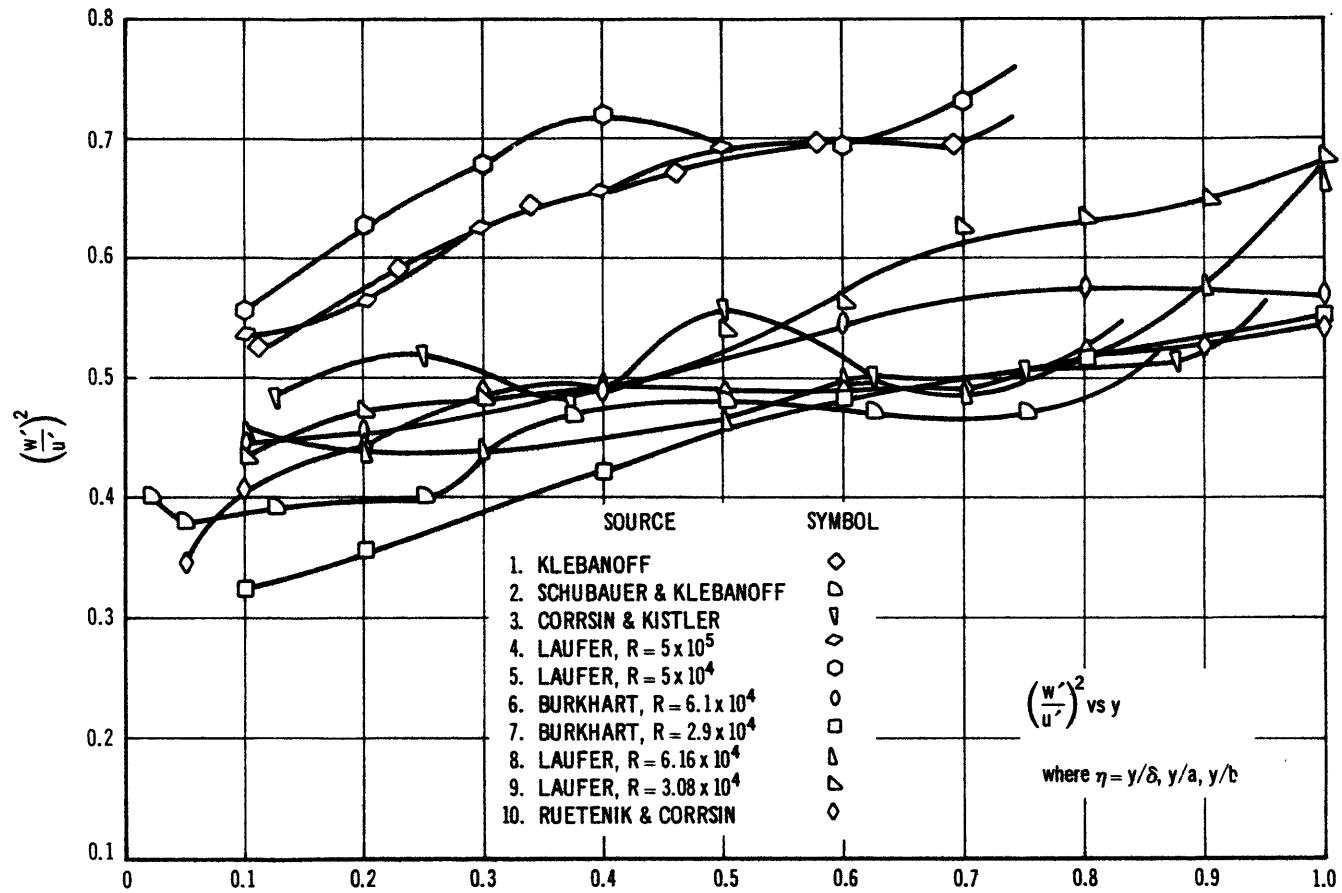


FIGURE 12—Comparison of Lateral Turbulence Intensities

5. Smooth Circular pipe, $R = 5 \times 10^4$; Laufer³⁶, CIT.
6. Rough circular pipe, $R = 6.1 \times 10^4$; Burkhardt³⁸,
Illinois.
7. Rough circular pipe, $R = 2.9 \times 10^4$; Burkhardt³⁸,
Illinois.
8. Smooth parallel plate flow, $R = 6.16 \times 10^4$;
Laufer³⁷, CIT.
9. Smooth parallel plate flow, $R = 3.08 \times 10^4$;
Laufer³⁷, CIT.
10. Smooth, two-dimensional diffuser, 2° included
angle; Ruetenik and Corrsin¹⁷, JHU.

In spite of the rather crude approach, Figure 11 appears to this writer to be singularly revealing. In the range of $\eta = 0.1$ to 0.7 it appears reasonable to represent $(v'/u')^2$ by a single straight line of constant slope. The portion of this line between $\eta = 0.7$ and $\eta = 1.0$ seems to be dependent on the form of outer limit imposed on the boundary layer. If a free stream exists, there is considerable evidence that u' , v' and w' approach a common limit as the intermittency goes to zero, so that $(v'/u')^2$ and $(w'/u')^2$ may be expected to approach unity. In the absence of a free stream, the limiting value of $(v'/u')^2$ at $\eta = 1.0$ is usually below unity. For the smooth wall case in the immediate vicinity of the wall, the

local boundary conditions and the continuity equation may be applied (see Reference 6, Article 11.2 and Reference 36, Figure 25) to show that v' varies about as y^2 while u' varies directly with y . Thus v'/u' should approach zero at the wall.

The physical pictures in two-dimensional flows of the types considered here imply the existence of vortices which provide strong mixing and momentum transport in the x - y plane so that any change in u' with x will produce a corresponding reaction in v' with x . Such variation should not appear in parallel equilibrium flows, rough or smooth, but only in boundary layer or diffuser flows where it is possible to manipulate both roughness and pressure gradient so that the u' distribution will change along the flow path.

Figure 12 does not present a clear-cut picture. On the one hand it would appear that either wall roughness or adverse pressure gradient serves to depress the values of $(w'/u')^2$ as indicated by comparison of curves 1, 2, and 3. On the other hand, there seems to be no obvious reason why the rough and smooth pipes should differ so sharply from each other. Particularly, since it has been claimed³⁸ that u' , v' , and w' depend only on U_τ and y/a for the equilibrium pipe flow case.

Batchelor³⁹ (Article 4.3) has considered the case of a wind-tunnel contraction in which pure stretching exists along the line of symmetry. The turbulence is assumed to be initially homogeneous and isotropic. This leads to the conclusion that $(v'/u')^2$ and $(w'/u')^2$ will increase rapidly, varying almost as c^3 for large values of c , where c is the contraction ratio of the wind-tunnel. For values of c close to unity, however, the change in $(v'/u')^2$ and $(w'/u')^2$ is quite small and may well be masked by experimental error in the measurement of v' and w' . In a similar fashion one may conclude that for an ideal divergence $(v'/u')^2$ and $(w'/u')^2$ will decrease as a result of compressive strain in the mean flow direction. Unfortunately the free-stream mean velocity ratios which have produced separation have been close to unity (about 0.7) and the scatter of experimental points is extremely large. One may also comment that neither the strain nor the vorticity are well-behaved as they might be in a homogeneous, isotropic medium.

Since our basic concern is the establishment of a proper level of transverse turbulence, the Schubauer and Klebanoff¹⁴ mean values have been used for all test stations. Figure 13 shows the values which were assumed in order to estimate the necessary corrections for both pitot tube and

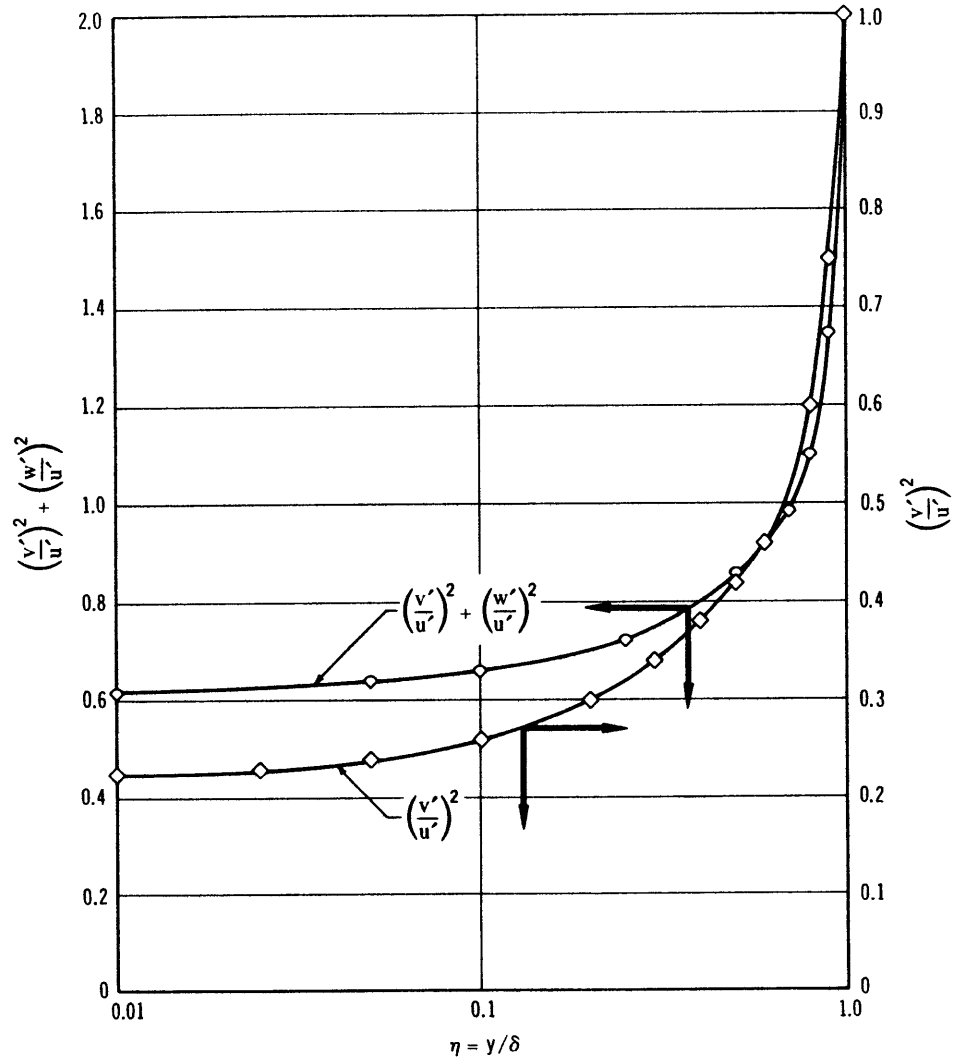


FIGURE 13—Working Values of $(\frac{v'}{u})^2$ and $(\frac{v'}{u})^2 + (\frac{w'}{u})^2$ To Be Used for Corrections

hot-wire anemometer. In view of the data which are presented in Figures 11 and 12, it seemed appropriate to use the lines shown. However, it is obvious that somewhat different values could have been chosen. Since the wall roughnesses project well beyond the viscous layer, the lines representing $(v'/u')^2$ and $(w'/u')^2$ have been extended to the wall.

4.3 TURBULENCE CORRECTIONS FOR THE HOT-WIRE

If a hot-wire probe in a boundary layer is oriented parallel to the wall, the wire will sense both longitudinal and normal fluctuations which are normal to the wire axis, but will exclude the lateral fluctuations which move parallel to its axis. The velocity picked up by the wire will be:

$$U_s = \sqrt{(U + u)^2 + v^2} \quad (11)$$

However, according to King's relationship for an electrically heated wire which is being cooled by the flow of air,

$$\frac{I^2 R_w}{R_w - R_g} = A + B \sqrt{U_s} \quad (12)$$

where I = electric heating current

R_w = electric resistance of heated wire

R_g = electric resistance of wire at air temperature

A, B are constants

U_s = sensed instantaneous velocity

we must deal with $\sqrt{U_s}$ in order to establish the influence of u' and v' on the measured value of the mean velocity. Starting from $\sqrt{U_s} = [(U + u)^2 + v^2]^{\frac{1}{2}}$ and expanding in series, we obtain:

$$\sqrt{U_s} = \sqrt{U} \left[1 + \frac{u}{2U} - \frac{1}{8} \frac{u^2}{U^2} + \frac{1}{4} \frac{v^2}{U^2} + \frac{1}{16} \frac{u^3}{U^3} - \frac{3}{8} \frac{uv^2}{U^3} + \dots \right] \quad (13)$$

The time average becomes:

$$\overline{\sqrt{U_s}} = \sqrt{U} \left[1 - \frac{1}{8} \frac{\overline{u^2}}{U^2} + \frac{1}{4} \frac{\overline{v^2}}{U^2} + \frac{1}{8} \frac{\overline{u^3}}{U^3} - \frac{3}{8} \frac{\overline{uv^2}}{U^3} + \dots \right] \quad (14)$$

and

$$\overline{U_s} = U \left(1 - \frac{1}{4} \frac{\overline{u^2}}{U^2} + \frac{1}{2} \frac{\overline{v^2}}{U^2} + \dots \right) \quad (15)$$

$$\overline{U_s} \approx U \left(1 - \frac{1}{4} \frac{\overline{u^2}}{U^2} + \frac{1}{2} \frac{\overline{v^2}}{U^2} \right) \text{ as originally} \quad (16)$$

obtained by Corrsin⁴⁰.

To appreciate the effect of this equation on the output of the amplifier, it is necessary to look at the arrangement of the circuit itself. This consists of the hot wire as an arm of an electrical bridge to which is applied a feedback amplifier which attempts to keep the resistance and temperature constant in the wire. The feedback circuit is thus continuously monitoring the fluctuations appearing at the hot wire and will include the v/U terms in its variations. Since the measuring circuit is observing the behavior of the

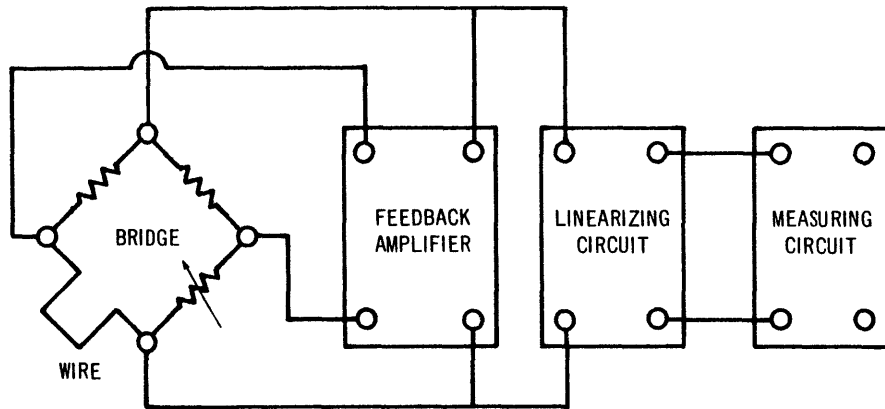


FIGURE 14—Constant Temperature Hot-Wire System

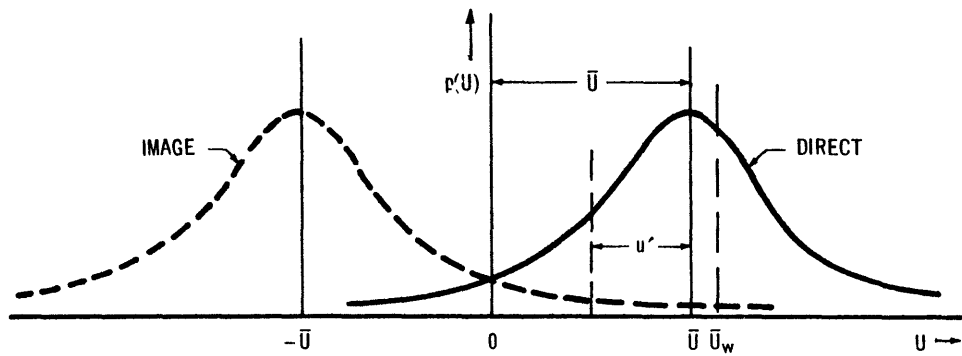


FIGURE 15—Normally Distributed Velocity Where $u' \rightarrow U$

feedback amplifier, it will read high by $\frac{1}{2} \overline{v^2}/U^2$ in its indication of U .

$$\text{Thus } U_w = U \left(1 + \frac{1}{2} \frac{\overline{v^2}}{U^2} \right), \text{ as a first approximation. (17)}$$

This agrees with equation 14 of the paper by W. Rose^{41*}.

In a similar fashion, Hinze⁴² (page 97-100), Parthasarathy and Tritton³⁵, and Rose^{41*} develop expressions for the longitudinal intensity,

$$\overline{u_w^2} = \overline{u^2} \left[1 + \frac{\overline{uv^2}}{Uu^2} + \frac{1}{4} \frac{\overline{v^4}}{U^2 \overline{u^2}} - \frac{1}{4} \frac{(\overline{v^2})^2}{U^2 \overline{u^2}} - \frac{\overline{u^2 v^2}}{U^2 \overline{u^2}} + \dots \right] \quad (18)$$

which consists only of higher order terms for which values are extremely small or not readily estimated in shear flows. For ideal isotropic flows, the corrections are small and occur in the second order terms. In the boundary layer case, the size of the first order term is unknown, while the second order terms tend to be smaller than those for the isotropic case. As an essential starting point, it was decided that this particular correction would be neglected.

4.4 ERROR IN MEAN VELOCITY MEASUREMENT DUE TO VELOCITY

REVERSALS

When turbulence levels exceed about one-third of the mean velocity, the inability of the hot-wire to distinguish

* As corrected by author.

between forward and backward air movement introduces an additional source of error in the readings supplied by the anemometer. Both mean velocities and root-mean square turbulence levels are affected by this source of error and must therefore be corrected. Ideally one should build a type of hot-wire which possesses the directional sensitivity to permit measurement of turbulence levels even at zero mean velocity. However, this approach will not serve to correct readings which have already been taken.

An approximate correction may be devised by assuming that the turbulence levels correspond to a normal Gaussian distribution. Using this assumption we may first attack the mean velocity, then the rms. turbulence level. Schematically we may show the distribution in two pieces; a direct, but clipped portion, and a reflection or image as shown in the sketch. Both direct and reflected curves are integrated from 0 to ∞ . The total area will continue to equal unity if the direct and image portions are added, so that the mean as read will be:

$$\bar{U}_w = \int_{U=0}^{U=+\infty} \frac{U}{\sqrt{2\pi} u'} e^{-\frac{(U - \bar{U})^2}{2u'^2}} dU + \int_0^{+\infty} \frac{U}{\sqrt{2\pi} u'} e^{-\frac{(U + \bar{U})^2}{2u'^2}} dU \quad (19)$$

if we let $y = U - \bar{U}$ and $z = U + \bar{U}$

and $x = y/\sqrt{2}u'$ or $z/\sqrt{2}u'$

this reduces to:

$$\bar{U}_w = \sqrt{\frac{2}{\pi}} u' \left[\int_{-\eta}^{+\infty} x e^{-x^2} dx + \int_{+\eta}^{+\infty} x e^{-x^2} dx \right] + \frac{U}{2} \frac{2}{\sqrt{\pi}} \int_{-\eta}^{+\eta} e^{-x^2} dx \quad (20)$$

$$\text{where} \quad \eta = \frac{U}{\sqrt{2}u'} \quad (21)$$

This may be solved directly to yield:

$$\bar{U}_w = \bar{U} \left(\frac{e^{-\eta^2}}{\sqrt{\pi}\eta} + \text{erf}(\eta) \right) = f_1(\eta) \quad (22)$$

$$\text{where} \quad \text{erf}(\eta) = \frac{2}{\sqrt{\pi}} \int_0^{\eta} e^{-x^2} dx \quad (23)$$

This is the same solution that Siao⁴³ obtained.

The foregoing analysis has assumed that the hot-wire remains normal to the mean velocity for all levels of u' . It would appear that the wire must be experiencing an average yawed flow having a component along the wire of order w' . Reference 41, Equations (10) and (11), and Reference 42, Equation 2-49, indicate that the effect of w' is small compared to either the influence of velocity reversal or that due to v' .

The indicated mean velocity, U_w , is thus subject to two principal corrections; the first due to the normal turbulence component v' and the second due to flow reversal. A more exact analysis would have treated both of these effects together. They are combined for computation in section 4-6.

4.5 ERROR IN TURBULENCE INTENSITY MEASUREMENT DUE TO VELOCITY REVERSALS

Precise corrections of measured values of u' appear to be quite difficult to evaluate since these should include terms involving v and w as well as the effect of instantaneous velocity reversal. v enters as a triple correlation, $\overline{uv^2}/U_1^3$, according to Equation 16 of Reference 41. Values of this triple correlation are not available for boundary layer flows. For wake flows Hinze⁴², article 6-6, shows such triple correlations to be at least an order of magnitude below $\overline{v^2}/U_1^2$ and since they go to zero in isotropic flows, it seems reasonable to believe they are very small in the present case. The order of magnitude of the w' terms is believed to be very small based upon the analysis for the single hot-wire given by Rose⁴¹. Since the only logical starting point for the turbulence corrections is a turbulence intensity u'/U or u'/U_1 , corrections to u' other than the one for velocity reversal have been omitted.

In an ideal sense, one may say that the intensity shown by the hot-wire consists of a portion due to the direct distribution and a portion due to the image. Since we are looking for the root-mean-square of the fluctuating portion

of the velocity, we may usually find this by taking the second moment about the mean. However, noting that the amplifier will yield an average, U_w , that is different from the true mean, it is necessary to take the second moment about the origin. Siao⁴³ has shown that this results in a very simple form. The averaged second moment of the measured velocities will be:

$$\overline{U_w^2} + \overline{u_w^2} = \int_0^{\infty} \frac{U^2 e^{-\frac{(U - \bar{U})^2}{2u^2}}}{\sqrt{2\pi}u} dU + \int_0^{\infty} \frac{U^2 e^{-\frac{(U + \bar{U})^2}{2u^2}}}{\sqrt{2\pi}u} dU \quad (24)$$

A direct evaluation of the right-hand side of this equation reveals that

$$\overline{U_w^2} + \overline{u_w^2} = \overline{U^2} + \overline{u^2} \quad (25)$$

so that

$$\frac{\overline{u_w^2}}{\overline{u^2}} = 1 + \frac{\overline{U^2}}{\overline{u^2}} \left(1 - \frac{\overline{U_w^2}}{\overline{U^2}}\right) \quad (26)$$

$$= 1 + 2\pi^2 [1 - (f_1(\eta))^2] \quad (27)$$

or

$$u_w'/u' = \sqrt{1 - 2\pi^2 [(f_1(\eta))^2 - 1]} = f_2(\eta) \quad (28)$$

where

$$\eta = \frac{U}{\sqrt{2}u'} = \frac{U}{\sqrt{2}u^2} \quad (21)$$

The lack of directional sensitivity on the part of the hot-wire thus tends to reduce the indicated turbulence intensity. If the intensity is non-dimensionalized by means of the free-stream velocity, U_1 , then $f_2(\eta)$ is the only

correcting factor needed since the anemometer is calibrated at U_1 which is at low-turbulence levels in these tests. These corrections are discussed more fully in the next section.

4.6 HOT-WIRE CORRECTIONS

As is often the case with data corrections, it turns out that the correct solution is needed in order to evaluate the correcting factors. The key relationships are functions of η , where $\eta = U/\sqrt{2u'}$, so that we need the true value of u'/U to obtain values of $f_1(\eta)$ and $f_2(\eta)$. Obviously, we may assume an appropriate range of values of η and by means of tables or graphs obtain solutions.

Initially we have two equations which are the results of the three preceding articles. For the mean velocity:

$$\frac{U}{U_w} = \frac{\left[1 - \frac{1}{2} \frac{\overline{v'^2}}{u'^2} + \dots\right]}{[\text{erf}(\eta) + e^{-\eta^2}/\sqrt{\pi}\eta]} = \frac{f_3(\eta, v'/u')}{f_1(\eta)} \quad (29)$$

$$= \left[1 - \eta^2 \left(\frac{1}{2} v'/u'\right)^2\right] / f_1(\eta) \quad (30)$$

and for the intensity:

$$\frac{u'}{u'_w} = \frac{1}{\sqrt{1 - 2\eta^2 [f_1(\eta)]^2 - 1}} = \frac{1}{f_2(\eta)} \quad (31)$$

combining Equations 30 and 31, we get:

$$\left(\frac{u'}{U}\right) \frac{f_3(\eta, v'/u')}{f_1(\eta)} = \left(\frac{u'}{U}\right)_w \quad (32)$$

This has been plotted in Figures 16a and 16b. Figure 16a is a direct plot for values of u'/U above 0.35. Figure 16b employs a more sensitive scale in the form $(u'/U) - (u'/U)_w$ for the lower range of values of u'/U . From these curves the corrected values of u'/U may be obtained by inserting the indicated values shown by the hot-wire anemometer.

Once the corrected value of u'/U is known, it is possible to obtain corrected values of U/U_1 from equation 30.

$$\frac{U}{U_w} = \frac{U}{U_1} \frac{U_1}{U_w} = \frac{f_3(\eta, v'/u')}{f_1(\eta)} \quad (33)$$

$$\text{or} \quad \frac{U}{U_1} = \left(\frac{U_w}{U_1}\right) \frac{f_3(\eta, v'/u')}{f_1(\eta)} = \left(\frac{U_w}{U_1}\right) F_h(\eta, v'/u') \quad (34)$$

$F_h(\eta, v'/u')$ versus u'/U is plotted in Figure 17.

It should be noted here that U_1 , the free-stream velocity exists in a low-turbulence region and was used as a reference calibration value at each test station. U_1 is therefore presumably free from error, at least, free of those errors which have just been discussed, and may be moved into and out of equations as a true constant.

The ratio u'/U_1 involves only the single correction factor $f_2(\eta)$ to modify u_w'/U_1 , but the local intensity ratio u'/U is of more significance in evaluating the corrections for mean velocity.

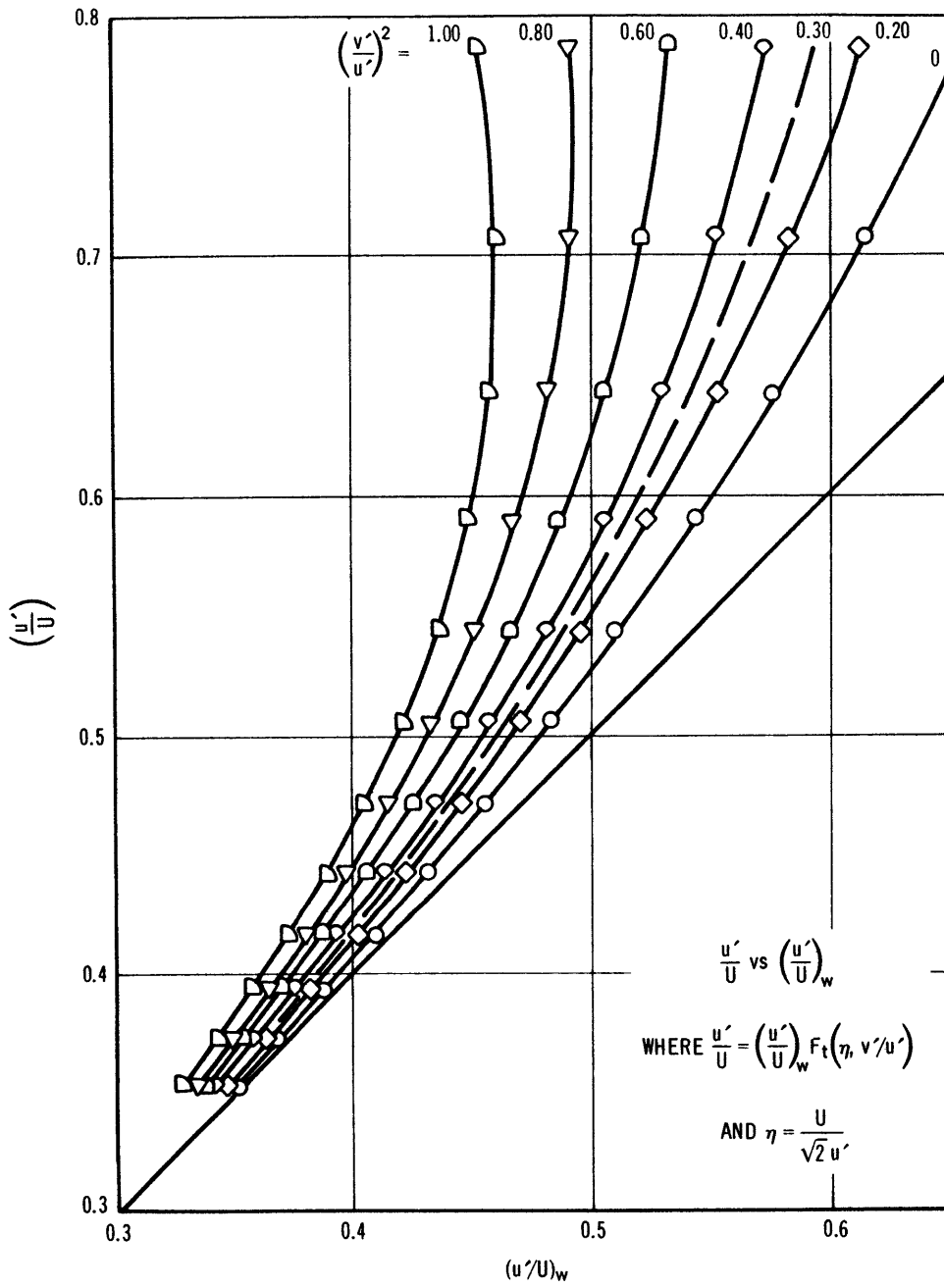


FIGURE 16a

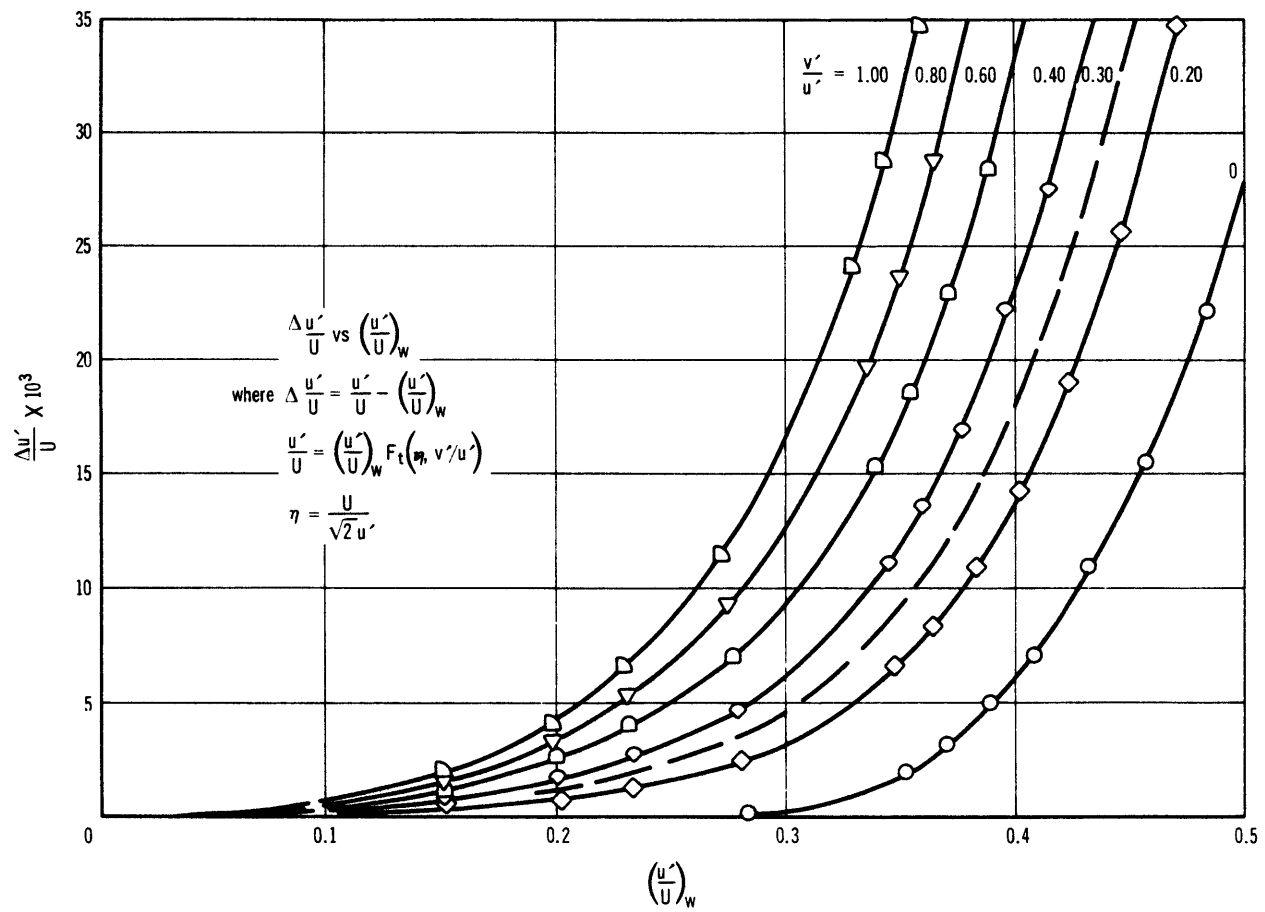


FIGURE 16b

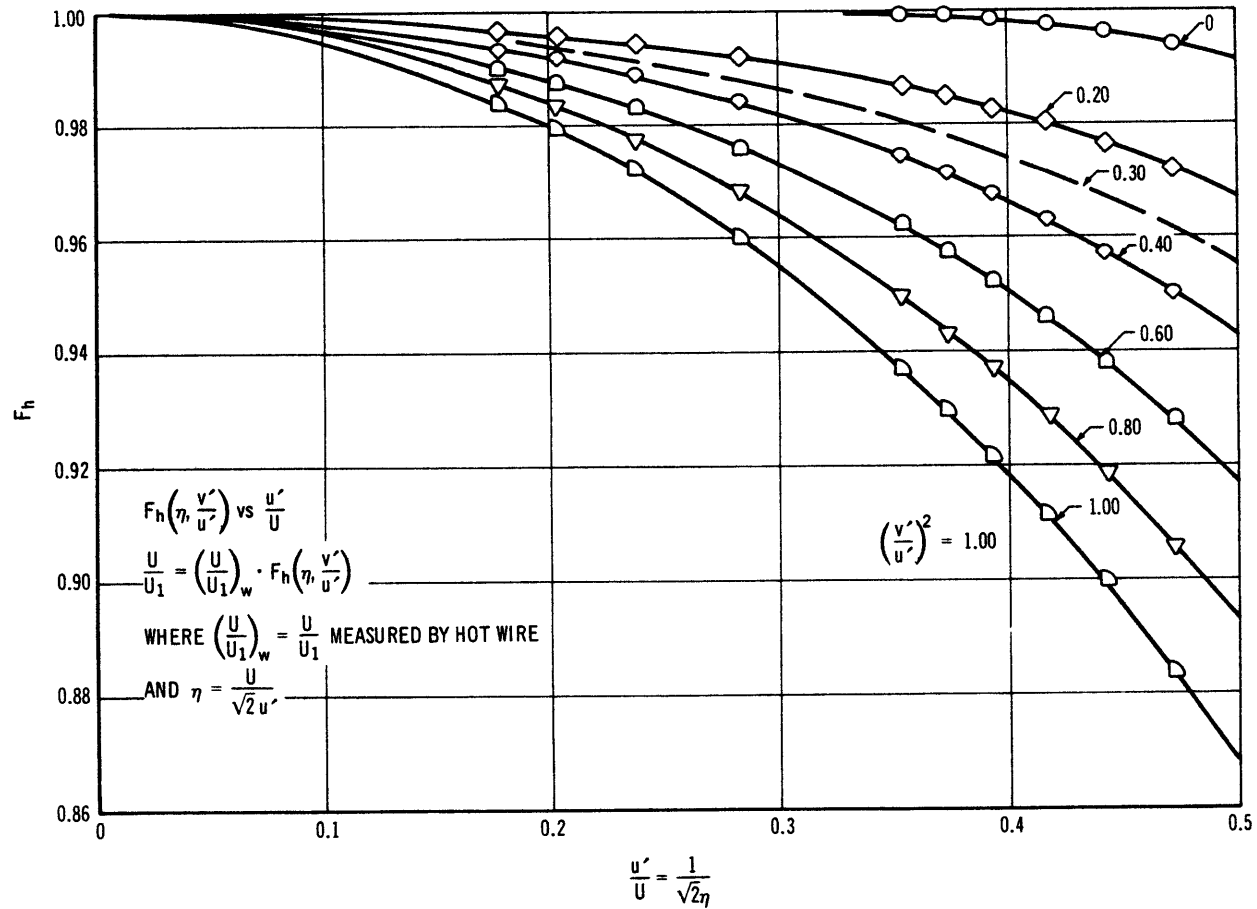


FIGURE 17

4.7 MEASUREMENT OF STATIC PRESSURE IN HIGH LEVEL TURBULENCE

At this point, we are concerned with the behavior of static probes, whether in combination with an impact tube or separated from such a tube, of cylindrical form having an hemispherical nose or leading edge cap with the axis of the cylinder aimed in the same direction as the mean velocity. Customarily, such probes have either an annular slot or a number of holes set normal to the axis of the cylinder some 5 to 15 diameters back from the leading edge. The slot or holes are then connected internally to the pressure sensing element. Recent tests by Strasberg⁴⁴ have shown that the probe having 4 holes set at 90° spacing in a plane perpendicular to the axis gives essentially the same readings as the annular slot. The 4 hole probe described earlier in Chapter 3 was used for all data reported here. The comments which follow are applicable to either type.

The first significant work which connects turbulence to static and impact tube measurements is that done by Goldstein⁴⁵ and Fage⁴⁶. They concluded that the longitudinal turbulent intensity, u' , would not affect static tube readings, but that some fraction of the normal components, v' and w' would enter the picture. The Goldstein equation is:

$$\overline{p_m} = \overline{p} + c\rho\overline{v^2} \quad (35)$$

where $c = \text{constant}$, $0 < c < \frac{1}{3}$

and $\underline{v} = \text{normal fluctuating vector of velocity}$.

The question of effective eddy size is not discussed.

A more recent paper by Toomre⁴⁷ considers the whole question of scale and type of flow in great detail. His first case is that of a static tube which is large compared to a characteristic eddy size so that the pressure fluctuations at the pressure taps would be uncorrelated. His analysis for this condition yields:

$$\overline{p_m} = \overline{p} + \frac{1}{2} \rho\overline{v^2}$$

for isotropic turbulence.

His second case is of more general significance since he first assumes that the static tube is small compared to the typical eddy size, a condition which fits a large number of experiments, including those performed by Fage⁴⁶.

Toomre's basic assumptions are that the eddies are extremely large so that the cylinder is subjected to cross flows and a uniform shear stress exists in the neighborhood of the cylinder. For a tube radius smaller than 1/10 of the typical eddy, the measured pressure is depressed as follows:

$$\overline{p_m} \cong \overline{p} - \frac{1}{2} \rho(\overline{v^2} + \overline{w^2}) \quad (36)$$

This is, of course, a reversal of sign from the Fage⁴⁶ analysis. It does more closely represent, however, the concept that the tube is on the average experiencing a yawed flow.

Hinze⁴² (page 134) approaches this more directly for the case of the small static tube on the basis of an average angle of yaw. He concludes that the measured pressure will be:

$$\overline{p}_m = \overline{p} - A \frac{\rho U^2}{2} \left[\frac{\overline{v^2} + \overline{w^2}}{2U^2} + \frac{1}{2} \left(\frac{\overline{v^2} + \overline{w^2}}{2U^2} \right)^2 + \dots \right] \quad (37)$$

and that the measured pressure will be below the true static.

There seems to be no serious disagreement between Hinze and Toomre on the required sign of the correction, but Toomre's value of $A = 2$ would appear to represent an upper limit on Hinze's A equal to or larger than unity.

Strasberg⁴⁴ conducted careful measurements of the fluctuating contribution but did not attempt to evaluate the algebraic sign. On the basis of Fage's experiments, he concluded that the indicated static pressure would be too high. Subsequent discussion with Dr. Strasberg reveals that he now believes the correction should be positive. The values which he obtained in the wake downstream of a cylinder appear to verify equation (36).

4.8 MEASUREMENT OF TOTAL PRESSURE IN HIGH LEVEL TURBULENCE

One may define an impact tube in an ideal sense as a thin-walled right circular cylinder having its axis perfectly lined up with the local mean velocity. Goldstein⁴⁵ proposed that such an ideal tube of small size would measure:

$$\overline{p_t} = \overline{p} + \frac{\rho U^2}{2} \left[1 + \frac{\overline{u^2} + \overline{v^2} + \overline{w^2}}{U^2} \right] \quad (38)$$

in the sense that this will be the impact pressure which results when an infinitesimal particle of fluid is brought completely to rest. Even if the tube is properly aimed along the direction of the mean velocity U , there are many factors which will affect this measurement:

- a. The lateral fluctuations will produce widely differing yawed flows as a function of tube size and geometry. Equation (38) is idealized and usually represents an upper limit on impact pressure in any practical case.
- b. The fluctuations are assumed to be slow enough that a quasi-steady Bernoulli equation can be used⁴⁸. It is obvious that with large fluctuations some form of unsteady Bernoulli equation ought to be applied. However, an unsteady correction has not been attempted in this present work.

c. Corrsin⁴⁸ has also called attention to the need to investigate the coupled system consisting of the unsteady external pitot flow, the internal fluid circuit, and the final manometric device.

d. For $\overline{u^2}/U^2$ greater than about 0.1, there will be instantaneous velocity fluctuations, $(U + u)$, which are reversed in direction. These will reduce the average pressure sensed by the impact tube since there will generally be negative pressures applied with the flow reversal. However, if the distribution of velocity fluctuations is a normal Gaussian one and the negative pressure coefficient is approximately unity, the pressure correction will be affected only slightly by reversal of the velocity direction.

Siao⁴³ has shown that for $u'/U = 0.60$, the correction is about 0.7%.

Assuming quasi-steady flow conditions the real point at issue, as noted by Hinze⁴², is that the influence of the lateral fluctuations is an unknown quantity dependent on impact tube geometry and not readily measurable. He makes the suggestion that a realistic estimate of the effect of the turbulence could be made by assuming a yawed tube at an angle φ such that $\tan \varphi = \sqrt{\overline{v^2} + \overline{w^2}} / (U + u')$. For extremely small v' and w'

$$\overline{p}_t \approx \overline{p} + \frac{\rho U^2}{2} \left[1 + \frac{\overline{u^2}}{U^2} - (B - 2) \left(\frac{\overline{v^2} + \overline{w^2}}{2U^2} \right) \right] \quad (40)$$

He indicates a measured value of B equal to 3 for static tests, presumably at low-turbulence level, on a yawed tube. This value of B does appear to give a reasonable fit to static yaw tests such as those reported in Figure 8 of Davies⁴⁹ for right-cylindrical impact tubes having a ratio of inner to outer diameter equal to 0.60. The suggestion that B may become sufficiently large to require no correction for turbulence effect on the impact tube does not seem plausible to this writer after much checking against experimental data.

4.9 FURTHER COMMENTS ON THE PITOT TUBE

There are additional factors which enter into the corrections for the pitot tube, or the impact and static tubes. These are largely dependent upon the geometries of tube shape, wall proximity, and boundary layer in addition to scale effect represented by a tube Reynolds number. The ideal impact tube has no physical size so that its axial center line matches the position of stagnation pressure. Where the mean velocity is distributed, a tube of finite dimensions will always show a displacement between its axis and the location of the stagnation pressure. Or stated in another fashion, there will always be a displacement

between the location of the indicated mean velocity and the axis of the tube. Static tubes are subject to an additional turbulence intensity correction since the normal turbulence component, v' , affects the local static pressure. The articles which follow will consider the effects which have been listed above.

4.9.1 The Reynolds number effect has been studied with great care by MacMillan⁵⁰, and the following remarks are based on his results. In his Figure 2, he shows that the flow past a sharp-edged right-cylindrical impact tube having a ratio of inner to outer radius equal to 0.60 may be expected to become dynamical and independent of Reynolds number for Reynolds numbers of 125 or greater. Here the Reynolds number is based on free-stream velocity and the external radius of the tube. For values of the Reynolds number below 125, the impact tube will indicate velocities which are too large and these must be corrected to a lower value.

The impact tube used in the present experiments was 0.025 inches O. D. by 0.016 inches I. D. so that $d/D = 0.64$ which is reasonably close to MacMillan's figure of 0.60. The limiting Reynolds number of 125 is reached at about 19 ft/sec. However, at the minimum indicated velocity of about 7 ft/sec recorded in these tests, the correction is

about 0.042 ft/sec or 0.6% downward. There seem to be only a very few test points for which the use of this correction can be justified.

4.9.2 The so-called displacement effect in pitot tubes accounts for the change in flow due to the presence of the tube and for the lack of coincidence of tube axis with the stagnation point. The presence of a wall and shear stress in the boundary layer will also influence the size of this effect.

Several interesting papers have been written on this subject. Among these should be mentioned those by Dhawan and Vasudeva⁵¹, Davies⁴⁹, and MacMillan⁵². MacMillan suggests that the key factors entering this correction are impact tube size, local shear and wall proximity. This may be expressed in a functional form as:

$$\frac{\epsilon}{D} = f_1 \left(\frac{y}{\delta}, \frac{y}{D}, \frac{U_\tau y}{\nu}, \frac{d}{D} \right) \quad \text{or} \quad f_2 \left(\frac{y}{\delta}, \frac{y}{D}, \frac{U_\tau D}{\nu}, \frac{d}{D} \right)$$

where

ϵ = displacement of measured U

D = external diameter of tube

y = distance from wall

δ = boundary layer thickness

U_τ = friction or shear velocity

ν = kinematic viscosity

d = internal diameter of tube.

On the basis of MacMillan's results ϵ/D for these tests will be at most about 0.14 or $\epsilon \cong 0.004$ inches. Since y' , the reference position for the rough wall, has at least a ± 0.005 inch tolerance, a correction for tube position does not appear to be very meaningful.

MacMillan also notes that the effect of wall proximity is felt out to about 2 tube diameters for a smooth wall. The present tests indicate a distortion of measurements consistently on the high side out to about 4 to 5 roughness heights, or 16 to 20 impact tube diameters, which would make one believe that k/D or y/k should be listed among the similarity terms. It is not clear at this time whether the observed distortion of velocity readings is a displacement effect. If it is, then the order of magnitude is vastly greater than anything which has been recorded for the smooth wall case.

Daily and Hardison⁵³ have prepared a review of the literature on impact probes and comment that the displacement, ϵ , runs about $0.18D$ for $0.1 < d/D < 0.5$ but is less for $d/D > 0.5$. This paper contains an extensive bibliography and a great deal of useful commentary on this subject.

4.9.3 The measurement of static pressure and the question of location of the static probe with respect to the

impact probe are intimately tied into the comments in the preceding section. There are three basic ways in which static pressure may be picked up. It may be measured by wall taps, provided the wall is smooth and that the taps are oriented normal to the wall, free of burrs, etc. A combined pitot tube may be used. In which case, the impact and static tubes are taking measurements at essentially the same axial location with respect to the wall. Finally, the impact and static tubes may be separated. They should be some 10 to 12 diameters of the static tube apart in order to avoid interference in the flow. They may be located at the same distance from the wall (in an x-z plane) or the static tube may be as far away as the free stream.

The roughened boundary prescribes certain limitations on the location of the static tube. The individual roughnesses produce local mean velocity variations which in turn produce local static pressure variations near the wall. Wall taps can not be used to give meaningful indications of static pressure. The combined pitot tube reflects this same variation in local static pressure for values of y less than some 4 to 5 times the roughness height. This leaves the separated impact and static tubes as the remaining possibility.

The type of impact-static tube used in these tests has already been described in Chapter 3. The static tube is located about 5 times the screen wire diameter (about 2.5 k) away from the impact tube in the y direction. A more convenient arrangement is that used by Moore⁷ in which a continuous static probe is placed in the free stream. This was contemplated in the present experiments, but rejected because of the relatively large curvatures in the streamlines in the free stream. However, static pressures were continuously monitored in the smooth parallel wall (in the x - y plane) of the wind-tunnel at a position in y beyond the boundary layer on the rough wall.

When the static tube is not in the same location as the impact tube, it is necessary to account for the change in $\overline{v^2}$ in order to compute a true static pressure at the location of the impact tube. A static tap located in a smooth wall or a static probe in a low-turbulence free stream will sense a maximum or limiting value of the static pressure.

In a turbulent boundary layer flow the y -component of the Navier-Stokes equations can be reduced to the form (Reference 6, Article 4)

$$\frac{\partial \overline{uv}}{\partial x} + \frac{\partial \overline{v^2}}{\partial y} = - \frac{1}{\rho} \frac{\partial p}{\partial y}$$

On integration from y to δ , this becomes:

$$\overline{p}_0 = \overline{p} + \rho \overline{v^2} - \rho \int_y^\delta \frac{\partial \overline{uv}}{\partial x} dy$$

where \overline{p}_0 = reference pressure

\overline{p} = local mean pressure

$\sqrt{\overline{v^2}}$ = turbulence intensity normal to wall.

$\rho \frac{\partial \overline{uv}}{\partial x} = - \frac{\partial \tau}{\partial x}$ = gradient of local shear stress in longitudinal direction.

Where a steeply adverse pressure gradient exists, the integral term may be significantly large enough compared to $\overline{\rho v^2}$ to warrant being retained. In the present research, its influence on the static pressure is generally small so the pressure equation may be simplified to the following form:

$$\overline{p}_0 = \overline{p} + \rho \overline{v^2} \quad (42)$$

This equation is in the form shown by Townsend⁵⁴, page 86, and is approximately verified by Newman²⁹.

For an impact tube at position i and a static tube at position s , we may write the following:

$$\overline{p}_i + \rho \overline{v_i^2} = \overline{p}_s + \rho \overline{v_s^2}$$

or $\overline{p}_i = \overline{p}_s + \rho \overline{v_s^2} - \rho \overline{v_i^2}$ (43)

Thus the measured static at point s will be:

$$\bar{p}_m = \bar{p}_s - A \frac{\rho U_s^2}{2} \left[\frac{\overline{v_s^2} + \overline{w_s^2}}{2U_s^2} \right] \quad (44)$$

and at point i :

$$\bar{p}_i = \bar{p}_m + A \frac{\rho U_s^2}{2} \left[\frac{\overline{v_s^2} + \overline{w_s^2}}{2U_s^2} \right] + \frac{\rho U_s^2}{2} \left(2 \frac{\overline{v_s^2}}{U_s^2} \right) - \frac{\rho U_i^2}{2} \left(2 \frac{\overline{v_i^2}}{U_i^2} \right) \quad (45)$$

4.9.4 In the experiments considered here, the impact tube was closer to the wall than the static tube was so that the impact tube would be at position y_i and the static tube at y_s .

The combined equation from parts 4.8 and 4.93 then becomes:

$$\begin{aligned} (\bar{p}_t - \bar{p})_{\text{measured}} &= A \frac{\rho U_s^2}{2} \frac{\overline{v_s^2} + \overline{w_s^2}}{2U_s^2} + \frac{\rho U_s^2}{2} 2 \frac{\overline{v_s^2}}{U_s^2} - \frac{\rho U_i^2}{2} 2 \frac{\overline{v_i^2}}{U_i^2} \\ &+ \frac{\rho U_i^2}{2} \left[1 + \frac{u_i^2}{U_i^2} - (B - 2) \frac{\overline{v_i^2} + \overline{w_i^2}}{2U_i^2} \right] \quad (46) \end{aligned}$$

or

$$\frac{\rho U_i^2}{2} = \frac{(\bar{p}_t - \bar{p})_m}{1 + \frac{u_i^2}{U_i^2} - (B-2) \left(\frac{\overline{v_i^2} + \overline{w_i^2}}{2U_i^2} \right) + A \left(\frac{\overline{v_s^2} + \overline{w_s^2}}{2U_s^2} \right) + 2 \left(\frac{\overline{v_s^2} - \overline{v_i^2}}{U_i^2} \right)} \quad (47)$$

There appear to be two limits on the possible range of values of A and B. These are:

- a. Goldstein - Toomre; $A = 2$, $B = 0$
- b. Hinze: $A = 1$, $B = 3$.

The former will give the largest possible correction and the latter the smallest possible in light of the foregoing discussion.

Equation (47) will then become, letting $U = u_1$;
 $u = u_1$; etc.

$$a. \quad \frac{\rho U^2}{2} = \frac{(\bar{p}_t - \bar{p})_m}{\left[1 + \frac{u^2 + \bar{v}^2 + \bar{w}^2}{U^2} + \frac{\bar{v}_s^2 + \bar{w}_s^2}{U^2} + 2 \frac{\bar{v}_s^2 - \bar{v}^2}{U^2} \right]}$$

and (48)

$$b. \quad \frac{\rho U^2}{2} = \frac{(\bar{p}_t - \bar{p})_m}{\left[1 + \frac{u^2}{U^2} - \frac{1}{2} \left(\frac{\bar{v}^2 + \bar{w}^2}{U^2} \right) + \frac{1}{2} \left(\frac{\bar{v}_s^2 + \bar{w}_s^2}{U^2} \right) + 2 \left(\frac{\bar{v}_s^2 - \bar{v}^2}{U^2} \right) \right]}$$

Since the desired correction is to be used to modify U_m/U_1 to the form U/U_1 and $(\bar{p}_t - \bar{p})_m = \rho U_m^2/2$, the "pitot" function will have the following form:

$$\frac{U}{U_1} = \left(\frac{U_m}{U_1} \right) F_p \quad (49)$$

where

$$F_p = \frac{1}{\sqrt{1 + \left(\frac{U_1}{U} \right)^2 \left[\frac{u^2 + \bar{v}^2 + \bar{w}^2}{U_1^2} + \frac{\bar{v}_s^2 + \bar{w}_s^2}{U_1^2} + 2 \frac{\bar{v}_s^2 - \bar{v}^2}{U_1^2} \right]}}$$

for the Goldstein-Toomre form, and

$$F_p = \frac{1}{\sqrt{1 + \left(\frac{U_1}{U} \right)^2 \left[\frac{u^2}{U_1^2} - \frac{1}{2} \left(\frac{\bar{v}^2 + \bar{w}^2}{U_1^2} \right) + \frac{1}{2} \left(\frac{\bar{v}_s^2 + \bar{w}_s^2}{U_1^2} \right) + 2 \left(\frac{\bar{v}_s^2 - \bar{v}^2}{U_1^2} \right) \right]}} \quad (50)$$

The only practical way to test the validity of these relationships would appear to be by comparison with the hot-wire results.

4.9.5 It should be noted at this point that the long form of these equations is necessary only if the impact and static tubes are separated and if the static tube is immersed in the shear flow. The special case where a combined impact-static type of pitot tube or a free-stream static tube is used greatly simplifies these equations and warrants comment even though neither of these was used in this experiment.

For the pitot tube, $v_s = v$, and $w_s = w$ so that equation (50) can be reduced to:

$$F_p = \frac{1}{\sqrt{1 + \left(\frac{U_1}{U}\right)^2 \left[\frac{u^2 + 2v^2 + 2w^2}{U_1^2} \right]}}$$

for Goldstein-Toomre, and

$$F_p = \frac{1}{\sqrt{1 + \left(\frac{U_1^2}{U^2}\right) \left(\frac{u^2}{U_1^2}\right)}} \quad (51)$$

for the Hinze form.

Where the static tube is immersed in a low-turbulence free stream or is simply a tap in a smooth wall in the boundary layer case, v_s and w_s are essentially zero, so that equations (50) may be expressed as follows:

$$F_p = \frac{1}{\sqrt{1 + \left(\frac{U_1}{U}\right)^2 \left[\frac{u^2 - v^2 + w^2}{U_1^2} \right]}}$$

for the Goldstein-Toomre form, and

$$F_p = \frac{1}{\sqrt{1 + \left(\frac{U_1}{U}\right)^2 \left[\frac{u^2}{U_1^2} - \frac{1}{2} \left(\frac{5v^2 + w^2}{U_1^2} \right) \right]}} \quad (52)$$

for the Hinze case. The latter form can lead to negative values within the brackets or F_p greater than unity even at very high turbulence levels. It is presumably this situation which Hinze⁴² had in mind when making his comments on page 136 regarding negligible corrections at high turbulence levels.

To anticipate the conclusions of article 4.10, it should be noted that equations (50), (51), and (52) represent extreme or limiting forms for the correction factor. Obviously, the proper value may be at either of these extremes or anywhere in between, assuming that the limits have been reasonably set. A compromise form which might be called "Hinze-Toomre" appears to give the best fit when comparing pitot tube data with that obtained using a hot wire. This form will be discussed in the next article and is presented here merely to summarize this commentary on special cases.

For the pitot tube, we let $A = 2$, $B = 3$, $v_s = v$, and $w_s = w$ in equation (47), so that equation (51) becomes:

$$F_p = \frac{1}{\sqrt{1 + \left(\frac{U_1}{U}\right)^2 \left[\frac{u^2}{U_1^2} + \frac{1}{2} \left(\frac{v^2 + w^2}{U_1^2} \right) \right]}} \quad (53)$$

Similarly for the free-stream static tube where $A = 2$, $B = 3$, $v_s = w_s = 0$, we get:

$$F_p = \frac{1}{\sqrt{1 + \left(\frac{U_1}{U}\right)^2 \left[\frac{u^2}{U_1^2} - \frac{1}{2} \left(\frac{5v^2 + w^2}{U_1^2} \right) \right]}} \quad (54)$$

which is identical to the Hinze form of equation (52) since the term involving the factor A will vanish when $v_s = w_s = 0$.

4.10 CONCLUSIONS

It has been noted in the preceding article that a solution for the correction factor, F_p , for the pitot tube mean velocities has been worked out. This lies between the extremes indicated in Equations (50) and also matches corrected mean velocities obtained with the hot-wire. The equation is as follows:

$$F_p = \frac{1}{\sqrt{1 + \left(\frac{U_1}{U}\right)^2 \left[\frac{u^2}{U_1^2} - \frac{1}{2} \left(\frac{v^2 + w^2}{U_1^2} \right) + \left(\frac{v_s^2 + w_s^2}{U_1^2} \right) + 2 \left(\frac{v_s^2 - v^2}{U_1^2} \right) \right]}} \quad (55)$$

The terms in the square brackets may be justified as follows:

- a. The first two terms represent a yawed impact tube having an average angle such that $\tan \varphi = \sqrt{\overline{v^2} + \overline{w^2}} / (U + u')$.
- b. The third term represents the effect of the flow of large eddies about a small static probe.
- c. The fourth term accounts for the reduction in local static pressure resulting from the normal turbulent velocity component.

A careful study of these terms reveals that they are of about the same order of magnitude throughout the boundary layer. The sum of the first three terms is always positive. The fourth term is positive at the wall and reverses sign at some point away from the wall for the case where the static tube is farther out in the boundary layer than the impact tube.

In order to compare the corrected mean velocities obtained by hot-wire and pitot tube data, it is necessary at this point to summarize briefly the steps taken to obtain the corrected values.

- a. Estimates of $(v'/u')^2$ and $(w'/u')^2$ are obtained from Figure 13.
- b. The longitudinal turbulence intensity is next evaluated from Figures 16a or 16b.

c. The mean velocity ratio U/U_1 may then be obtained from Figure 17 for the hot-wire.

d. As a result of the first three steps, it is now possible to tabulate corrected values of U/U_1 , u'/U_1 , and u'/U and estimated values of v'/u' , w'/u' , v'/U_1 , and w'/U_1 as functions of y' at each station. These are needed for the analyses which are given in Chapter 5.

e. The values given in step (d) may now be used to compute F_p in order to correct the pitot tube mean velocities.

Equation 55 assumes that local mean velocities and turbulence intensities are known. While this was the case for data reported here, it is not generally true. Usually, one would seek the value of U/U_1 based on knowledge of U_m/U_1 and measured or estimated values of u'/U_1 , v'/U_1 and w'/U_1 . Equation 55 may be reorganized to use these data in the following form:

$$F_p = \sqrt{1 - \left(\frac{U_1}{U_m}\right)^2 \left[\frac{u'^2}{U_1^2} - \frac{1}{2} \left(\frac{v'^2 + w'^2}{U_1^2} \right) + \left(\frac{v'_s + w'_s}{U_1^2} \right) + 2 \left(\frac{v'_s - v'^2}{U_1^2} \right) \right]} \quad (56)$$

Unfortunately, this equation is no easier to apply than equation 55.

The preceding conclusions are the result of a tedious trial-and-error process so far as verification of the pitot

tube mean velocities are concerned. Solutions which appear reasonable do not necessarily fit the experimental results, and because the experimentally evaluated data are in themselves subject to a variety of error such as amplifier drift and leaky manometer connections, it has been necessary to check and rework the data in order to improve reliability. As a consequence, some data have had to be rejected.

Figures (18) to (22) present the corrected values for mean velocities and longitudinal turbulence intensities. Under the circumstances, it is believed that these represent a best-fit. In any event, they are the result of employing a single consistent set of corrections. Figures 18 and 19 show comparisons of raw and corrected data for stations 9 and 11 of the pressure gradient 2, rough wall test data. The hot-wire mean velocity data have been corrected by the factor F_h given by Equation 33 and the pitot-tube data by F_p as given in Equation 55. These two stations were chosen largely because both hot-wire and pitot-tube readings were believed to be reliable since they had been repeated many times. Stations 9 and 11 also exhibited interesting distributions of u'/U_1 in terms of magnitude and shape. Figures 20 and 21 show the variation in F_h and F_p with distance from the wall. All of the corrected data are summarized in Table 4.1. The mean velocity error appears to

be quite small, having maximum values of the order of 1% of U_1 .

Figure 22 is intended to present an order of magnitude comparison of mean velocity pitot-tube corrections for flow over rough and smooth surfaces. The data shown are for flows having the same pressure distributions. The smooth wall corrections are somewhat greater, or F_p is smaller, for flows which separate. However, the correction for smooth wall flows even at separation is only one-third to one-half that for station 11 in the rough wall case.

TABLE 4.1

Comparison of Hot-Wire and Pitot-Tube CorrectionsStation 9

y'	Corrected		Hot-Wire		Pitot-Tube		$\Delta U/U_1$
	u'/U	F_h	U/U ₁	F_p	U/U ₁	%	
0.130	0.626	0.925	0.151	0.710	0.156	+ 3.3	
0.160	0.573	0.945	0.171	0.750	0.171	0.0	
0.205	0.565	0.948	0.189	0.779	0.190	+ 0.5	
0.250	0.515	0.958	0.212	0.809	0.210	- 0.9	
0.325	0.503	0.960	0.232	0.829	0.232	0.0	
0.400	0.484	0.965	0.262	0.854	0.258	- 1.5	
0.550	0.416	0.976	0.306	0.883	0.295	- 3.6	
0.700	0.366	0.980	0.352	0.906	0.340	- 3.4	
1.000	0.326	0.984	0.416	0.931	0.410	- 1.4	
1.300	0.280	0.987	0.486	0.948	0.488	+ 0.4	
1.600	0.239	0.990	0.556	0.965	0.561	+ 0.9	
1.900	0.208	0.992	0.615	0.977	0.637	+ 3.6	
2.200	0.165	0.994	0.708	0.987	0.708	0.0	
2.650	0.122	0.997	0.821	0.993	0.785	- 4.4	
3.100	0.085	0.998	0.904	0.997	0.892	- 1.3	
3.550	0.052	0.999	0.942	0.999	0.951	+ 1.0	
4.000	0.027	1.000	0.984	1.000	0.984	0.0	

Station 11

0.130	0.386	0.982	0.111	0.792	0.113	+ 1.8
0.160	0.412	0.978	0.114	0.784	0.107	- 6.1
0.205	0.441	0.974	0.117	0.781	0.112	- 4.3
0.250	0.457	0.971	0.123	0.791	0.118	- 4.1
0.325	0.512	0.957	0.122	0.778	0.119	- 2.5
0.400	0.470	0.968	0.136	0.805	0.129	- 5.1
0.550	0.474	0.967	0.150	0.817	0.145	- 3.3
0.700	0.540	0.950	0.154	0.801	0.152	- 1.3
1.000	0.467	0.965	0.190	0.828	0.180	- 5.3
1.300	0.495	0.958	0.209	0.829	0.207	- 1.0
1.600	0.470	0.961	0.236	0.831	0.230	- 2.5
1.900	0.450	0.964	0.272	0.851	0.270	- 0.7
2.200	0.446	0.963	0.308	0.869	0.307	- 0.3
2.650	0.373	0.974	0.384	0.901	0.372	- 3.1
3.100	0.335	0.978	0.448	0.930	0.446	- 0.4
3.550	0.286	0.983	0.512	0.946	0.518	+ 1.2
4.000	0.247	0.987	0.593	0.960	0.594	+ 0.2
4.600	0.195	0.991	0.701	0.979	0.697	- 0.6
5.100	0.149	0.994	0.798	0.988	0.793	- 0.6
5.600	0.121	0.996	0.855	0.995	0.855	0.0

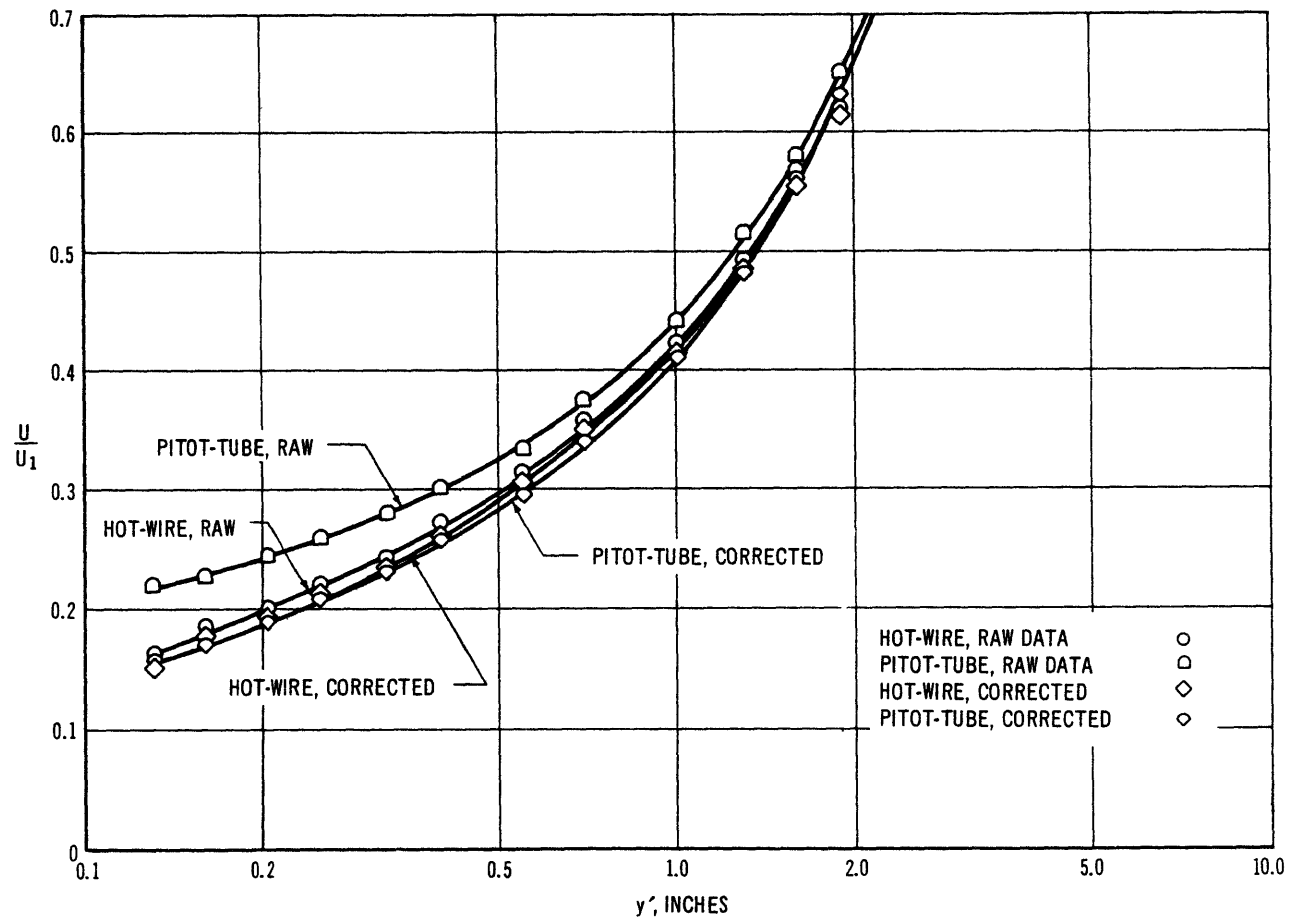


FIGURE 18—Rough Wall, Pressure Gradient 2, Station 9

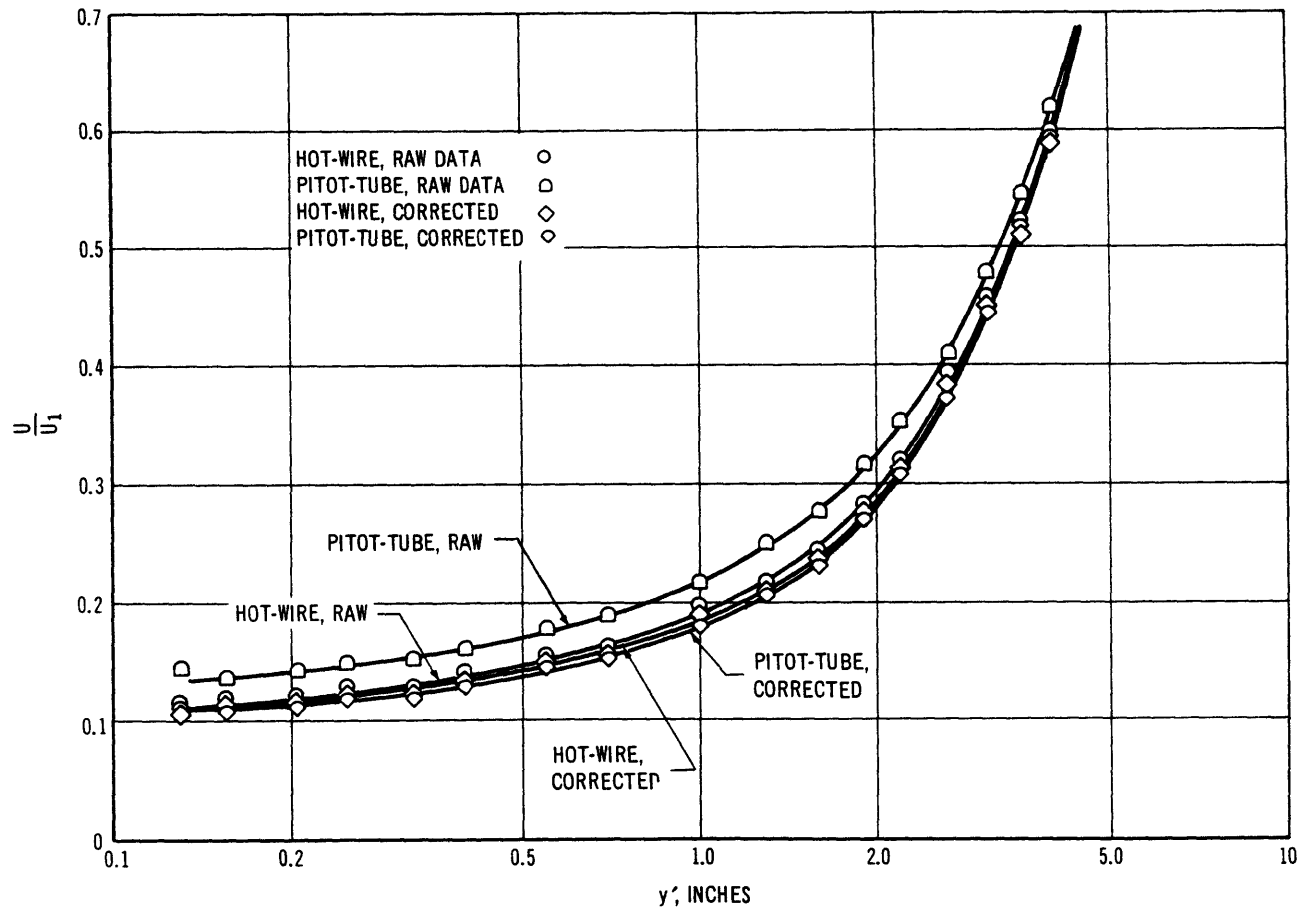


FIGURE 19—Rough Wall, Pressure Gradient 2, Station 11

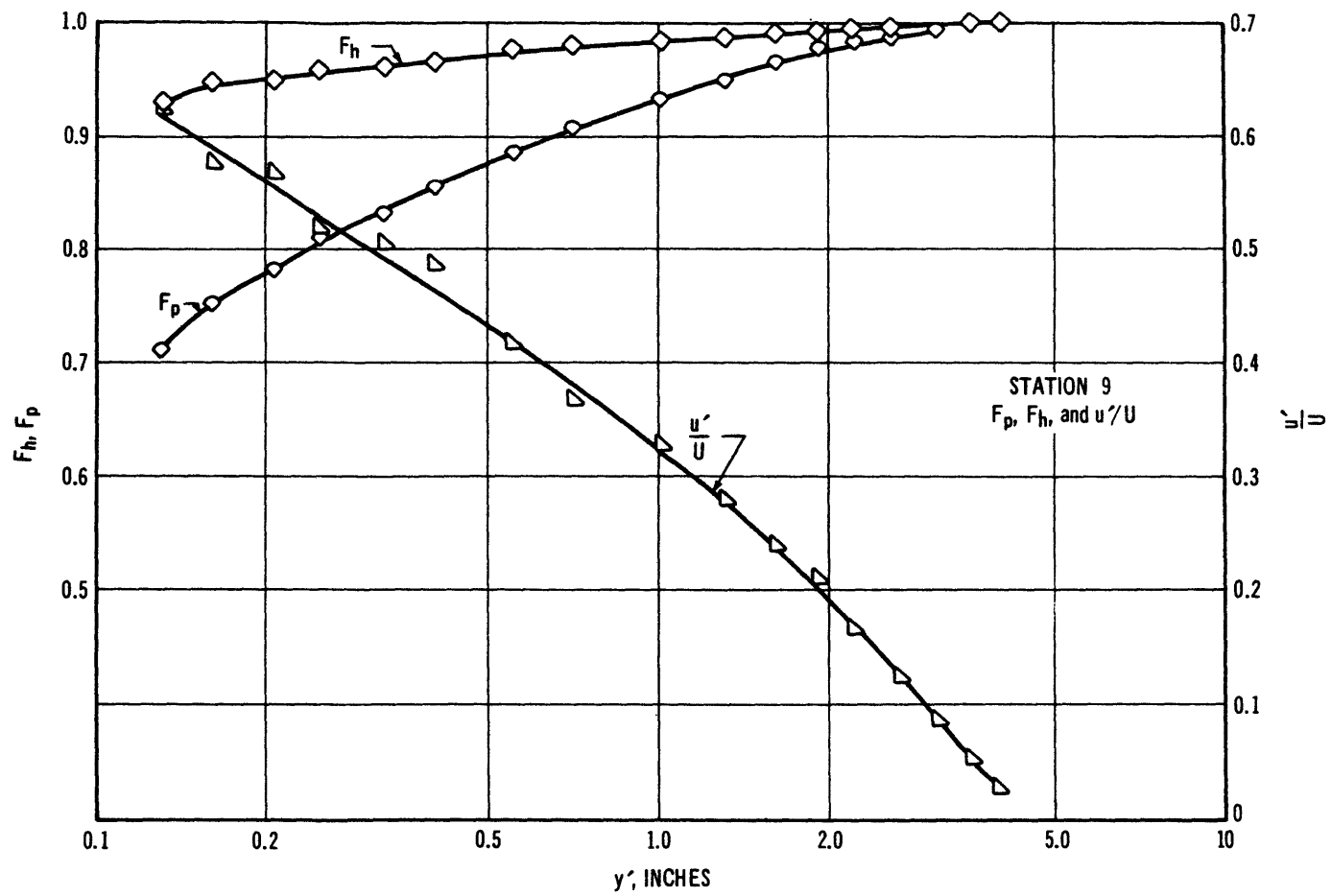


FIGURE 20—Rough Wall, Pressure Gradient 2

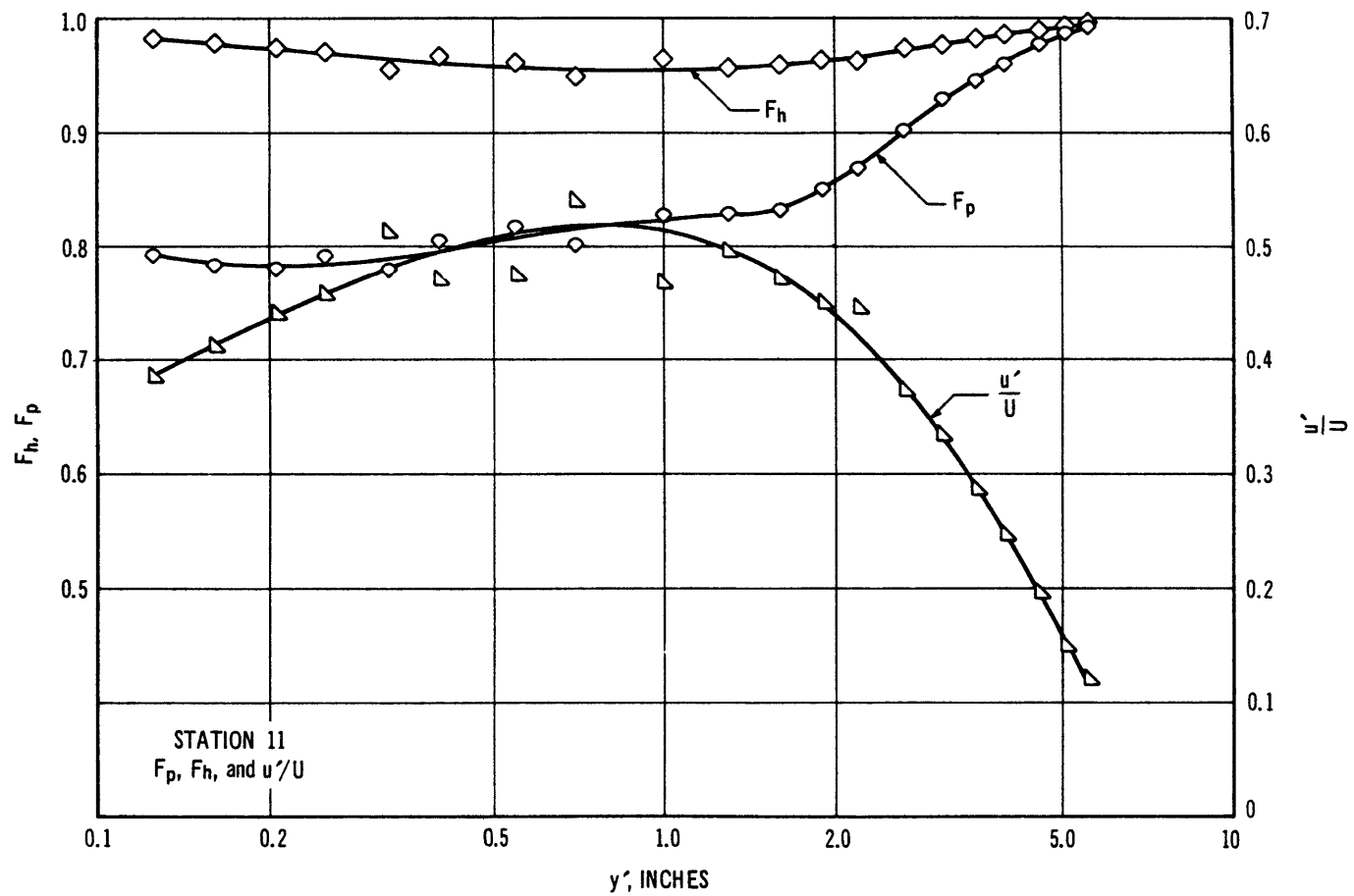


FIGURE 21—Rough Wall, Pressure Gradient 2

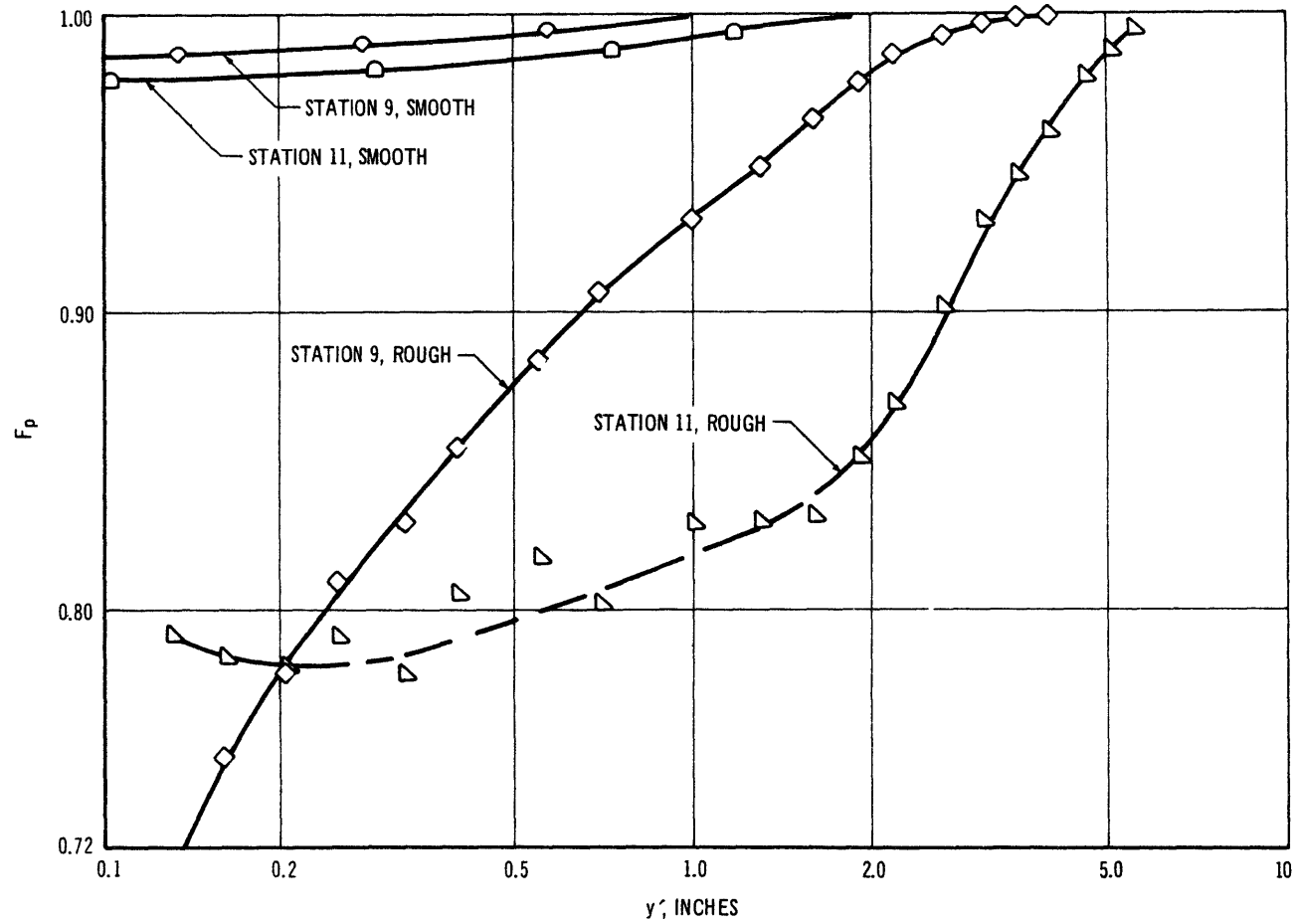


FIGURE 22—Comparison of F_p Values for Smooth and Rough Walls, Pressure Gradient 2

5. ANALYSIS OF THE VELOCITY AND SHEAR FIELDS

There are many facets to the behavior of flow in a boundary layer. All of these deserve examination in order to make meaningful comparisons between the flows over rough and smooth boundaries. Growth, mixing, shear stress and mean velocity distributions carry many implications about physical behavior. For this reason, it appeared necessary to calculate and present not only the mean velocity and shear stress fields associated with the various test conditions, but also the customary mean velocity parameters.

This chapter develops the analytical relationships needed to calculate the fields of interest. Computer programs were written to solve these equations. The results of these programs are plotted and discussed in the next chapter.

5.1 THE MEAN VELOCITY FIELD

The mean velocity field is most readily presented in terms of the stream function, ψ , which is defined as:

$U = \partial\psi/\partial y$ or in a practical way as

$$\psi = \int_0^y U \, dy \quad \text{where} \quad V \ll U \quad (57)$$

Even when V approaches $0.1 U$, as it does near separation,

equation (57) is less than 0.5% in error. Once ψ has been evaluated as a function of y for the various stations, it is then possible to determine V from the simple equation:

$$V = - \frac{\partial \psi}{\partial x} \quad (58)$$

5.2 COMPUTATION OF ψ AND V

As a consequence of the corrections supplied by Chapter 4, it is now possible to work with the corrected values of U/U_1 as a function of y or y' . The procedure followed was relatively simple. Experimental data at each station ($x = x_1$) were put on punch cards and U_1/U_0 was also recorded. $U_0/U_0 = 1$ was taken at the throat section, or first section for each test. Values of

$$\delta_1^* = \int_0^{\delta} (1 - U/U_1) dy \quad \text{and} \quad \theta_1 = \int_0^{\delta} \frac{U}{U_1} \left(1 - \frac{U}{U_1} \right) dy$$

were computed by the trapezoidal rule using finer increments near the wall. The subscript 1 refers to the particular station, $x = x_1$, in each case. In order to provide uniform scales in x and y , a reference length equal to θ_0 at the first station was used to nondimensionalize all lengths.

We may now write $\frac{\psi}{U_1} = \int_0^y \frac{U}{U_1} dy$ and put this into a uniform scale by writing:

$$\frac{\psi}{\theta_o U_o} = \frac{\psi}{U_1} \frac{1}{\theta_o} \frac{U_1}{U_o} \quad (59)$$

The computer was then instructed to tabulate y/θ_o and $\psi/\theta_o U_o$ at each x_1/θ_o . Since the values of y/θ_o became somewhat random at each station and quite different with a change in stations, it was decided to introduce an interpolation routine which would give consistent values of y/θ_o at all stations. These values were more finely spaced near the wall; i.e. $\Delta y/\theta_o = 0.02$ out to $y/\theta_o = 0.10$, 0.1 out to 1.0, and 0.5 out to 39.5 for the rough wall approaching separation.

A least squares fit was used to establish the value of

$$\frac{v}{U_o} = - \frac{\partial(\psi/\theta_o U_o)}{\partial(x/\theta_o)}$$

Values of U/U_o and V/U_o were then converted back to U/U_1 and V/U_1 . The U/U_1 tabulation served as a partial check on the process. The maximum value of V/U_1 was less than 0.10, so that equation (57) was well within the 0.5% limiting error.

5.3 THE WALL SHEAR STRESS

The wall shear stress has been discussed in Chapter 2 in which it is pointed out that the effects of three-dimensional flows tend to introduce serious errors in any

direct computational solution. Nevertheless, this computation was made in order to compare the values with those estimated by the slope-comparison method.

If we start from the boundary layer approximation of the Navier-Stokes equation given as equation 4.5 of reference 6, pages 13 and 16, we have:

$$U \frac{\partial U}{\partial x} + v \frac{\partial U}{\partial y} = - \frac{1}{\rho} \frac{dP_1}{dx} + \frac{\partial}{\partial y} (-\overline{uv}) - \frac{\partial}{\partial x} (\overline{u^2} - \overline{v^2}) \quad (60)$$

where P_1 and U_1 are dependent on x_1 only

and U , v , \overline{uv} , $\overline{u^2}$, $\overline{v^2}$ are functions of x and y .

Since $-\frac{1}{\rho} \frac{dP_1}{dx} = U_1 \frac{dU_1}{dx}$ outside the boundary layer, equation 60 becomes:

$$U \frac{\partial U}{\partial x} + v \frac{\partial U}{\partial y} = U_1 \frac{dU_1}{dx} + \frac{\partial}{\partial y} (-\overline{uv}) - \frac{\partial}{\partial x} (\overline{u^2} - \overline{v^2}) \quad (61)$$

Thus:

$$(-\overline{uv}) = \tau/\rho = \int_0^y \left[U \frac{\partial U}{\partial x} + v \frac{\partial U}{\partial y} - U_1 \frac{dU_1}{dx} + \frac{\partial}{\partial x} (\overline{u^2} - \overline{v^2}) \right] dy + \tau_0/\rho \quad (62)$$

since $c_\tau = \frac{\tau}{\rho U_1^2}$, $c_f = c_\tau$ and $\tau = \tau_0$ at $y = 0$, and

$$\frac{\tau_0}{\rho} = - \int_0^\delta \left[U \frac{\partial U}{\partial x} + v \frac{\partial U}{\partial y} - U_1 \frac{dU_1}{dx} + \frac{\partial}{\partial x} (\overline{u^2} - \overline{v^2}) \right] dy \quad (63)$$

we get

$$c_\tau = - \frac{2}{U_1^2} \int_0^\delta \left[U \frac{\partial U}{\partial x} + v \frac{\partial U}{\partial y} - U_1 \frac{dU_1}{dx} + \frac{\partial}{\partial x} (\overline{u^2} - \overline{v^2}) \right] dy \quad (64)$$

Since U_1 is a function of x , the following non-dimensional form may be written to suit the terms in the velocity field:

$$c_\tau = -2 \int_0^\delta \left\{ \frac{U}{U_1} \frac{\partial U/U_1}{\partial x} + \frac{v}{U_1} \frac{\partial U/U_1}{\partial y} - \left[1 - \frac{U^2}{U_1^2} - 2 \frac{\overline{u^2}}{U_1^2} \left(1 - \frac{\overline{v^2}}{U_1^2} \right) \right] \frac{1}{U_1} \frac{dU_1}{dx} + \frac{\partial}{\partial x} \left[\frac{\overline{u^2}}{U_1^2} \left(1 - \frac{\overline{v^2}}{U_1^2} \right) \right] \right\} dy \quad (65)$$

This form will be used later to evaluate the distribution of shear stress in the boundary layer.

By means of the usual parameters δ^* , θ , $H = \delta^*/\theta$, and the continuity equation,

$$\frac{\partial U}{\partial x} + \frac{\partial V}{\partial y} = 0,$$

equation 63 can be simplified to the momentum form for the wall shear at a boundary layer (see Reference 55, article 83, Equation 218)

$$c_f = 2 \frac{d\theta}{dx} + 2(H+2) \frac{\theta}{U_1} \frac{dU_1}{dx} - \frac{2}{U_1^2} \frac{d}{dx} \int_0^\delta (\overline{u^2} - \overline{v^2}) dy \quad (66)$$

θ and H are calculated from the velocity field at each station, so that the first two terms on the right may be determined with reasonable accuracy. However, the turbulence term is significantly large in an adverse pressure gradient and subject to a good deal of error in measurement so far as the $\overline{v^2}$ term is concerned. The large inaccuracies in the $\overline{v^2}$ and the effects of three-dimensional flows tend

to make this equation highly inaccurate in the prediction of c_f . Values of c_f based on estimates of $\overline{v^2}$ are presented in the next chapter.

5.4 SHEAR STRESS DISTRIBUTION

The general expression for shear stress given in equation (65) may be evaluated from the velocity field with the addition of the turbulence properties, $\overline{u^2}/U_1^2$ and $\overline{v^2}/\overline{u^2}$. As will be seen in Chapter 6, the computed results leave much to be desired in terms of precise numerical values and smoothness in both the x and y directions.

6. PRESENTATION OF RESULTS

The boundary layer characteristics are presented in four sets of curves in all of which the notation has been as follows:

- (a) Pressure Gradient 1, Rough Wall
- (b) Pressure Gradient 2, Rough Wall
- (c) Pressure Gradient 3, Smooth Wall

Pressure gradient 1 was quite small and had an included divergence angle of about 2.9° as noted previously. Pressure gradient 2 was very strong, having a divergence angle of about 11.8° for the rough wall, and a rough wall boundary layer which nearly separated. The smooth wall tests were run with a pressure gradient which closely approximates pressure gradient 2. The angle of divergence for the smooth wall is a good deal smaller than that for the corresponding rough wall case due to the reduction in δ^* on the test wall.

The resulting data are given in four sets of curves with (a), (b) and (c) of each set corresponding to the cases cited above. Figure 23 displays the variation in the standard boundary layer characteristics U_1/U_0 where U_1 is the free stream velocity and U_0 is the reference value; the displacement thickness, δ^* ; the momentum thickness, θ ;

and the shape parameter, $H = \delta^*/\theta$. Figure 24 shows the streamlines for each of the cases and also presents estimates of the boundary layer thickness, δ . Figure 25 compares the various schemes for evaluating c_f , the wall shear or skin friction coefficient. Figure 26 presents the values of c_τ , the shear coefficient, as computed by inserting measured data in the integrated form of the turbulent Euler equations.

In Figure 23 the free-stream velocity U_1 was measured by static pressure taps in the floor of the wind-tunnel and also by pitot-tube in the low-turbulence free stream. The measured values of U_1/U_0 were fed into the computer program. δ^* , θ and H are taken from the computer runs described in Chapter 5. All input data were corrected hot-wire measurements. Since, in general, the quality of data taken at individual stations was judged by the appearance of the pitot-tube measurements and it was not certain how the hot-wire readings should look, several rather poor sets of hot-wire data have come through to final presentation. In particular, these are stations 9 and 11 for pressure gradient 1, rough wall, and stations 12 and 13 for pressure gradient 2, smooth wall. The rest of the data appear to be reasonably satisfactory, at least they are sufficiently correct that qualitative conclusions may be drawn from them.

There are certain strong similarities between pressure gradient 1, rough wall, and pressure gradient 2, smooth wall. Relative variations in δ^* , θ , and H are of the same order of magnitude as shown in Figures 23 (a) and 23 (c). Values of the wall shear coefficient, c_f , shown in Figure 25 drop a little more sharply for the smooth wall to about 0.0008 or a third of the constant-pressure value compared to 0.004 for the rough wall, which is about half the constant-pressure value. Figure 33 also shows this same similarity with both of these cases having a top value of the pressure gradient parameter, β , near 5. Characteristically the streamlines flow into the boundary layer in a constant-pressure situation at a relative slope equal to δ^*/δ which approximates 1/8. To put it another way, the slope of the outer edge of the boundary layer $d\delta/dx$ is about 8 times as great as $d\delta^*/dx$ which is the streamline slope at $y = \delta$, or $d\delta^*/dx = V_1/U_1$ at the edge of the free-stream. Variation in pressure along the wall will change the ratio δ^*/δ quite sharply. Adverse pressures tending toward separation will make δ^*/δ increase rapidly. Examination of Figures 24 (a) and (b) illustrates this contrast. In figure 24 (a) the behavior is similar to the constant pressure case, whereas Figure 24 (b) is like the case for separated flows.

Values of the wall shear coefficient c_f are presented in Figures 25 (a), (b), and (c). These have been evaluated by three methods:

1. Direct computation using experimental data applied to Equation 65.
2. Evaluation of the momentum equation 66 using faired values of $d\theta/dx$ and U_1/dx . While Equation 66 is essentially a limiting case of Equation 65, this computational procedure reduces the scatter of computed points to some extent.
3. The slope-comparison method using either Equation 8 or 10 in Chapter 2. This is discussed in more detail in Chapter 7.

It is evident that the direct computation and momentum methods are seriously affected by the fact that the various terms are usually opposite in sign and very large compared to the resulting differences. The momentum method benefits slightly by the fairing of $d\theta/dx$ and dU_1/dx in the graphical differentiation process, but it still leaves much to be desired so far as a smooth and reasonable variation of c_f with x is concerned.

This writer still prefers the slope-comparison approach first suggested by Clauser²⁰. Although this requires a bit

of fairing also, it involves only a single constant for each station, and erroneous values show up quickly. Although no direct evidence exists for the validity of this scheme for flow over a rough wall, this writer has found that it checks very well with the work of Ludwig and Tillmann¹⁵, Moses²³, and Hsu²⁸ in which the values of c_f were determined by other experimental means. The latter flows were over smooth boundaries in a variety of adverse pressure gradients. It is interesting to note that it is the corrected hot-wire data which seem to give the closest check. As separation is approached, the linear-logarithmic part of the mean velocity curve ceases to exist. However, as shown in Chapter 7, the Coles'¹⁹ "Wake Function" gives a good indication of c_f for both smooth and rough boundaries near separation. Figures 25 (a) and (c) have been evaluated by the slope method. Figure 25 (b) required the use of the Coles' "Wake Function" to check values of c_f at stations 10, 11, 12 and 13.

Figures 26 (a), (b) and (c) present the distributions of shear coefficient c_τ versus y'/θ_o . The curves have the right orders of magnitude and general shapes. However, the strange variations from station to station and negative values of c_τ shown are presumably erroneous. The Schubauer and Klebanoff¹⁴ results were used as a check on the computer

program and exhibited the same peculiarities. Several runs were hand-checked and gave essentially the same numerical answers. It must therefore be concluded that the terms in Equation 65 are extremely sensitive to the normal errors in measurement.

Careful study of the behavior of the individual mean velocity terms in Equations 65 and 66 reveals a tendency to amplify what at first appear to be small errors. In addition, the adverse pressure gradients tend to increase the magnitudes of these terms. Since the largest terms are opposite in sign, the resulting differences scatter rather badly from station to station. The gradients of the integrals which contain turbulence terms remain quite small even close to separation and appear to make little contribution to the computed shear coefficients. Similar results were observed by Sandborn and Slogar⁵⁶. They carried out the same detailed study of evaluation of c_f by the momentum method and came to essentially the same conclusions.

Where c_f is systematically high or low as in Figure 25b, it seems reasonable to suspect the existence of secondary or three-dimensional flows. In order to check the wind tunnel for such flows certain tests were run. At each pressure condition, measurements of mean velocity and longitudinal turbulent intensity were made at points 16

inches up and down from the horizontal center line at two or three stations in the maximum pressure region. The resulting values of U/U_1 and u'/U_1 versus y appear to be nearly identical for the upper, lower and center-line positions. dU/dz appears to be zero based on the measurements taken. On the other hand, a small value of W , the mean velocity component parallel to the wall, would not be revealed by such measurements. It is doubtful that ordinary yaw meters would be able to detect the small angles probably associated with these velocities.

In order to evaluate the role played by dU/dz we must return to Equation 61 in Article 5.3. This equation had originally been simplified by the assumption that $W\partial U/\partial z$ was very small compared to $U\partial U/\partial x$. If we retain $W\partial U/\partial z$ in Equation 61, note that the continuity equation is

$$\frac{\partial U}{\partial x} + \frac{\partial V}{\partial y} + \frac{\partial W}{\partial z} = 0 ,$$

and assume that W is independent of y , we get the following modification of c_τ in Equation 65:

$$\Delta c_\tau = - \frac{2}{U_1} \left(\frac{\partial W}{\partial z} \right) \int_y^\delta \left(1 - \frac{U}{U_1} \right) dy \quad (67)$$

Equation (67) will reduce to the following form at the wall:

$$\Delta c_f = - \frac{2\delta^*}{U_1} \left(\frac{\partial W}{\partial z} \right) \quad (68)$$

The latter can be used to modify Equation 66.

The flow convergence produced by a 1° angle at $z = 16$ inches is sufficient to yield positive values of c_f and c_τ throughout Figures 25b and 26b. Such a convergence approximates that produced by the growth of the boundary layers on the top and bottom surfaces of the wind-tunnel test section. Unfortunately, when the same correction is applied to the c_f and c_τ of the smooth wall which should have approximately the same convergence, the resulting values of c_f and c_τ are obviously much too large. The only conclusion that may be drawn is that it is possible to account for systematic error in these coefficients by small amounts of convergence or divergence in the $x - z$ plane, but even this accounting does not seem completely satisfactory. Other papers, such as that by Moses²³ and a very recent one by Mellor⁵⁷ have used eddy viscosity distributions and Coles' Functions to obtain both shear stress and mean velocity distributions which appear well-behaved and check the experimental data quite well. These approaches may prove useful when more data have been collected for boundary layer flows over rough surfaces in adverse pressure gradients.

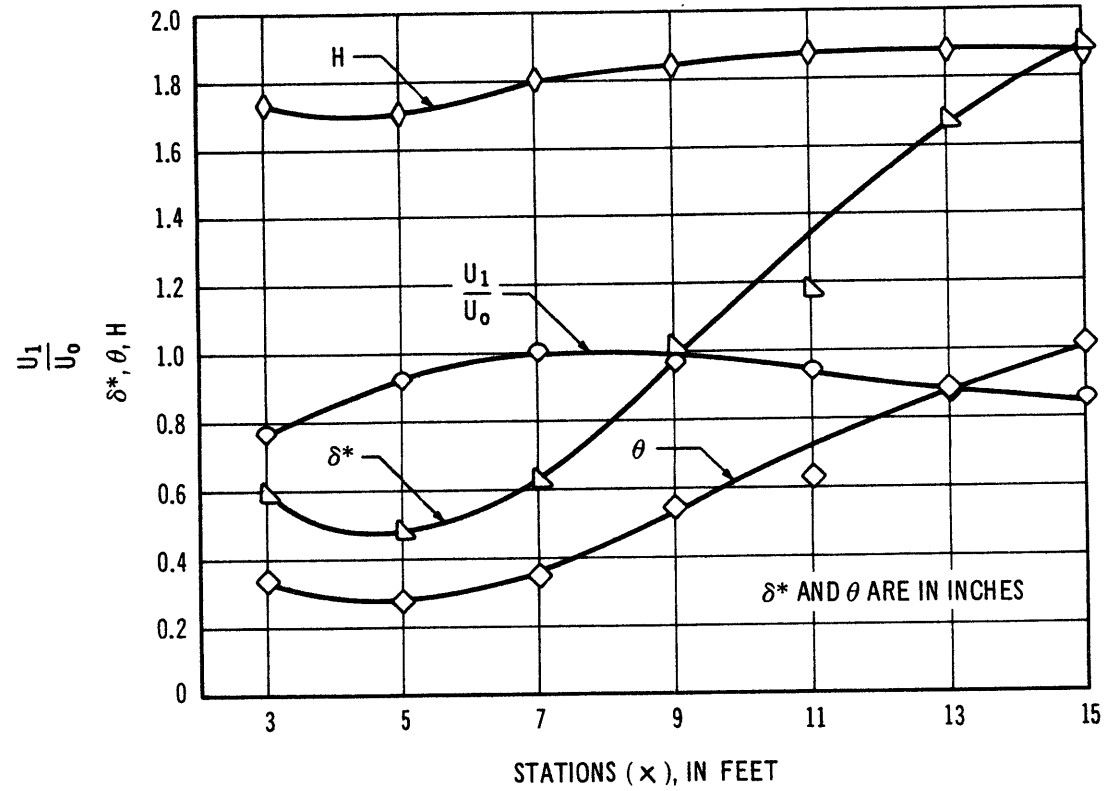


FIGURE 23a—Boundary Layer Characteristics, Pressure Gradient 1, Rough Wall

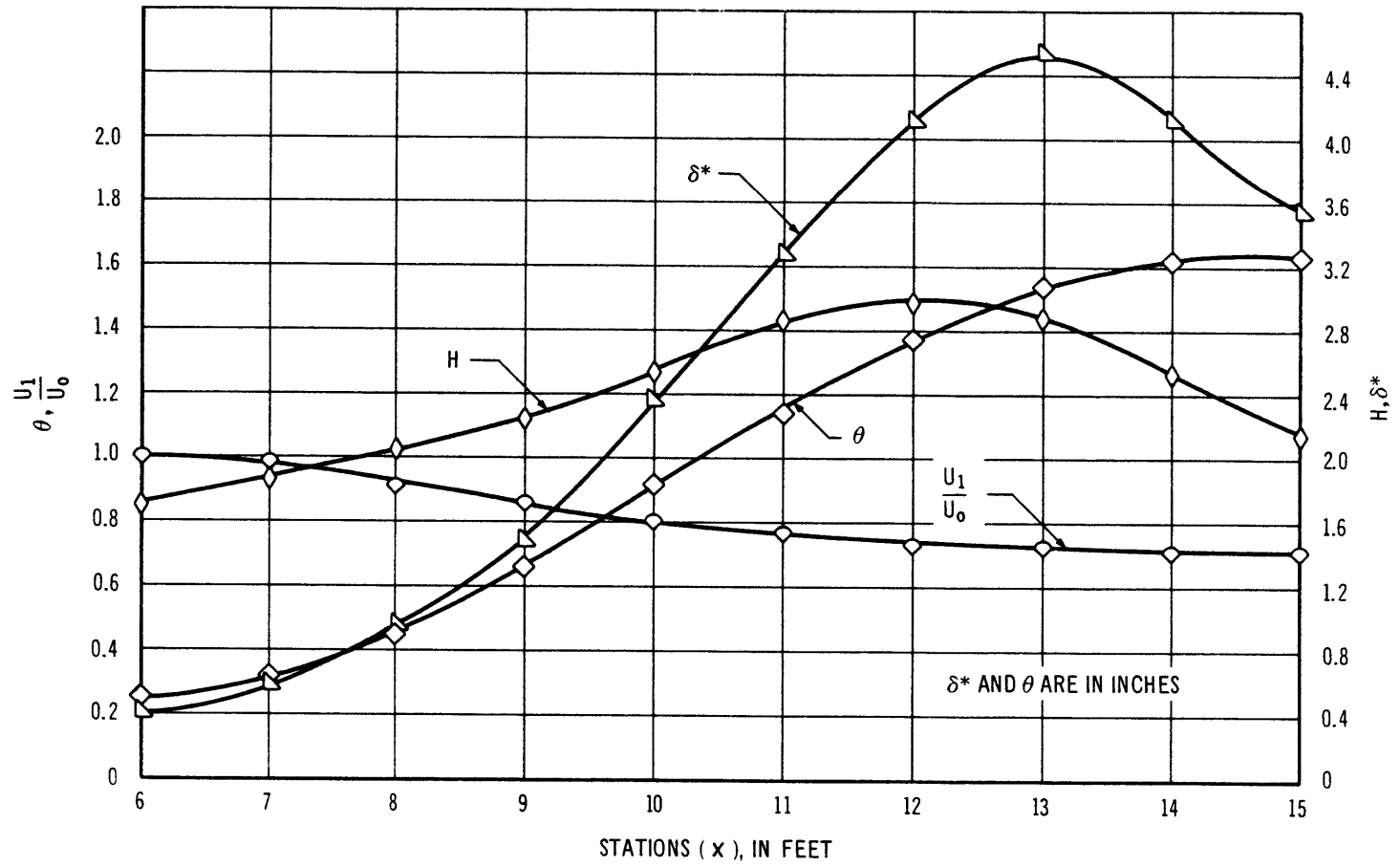


FIGURE 23b—Boundary Layer Characteristics, Pressure Gradient 2, Rough Wall

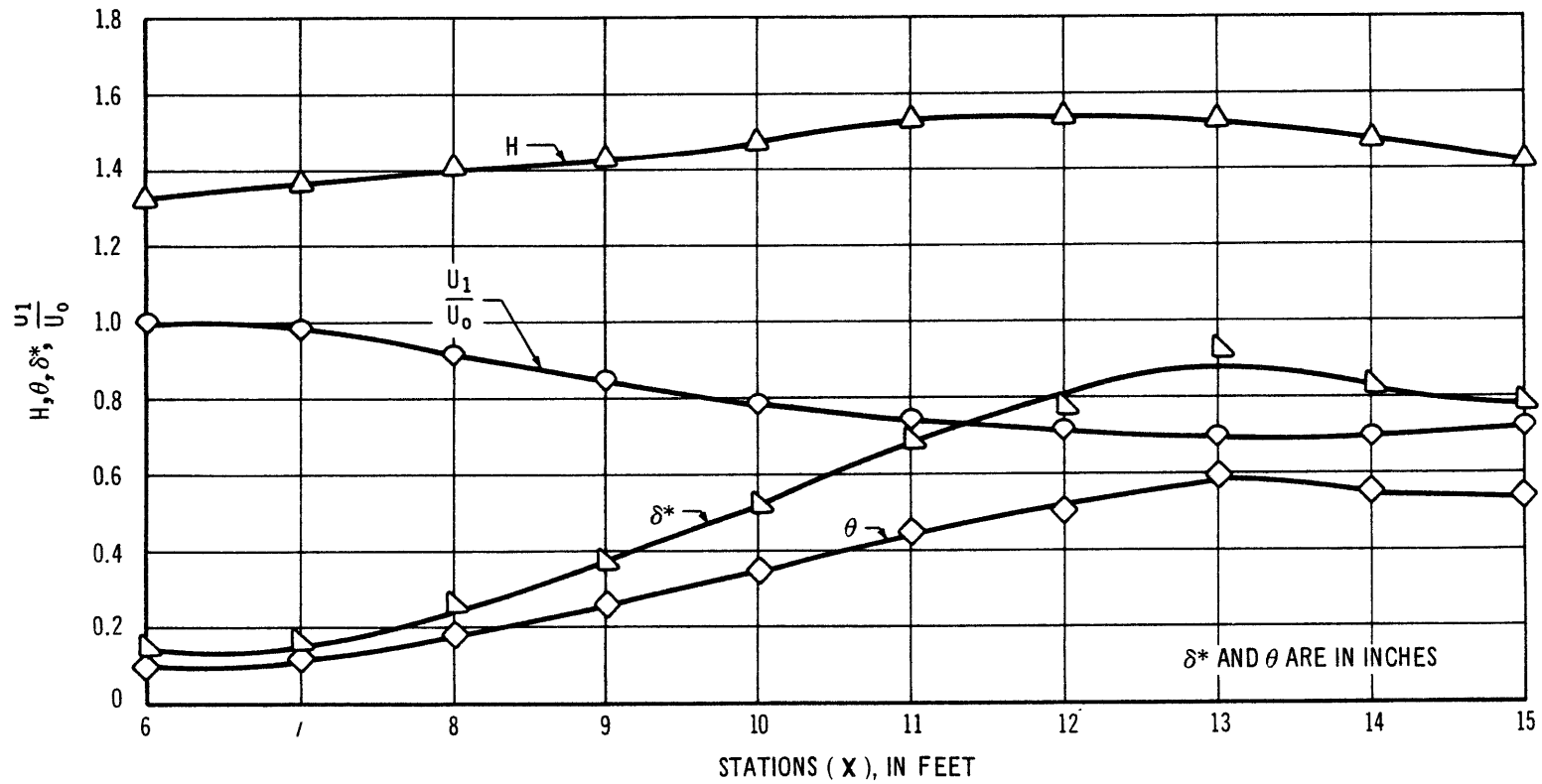


FIGURE 23c—Boundary Layer Characteristics, Pressure Gradient 2, Smooth Wall

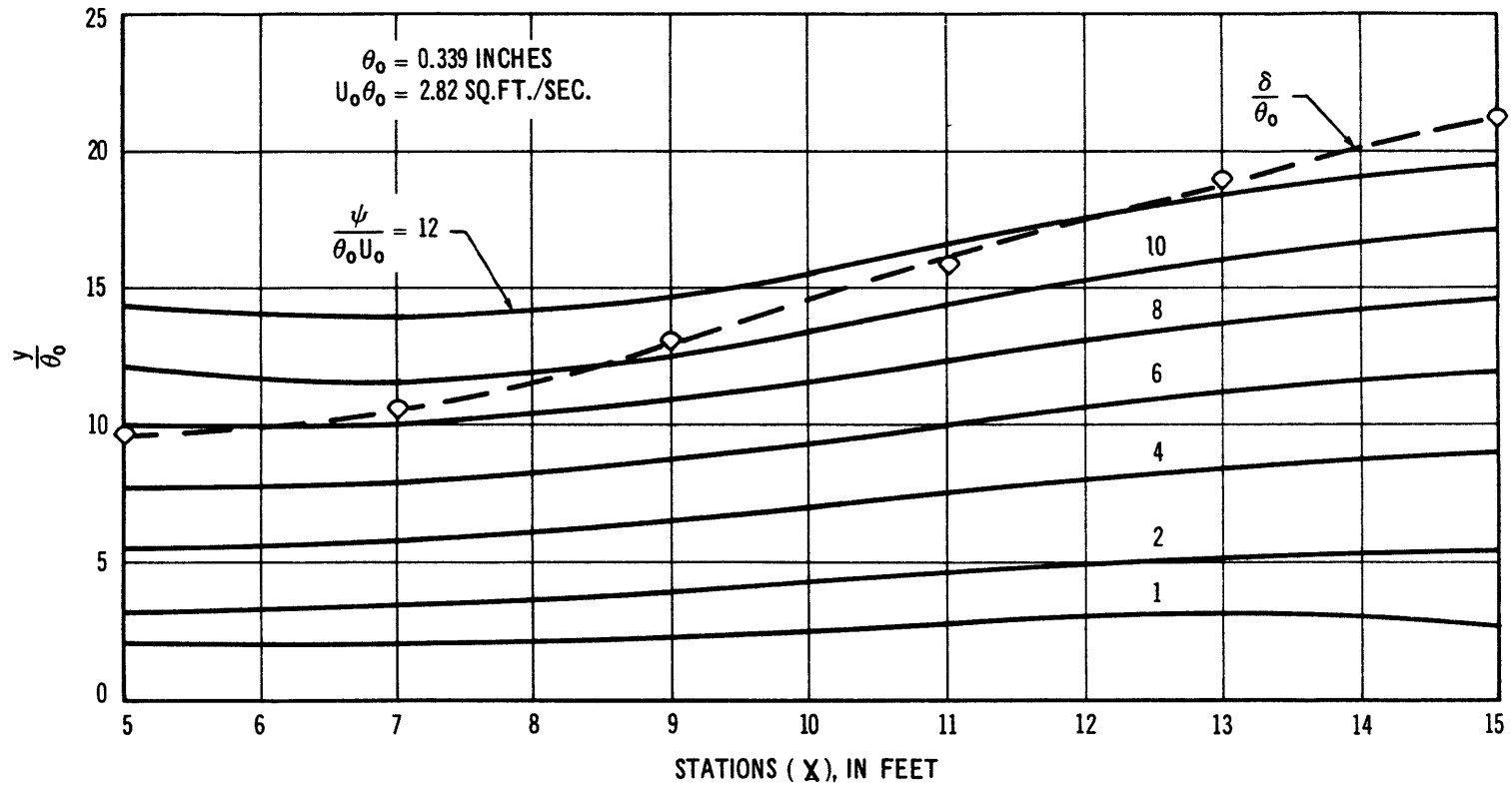


FIGURE 24a—Streamline Distribution, Pressure Gradient 1, Rough Wall

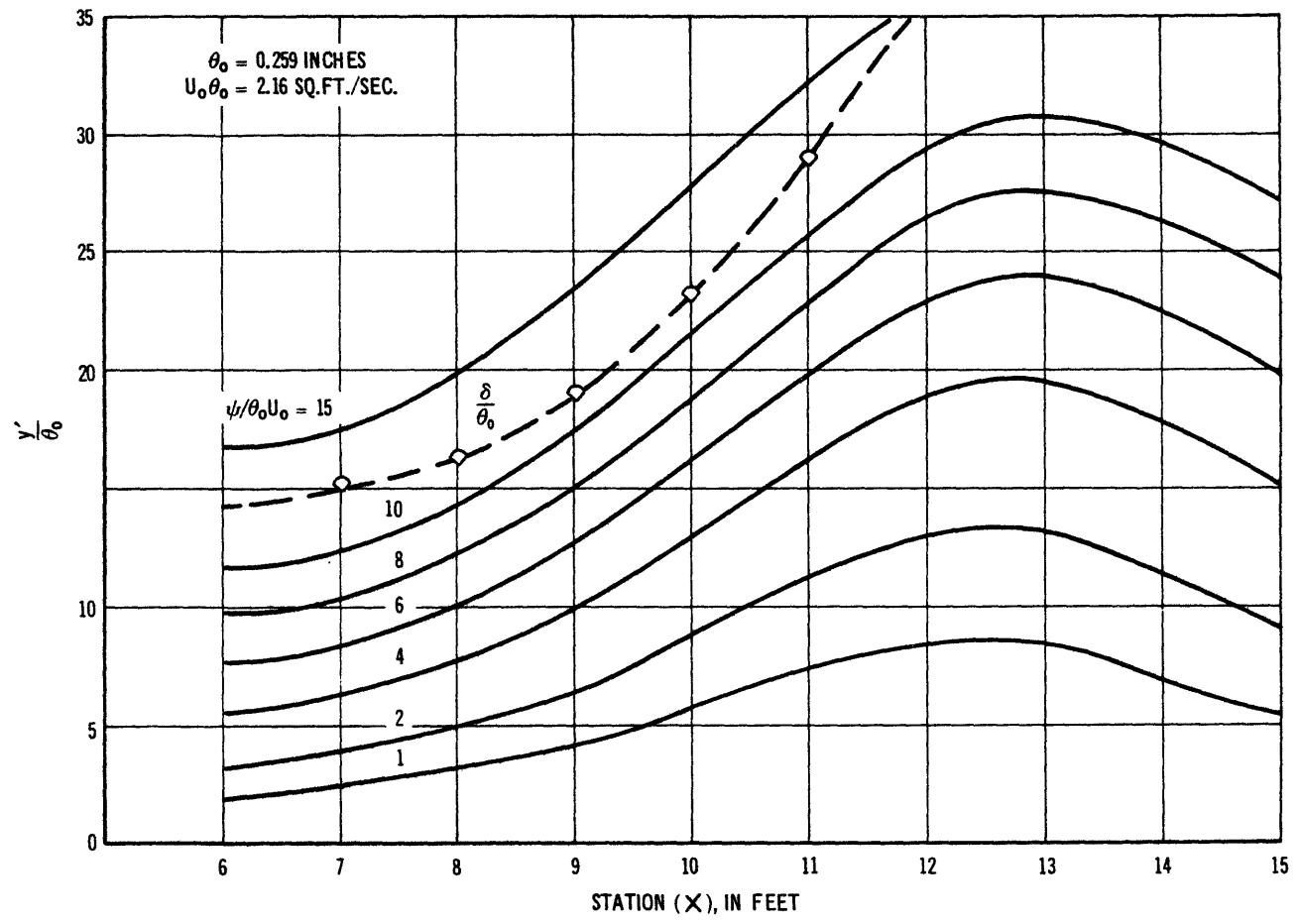


FIGURE 24b—Streamline Distribution, Pressure Gradient 2, Rough Wall

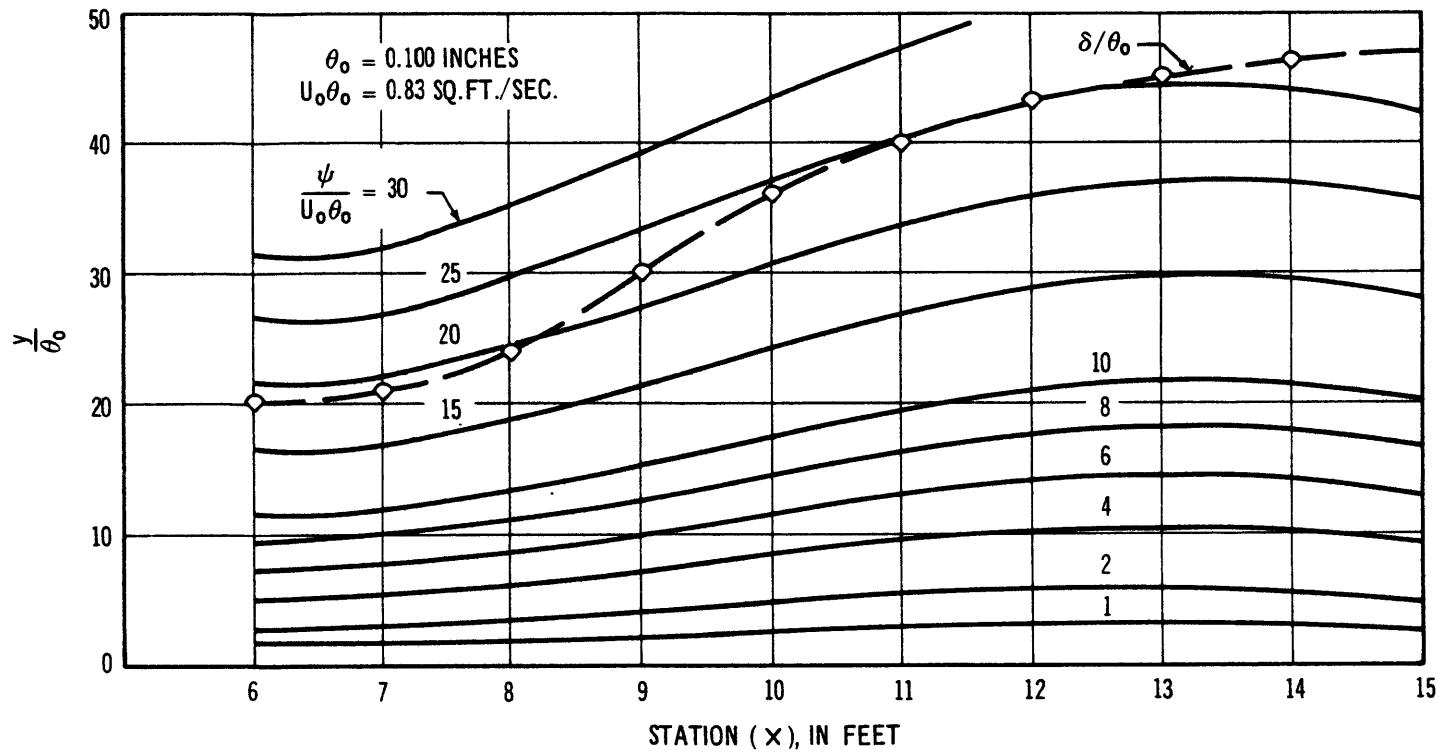


FIGURE 24c—Streamline Distribution, Pressure Gradient 2, Smooth Wall

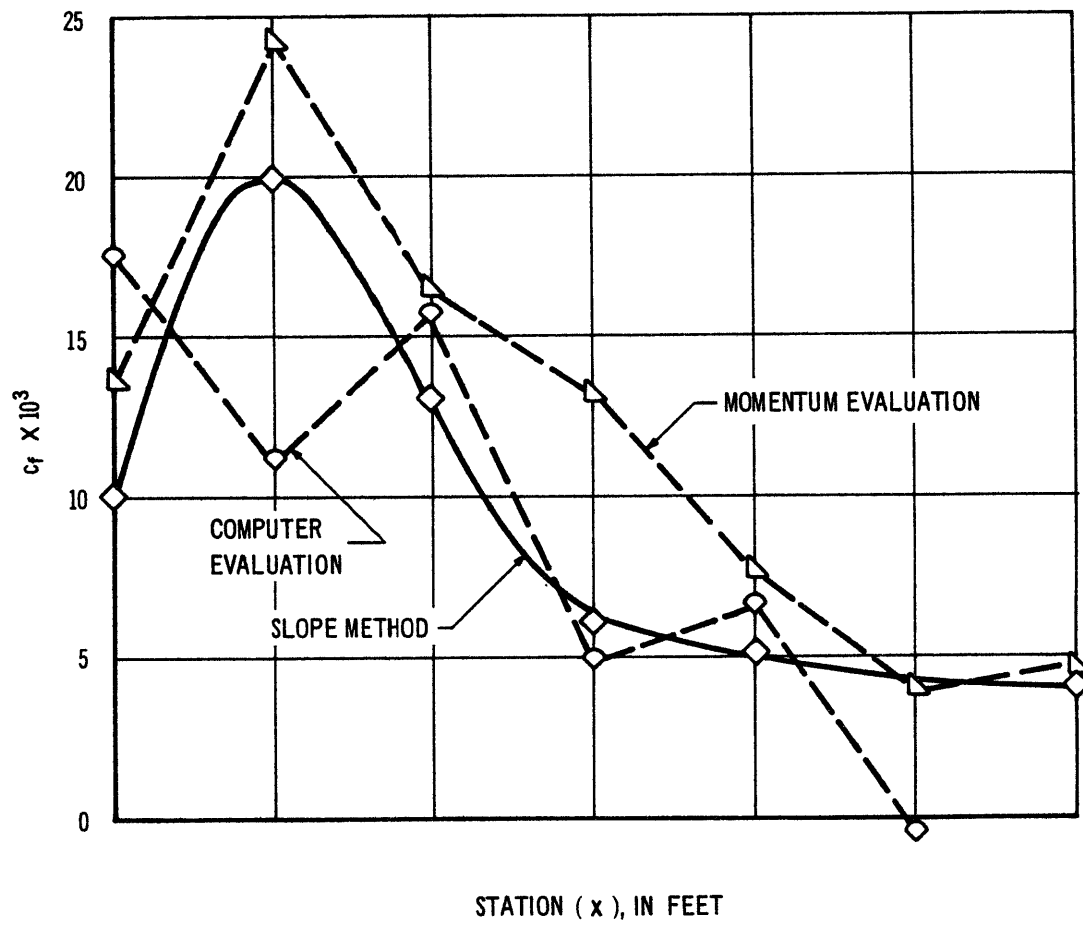


FIGURE 25a—Wall Shear Coefficient, Pressure Gradient 1, Rough Wall

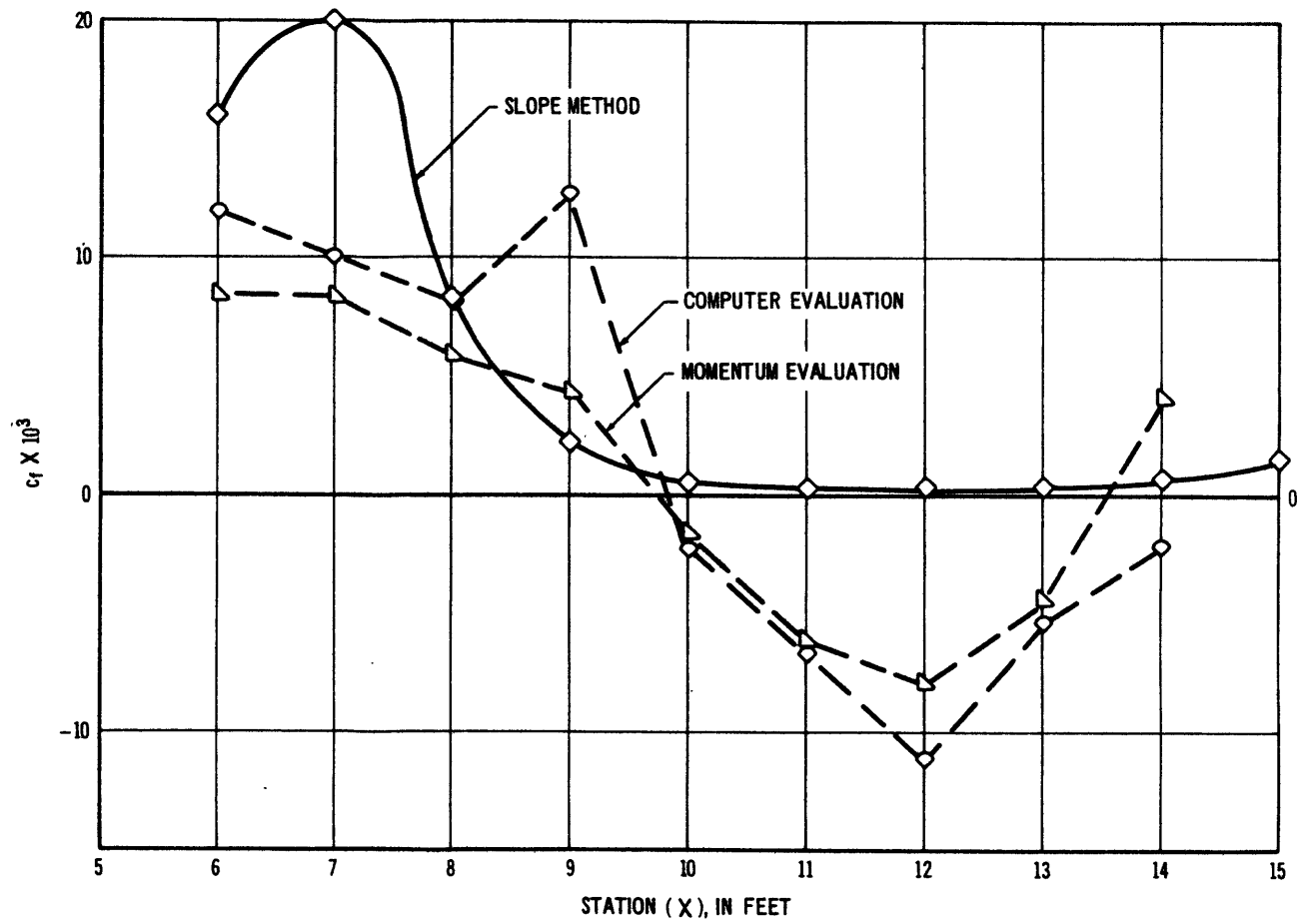


FIGURE 25b—Wall Shear Coefficient, Pressure Gradient 2, Rough Wall

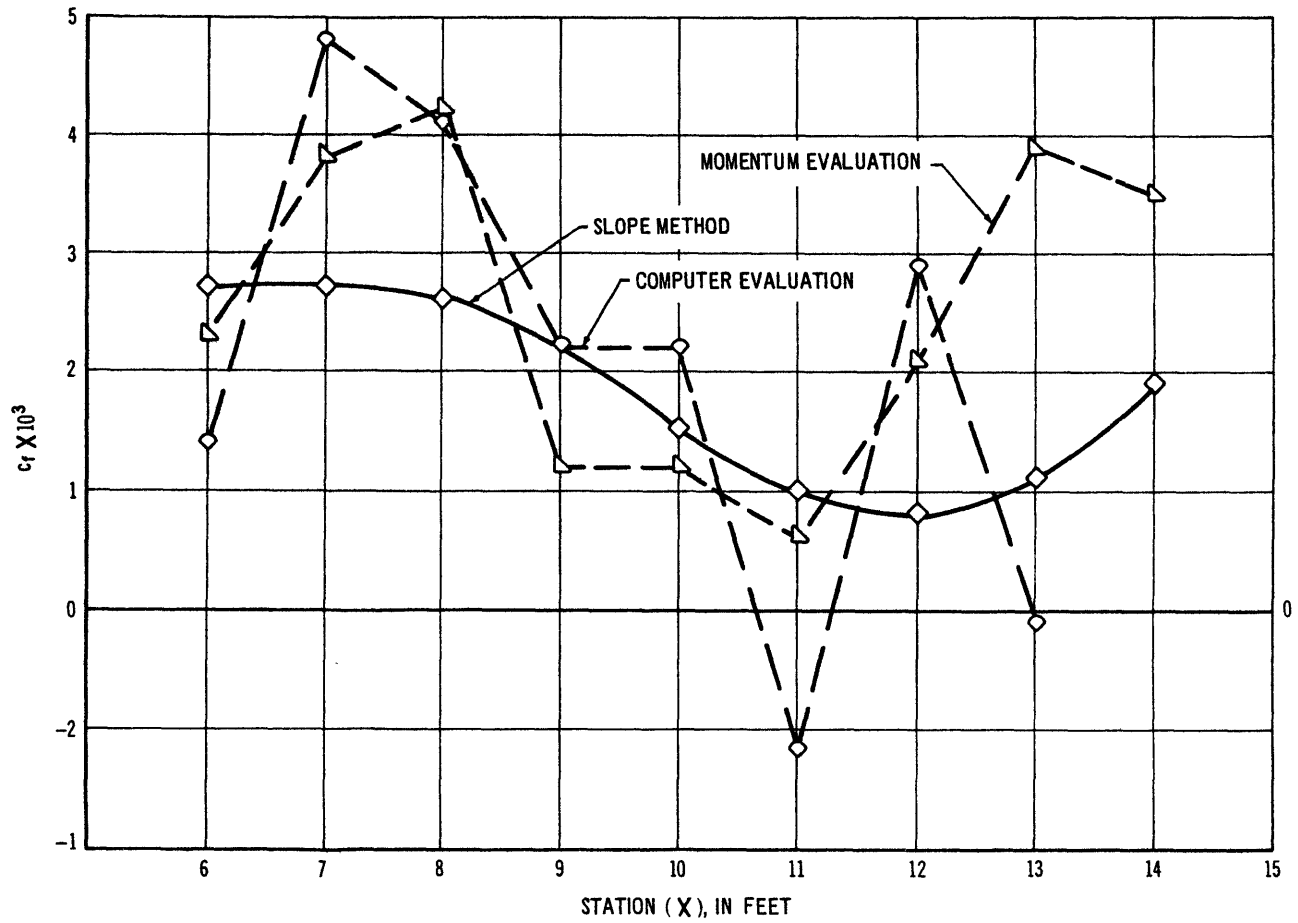


FIGURE 25c-Wall Shear Coefficient, Pressure Gradient 2, Smooth Wall

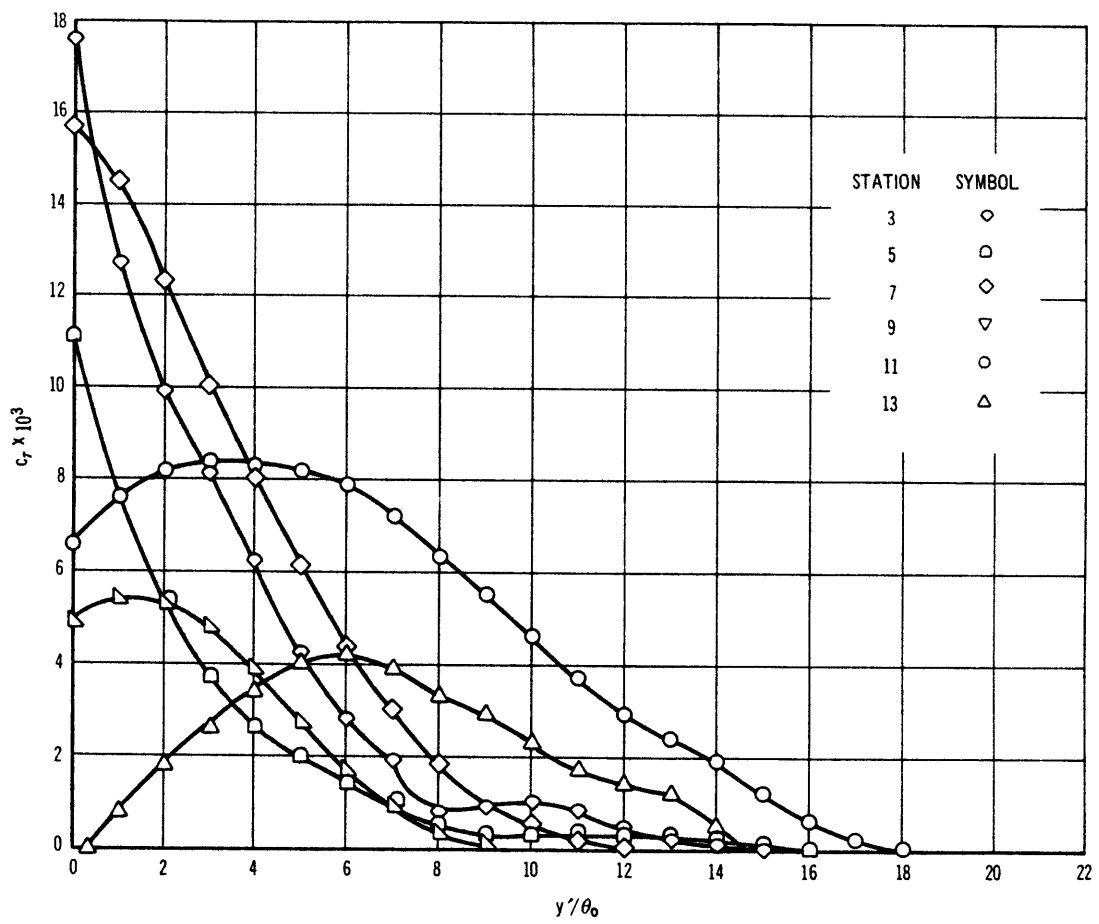


FIGURE 26a—Shear Coefficients Computed From Measured Data, Pressure Gradient 1, Rough Wall

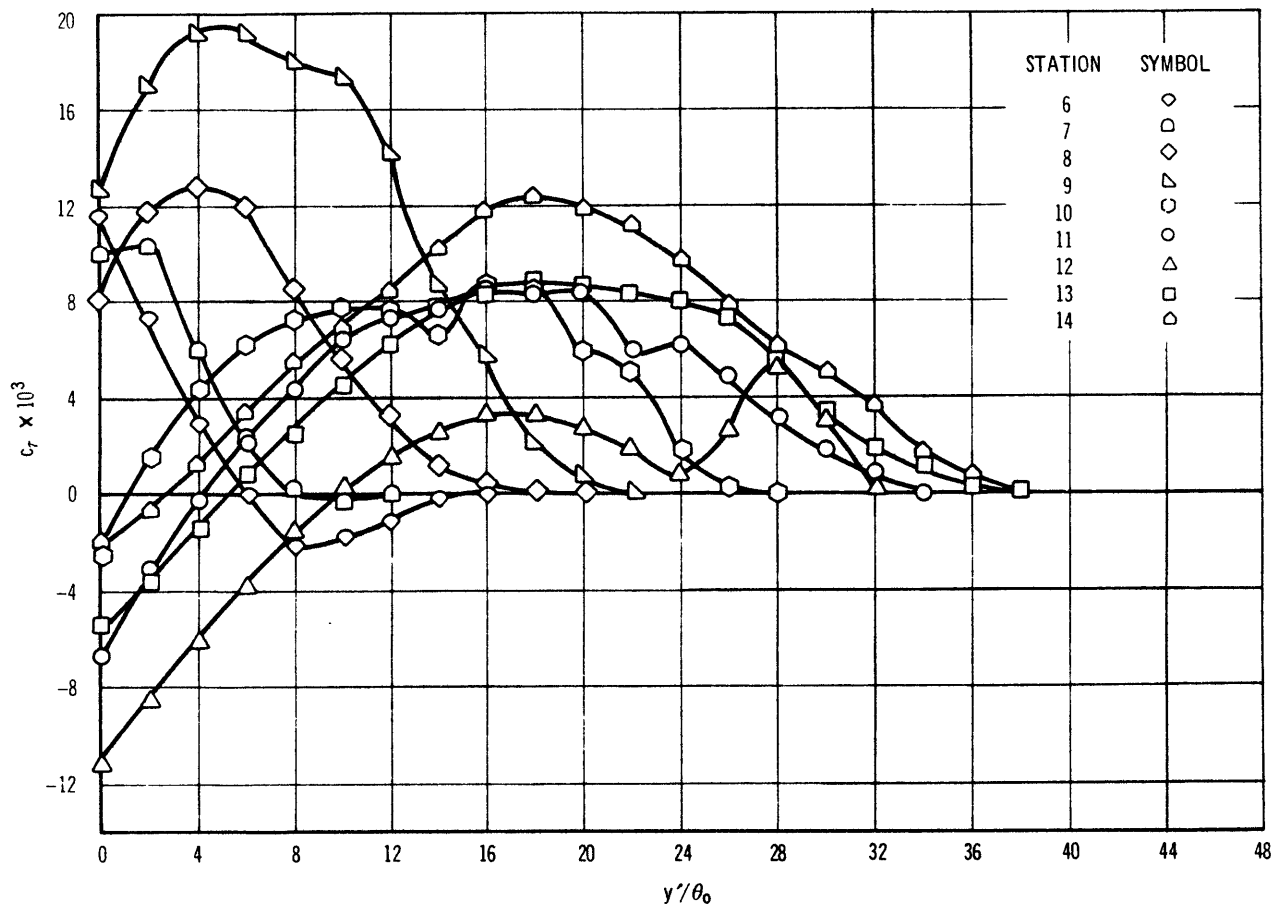


FIGURE 26b—Shear Coefficients Computed From Measured Data, Pressure Gradient 2, Rough Wall

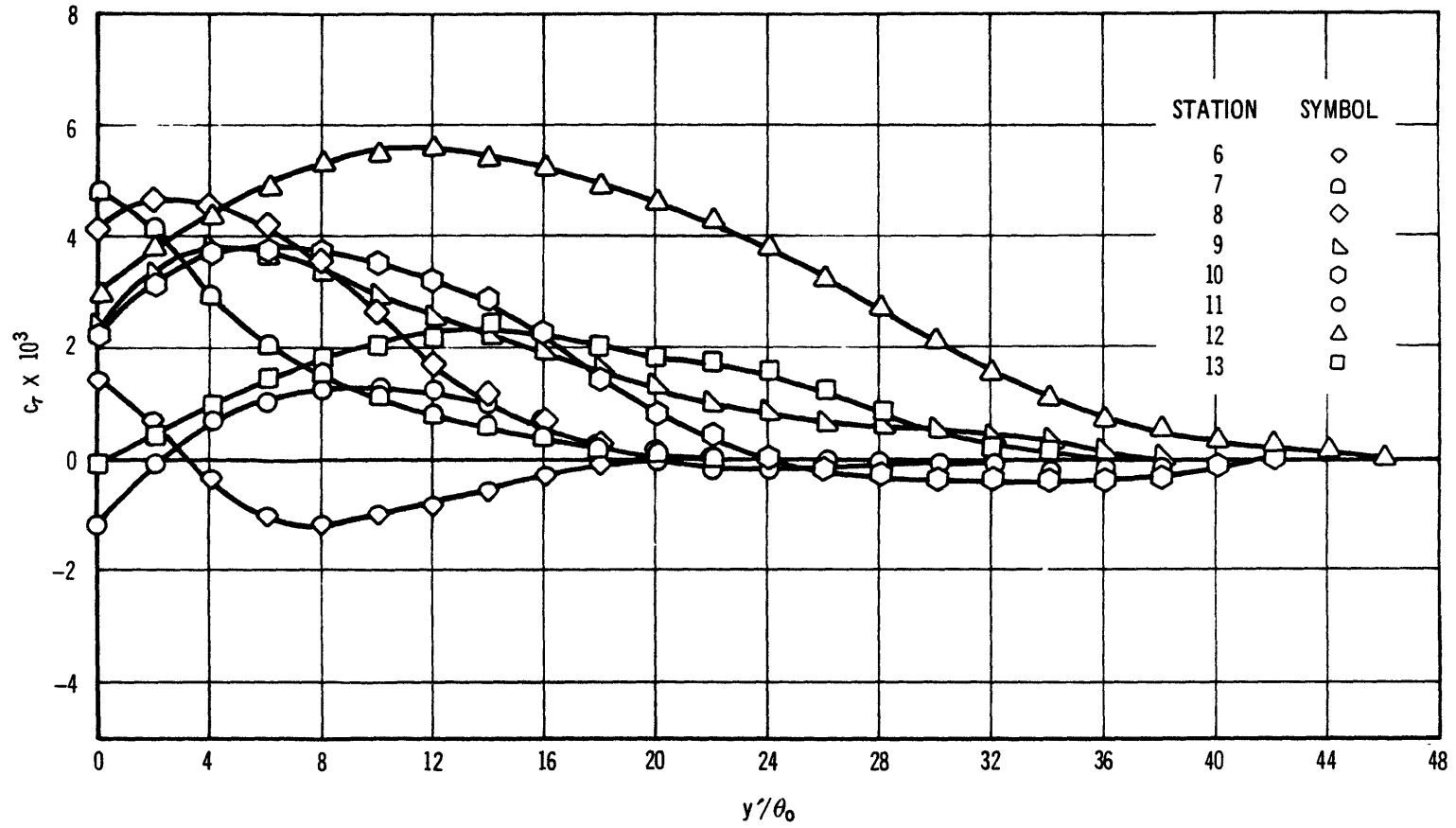


FIGURE 26c—Shear Coefficients Computed From Measured Data, Pressure Gradient 2, Smooth Wall

7. COMPARISON WITH THE LAW OF THE WAKE

Very early in this series of experiments it was observed that the Coles "Law of the Wake"¹⁹ provided an alternate means of estimating the skin friction coefficient, c_f . It was known both from the Coles paper and from the work of Moses²³ that the velocity distribution U/U_1 for smooth boundaries could be matched quite well at different stations as separation was approached. The principal difference between this method and that discussed under the "Logarithmic Velocity Law" in Section 2.1 is that the "Law of the Wake" should give the completed velocity distribution at a given station out to $y = \delta$. The effect of roughness on the wake region is not known, but if one assumes that the influence of roughness is the same for the adverse pressure case as for the constant pressure condition, it is possible to obtain an equation for U/U_1 .

7.1 THE ROUGH-WALL FUNCTION

Coles¹⁹ has provided a derivation for the mean velocity distribution which is reproduced here in a modified form in order to include the effect of roughness.

Commencing with equation 7 of reference 19,

$$\frac{U}{U_\tau} = f \left(\frac{yU_\tau}{\nu} \right) + \frac{\Pi}{K} w \left(\frac{y}{\delta} \right) \quad (69)$$

where w is the wake function, "supposedly common to all two-dimensional boundary-layer flows", and Π is a profile parameter which is independent of x and y . $f\left(\frac{yU_\tau}{\nu}\right)$ represents the "inner" or "logarithmic" region, so that:

$$f\left(\frac{yU_\tau}{\nu}\right) = \frac{1}{K} \ln\left(\frac{yU_\tau}{\nu}\right) + 4.9 - \frac{\Delta U}{U_\tau} \quad (70)$$

as given in equation (6) of this paper. Then letting $y/\delta = \eta$

$$\frac{U}{U_\tau} = \frac{1}{K} \ln\left(\frac{yU_\tau}{\nu}\right) + 4.9 - \frac{\Delta U}{U_\tau} + \frac{\Pi}{K} w(\eta) \quad (71)$$

At $y = \delta$, $U = U_1$ to give:

$$\frac{U_1}{U_\tau} = \frac{1}{K} \ln\left(\frac{\delta U_\tau}{\nu}\right) + 4.9 - \frac{\Delta U}{U_\tau} + \frac{\Pi}{K} w(1) \quad (72)$$

Combining these, we get a velocity defect relationship in the following form:

$$\frac{U - U_1}{U_\tau} = \frac{1}{K} \ln(\eta) + \frac{\Pi}{K} [w(\eta) - w(1)] \quad (73)$$

As shown by Coles,¹⁹ $w(\eta)$ is subjected to the normalizing conditions $w(0) = 0$, $w(1) = 2$, and $\int_0^2 \eta dw = 1$.

For the screen type of roughness used in this study, Hama¹ has shown that the change in velocity defect for the constant pressure case may be represented by:

$$\frac{\Delta U}{U_\tau} = \frac{1}{K} \ln\left(\frac{kU_\tau}{\nu}\right) - 1.2 \quad (74)$$

so that:

$$\frac{U_1}{U_\tau} = \frac{1}{K} \ln \left(\frac{\delta U_\tau}{\nu} \right) + 4.9 + 1.2 - \frac{1}{K} \ln \left(\frac{k U_\tau}{\nu} \right) + 2 \frac{\Pi}{K} \quad (75)$$

or

$$\frac{2\Pi}{K} = \frac{U_1}{U_\tau} - \frac{1}{K} \ln \left(\frac{\delta}{k} \right) - 6.1$$

then:

$$\frac{U - U_1}{U_\tau} = \frac{1}{K} \ln (\eta) + \left[\frac{U_1}{U_\tau} - \frac{1}{K} \ln \left(\frac{\delta}{K} \right) - 6.1 \right] \left(\frac{1}{2} w (\eta) - 1 \right) \quad (76)$$

This is written more conveniently as:

$$\frac{U}{U_1} = \frac{1}{2} w(\eta) + \alpha \left\{ \log_{10} (\eta) + \left[\log_{10} \left(\frac{\delta}{k} \right) + 1.1 \right] \left[1 - \frac{1}{2} w(\eta) \right] \right\} \quad (77)$$

$$\text{where } \alpha = \frac{2.303}{K} \sqrt{\frac{c_f}{2}} \cong 5.6 \sqrt{\frac{c_f}{2}} = 5.6 \frac{U_\tau}{U_1}$$

for $K \cong 0.41$, and $6.1 K/2.303 \cong 1.1$.

Thus $U/U_1 = f(\eta, \alpha, \delta/k)$ for the rough case.

Several basic assumptions enter into the use of equation (77). These might be listed as follows:

1. The function $w(\eta)$ is taken to be universal, according to Coles¹⁹. (See also the discussion in Hinze⁴², pp 507 to 514). It may be applied to rough as well as smooth boundaries.

2. Equation (74) may be used with an adverse pressure gradient. Presently available data are not sufficient to justify this assumption, but it appears to be approximately correct up to the point where c_f becomes very small near separation.

3. A further restriction is that the roughness is large so that the flow is essentially "fully rough", otherwise equation (74) will not apply.

A computer routine was set up for evaluating equation (77), as well as for the smooth wall case which is represented by the following equation:

$$\frac{U}{U_1} = \frac{1}{2} w(\eta) + \alpha \left\{ \log_{10}(\eta) + \left[\log_{10}(\alpha R_\delta) + 0.13 \right] \left[1 - \frac{1}{2} w(\eta) \right] \right\} \quad (78)$$

$$\text{where } R_\delta = \frac{U_1 \delta}{\nu}$$

thus $\frac{U}{U_1} = f(\eta, \alpha, R_\delta)$ for the smooth wall case.

Both cases were calculated using $\eta = 0$ to 1.00 by 0.05 intervals and $\alpha = 0$ to 0.40 by 0.05 intervals. The rough wall case was evaluated for $\delta/k = 20, 40, 60, 80$ and 100, and the smooth wall case for $R_\delta = 10^4, 10^5$ and 10^6 .

7.2 COMPARISON OF FUNCTIONS WITH EXPERIMENTAL DATA

A comparison with the Coles function of mean velocity distributions obtained using the rough wall subjected to the strongly adverse pressure gradient leaves much to be desired. The rapid deceleration between Stations 6 and 9 is illustrated in Figure 27. Here the zone close to the wall is being modified so rapidly by the pressure gradient in such a short distance along the wall that the outer part of the boundary layer has not had an opportunity to adjust to upstream conditions. Figure 28 shows stations 11 and 12 compared to the fully rough Coles function (Equation 77), and Figure 29 shows these same stations compared to the Coles function for a smooth wall (Equation 78). The flow is very close to separation here, and one senses that the outer or wake portion of the boundary layer has enlarged inward toward the wall and has effectively eliminated the inner or logarithmic region.

Clearly there are physical effects taking place here which for a variety of reasons make it obvious that attempting to evaluate the skin friction coefficient by such comparisons is not going to produce satisfactory results. However, this writer believes that the Coles approach in itself is reasonably valid, but that there are other factors

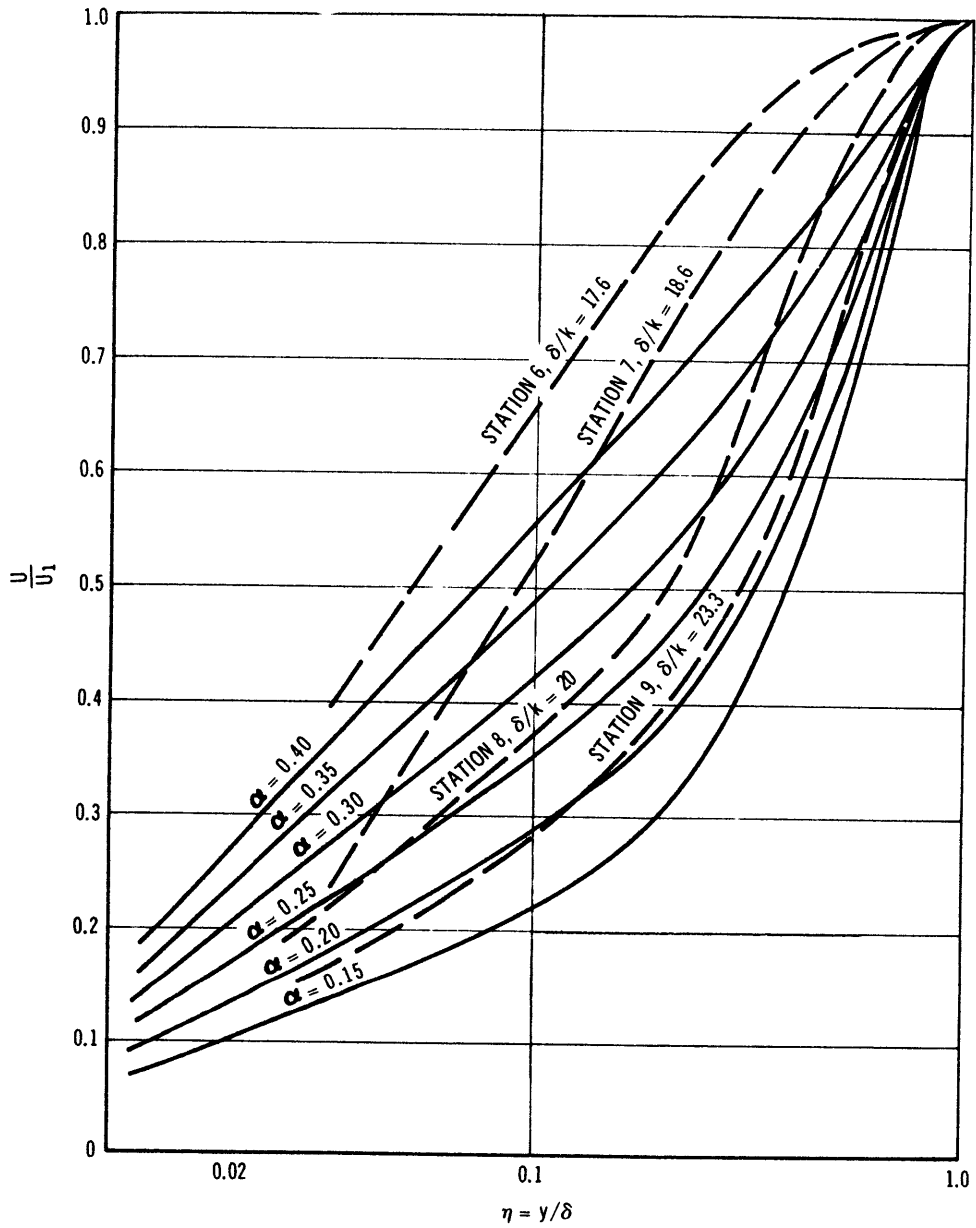


FIGURE 27—Comparison of Rough Coles Function, $\delta/k = 20$,
With Experimental Data, Pressure Gradient 2

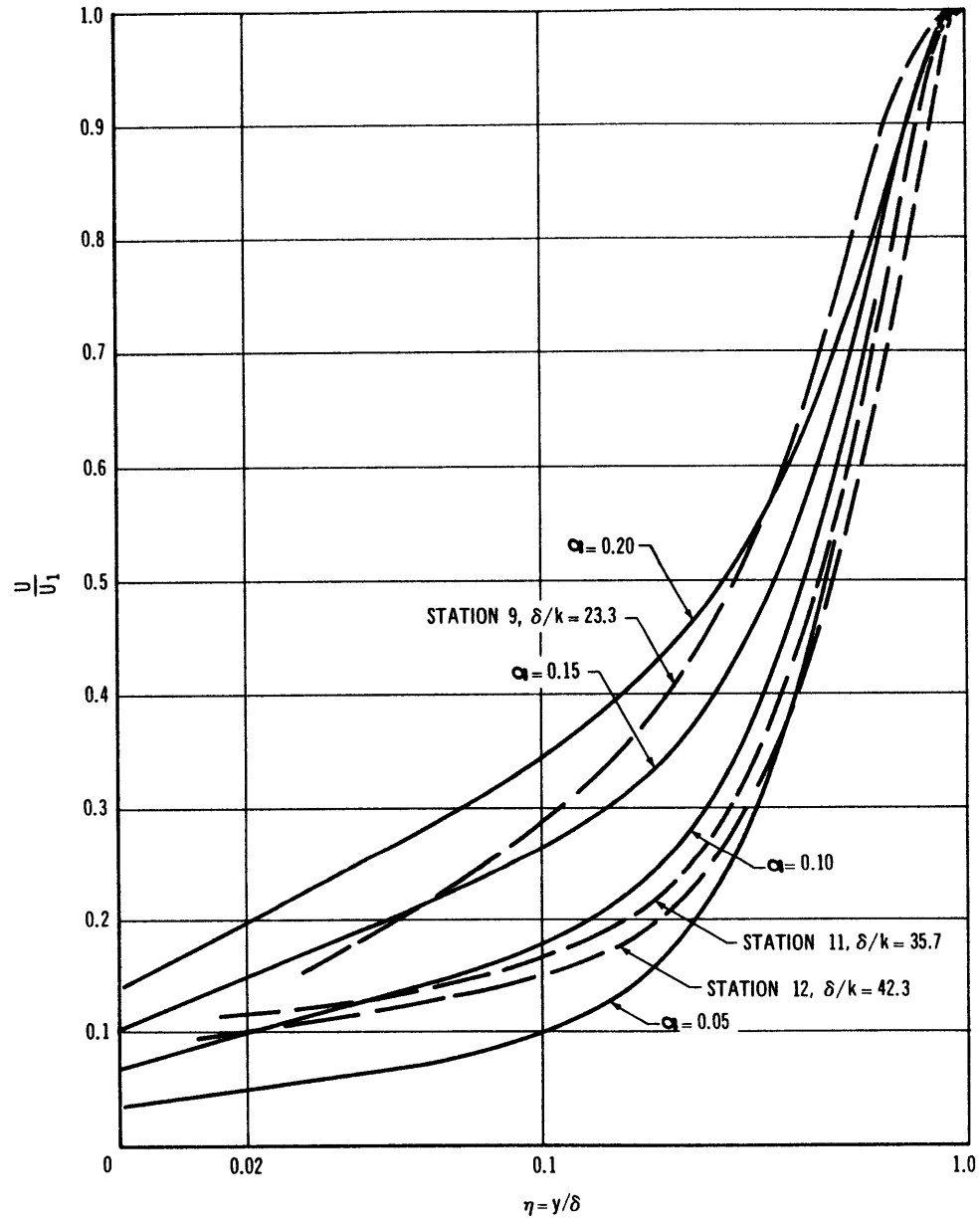


FIGURE 28—Comparison of Rough Coles Function, $\delta/k = 40$,
With Experimental Data. Pressure Gradient 2

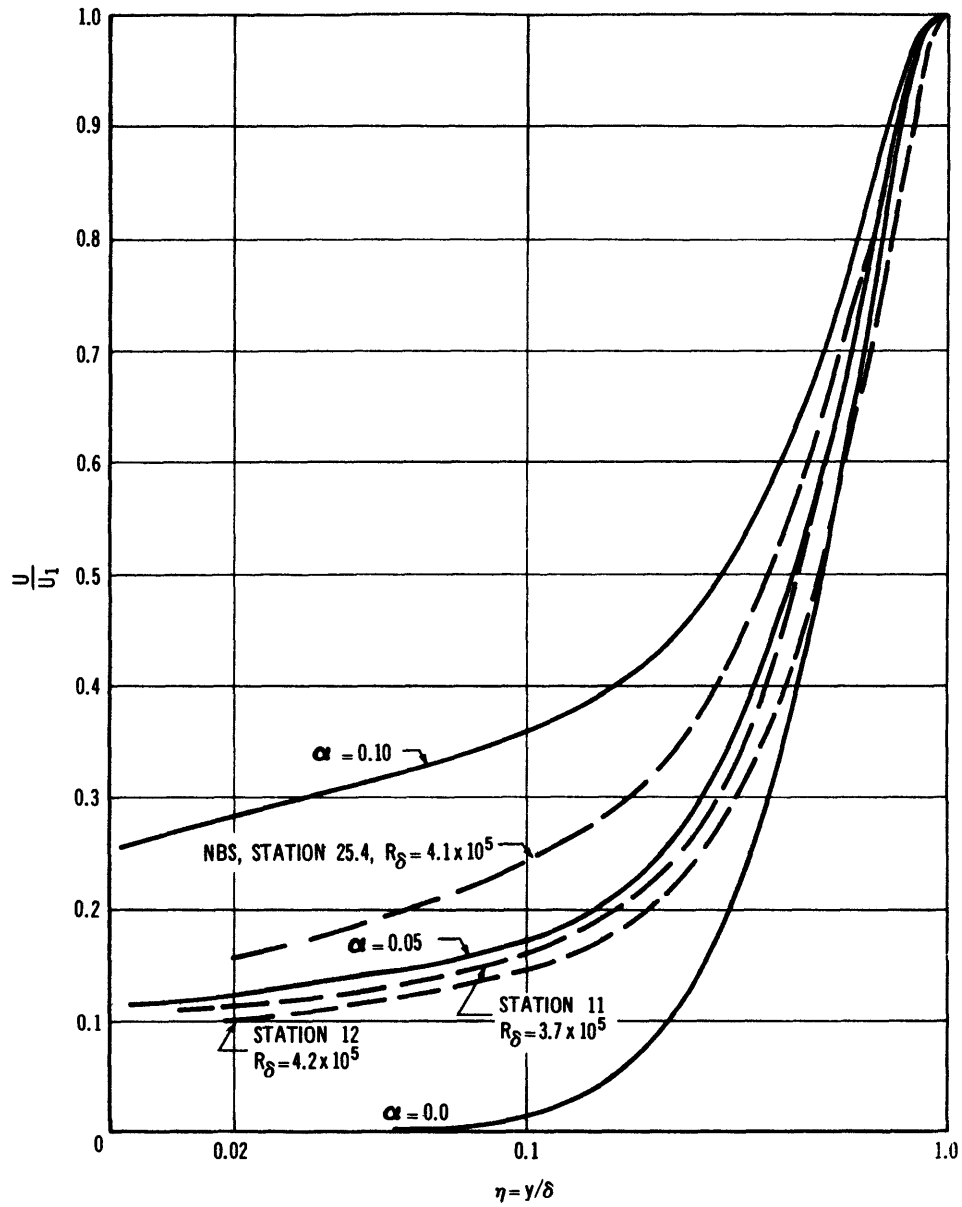


FIGURE 29—Comparison of Smooth Coles Function, $R_\delta = 4 \times 10^5$, With Experimental Data; Pressure Gradient 2, Stations 11 and 12, Rough Wall; NBS, Station 25.4, Smooth Wall

which have produced the observable differences shown in these three Figures.

The first of these factors applies to the assumptions regarding Equation (74). A comparison of Figures 28 and 29 makes it very clear that the effect of roughness departs very radically from that given by Equation (74) as separation is approached. The roughness of the wall can have little or no influence on the general character of the flow as the wall shear goes to zero. The flow will be completely dominated by the pressure change and the accumulated effects of boundary layer behavior upstream. This is directly indicated by the shape of the velocity distributions in Figure 29; i.e. that a very rough wall affects the flow like a smooth one when separation is impending, or when c_f approaches zero.

The flow between Stations 6 and 9 is subject to initial conditions which were not present in the data which Coles used to set up his wake function. The wind-tunnel configuration in the present set of tests was such that it was necessary to accelerate the flow ahead of Station 6. This thinned out the boundary layer over a very rough surface giving an extremely high skin friction coefficient. The flow was then rather abruptly decelerated without benefit of a constant pressure zone, or a zone having a reasonably

parallel free stream external to the boundary layer. It is possible that a more gradual change would have allowed the whole thickness of the boundary layer to adapt to the new regime, thus producing a more favorable comparison with the rough-wall function. The fact that Station 9 compares well with the Coles function for a roughened wall (Figures 27 and 28) implies that Equation 74 may be correct in an adverse pressure gradient until the wall shear becomes quite small.

8. COMPARISON OF ROUGH AND SMOOTH WALL DATA

One of the principal objectives of this investigation has been to determine whether boundary layer flows in an adverse pressure gradient tend to separate more readily in the presence of a rough or a smooth wall. Existing data, including those of the present experiments, are rather qualitative in nature but seem to favor the smooth wall if resistance to separation is desired.

A number of comparisons are presented which make use of the experiments of Schubauer and Klebanoff¹⁴, Moses²³, and those of the writer. No attempt has been made to evolve a special similarity form for prediction of separation, although a variety of the usual variables are considered and discussed.

8.1 Although the experimental data taken by Schubauer and Klebanoff¹⁴ made use of a different wind tunnel arrangement, conditions were similar enough to make a comparison of their data and some of the present work justifiable. In the NBS experiments the pressure gradient was produced by a curved test wall whereas the pressure gradients of the present tests were produced by having a curved smooth wall opposite the test wall. Both flows involve a region of favorable pressure gradient in which the flow is accelerated followed by a

region of adverse pressure gradient in which the flow is retarded to the point of separation. The NBS flow actually separates while the TMB flow approaches separation very closely since c_f approaches zero. In the adverse pressure regions both experiments exhibit remarkably similar values of the momentum thickness.

The data chosen for comparison in the two sets of experiments were obtained at stations where the local flow conditions were similar. The first NBS station selected was the one located 17.5 ft from the leading edge of the test wall at which the pressure gradient changed signs ($dp/dx = 0$), and a nearly parallel flow existed. The third point was Station 25.4, the point of incipient separation. An intermediate station was picked in an arbitrary fashion by taking one which had a momentum thickness equal to one-half that at the third station. The three TMB stations were selected in essentially the same manner. The first one, Station 7, was chosen to give a condition of nearly parallel flow based on c_f and H , the third, Station 11, to show conditions at impending separation, and the second, Station 9, had about half the momentum thickness of the third.

The data from each of the positions are presented in Figures 30, 31, and 32. In Figure 30 U/U_1 is plotted against y' , in Figure 31 u'/U_1 is plotted against y' ,

and in Figure 32 u'/U is plotted against y' . In these graphs y' represents the distance from the "effective" origin (see Figure 2) for the TMB data and the distance from the smooth wall for the NBS data. The value of y' which indicates the outer extremities of the roughness for the TMB test wall is located at about 0.1 inches on each of the plots.

VELOCITY PROFILES

There are, of course, significant differences in the three parameters, wall shear stress, free stream velocities, and longitudinal distances, required to produce the observed changes in momentum thickness θ and shape parameter H necessary to induce separation on smooth or rough boundaries. In Figure 30 we may observe the effects of these differences on the velocity distributions. The TMB rough wall velocity profile at Station 7 has a relatively low velocity near the wall due to the high value of c_f . As the wall face is located at $y' = 0.1$ inches, the linear portion of the velocity distribution is considerably shorter than that for the corresponding NBS data at Station 17.5, since both distributions appear to start the upward curving portion of the outer layer at about the same value of y' . Both Coles¹⁹ and Perry and Joubert²⁵ have shown that the latter conclusion is to be expected as a consequence of the large portion

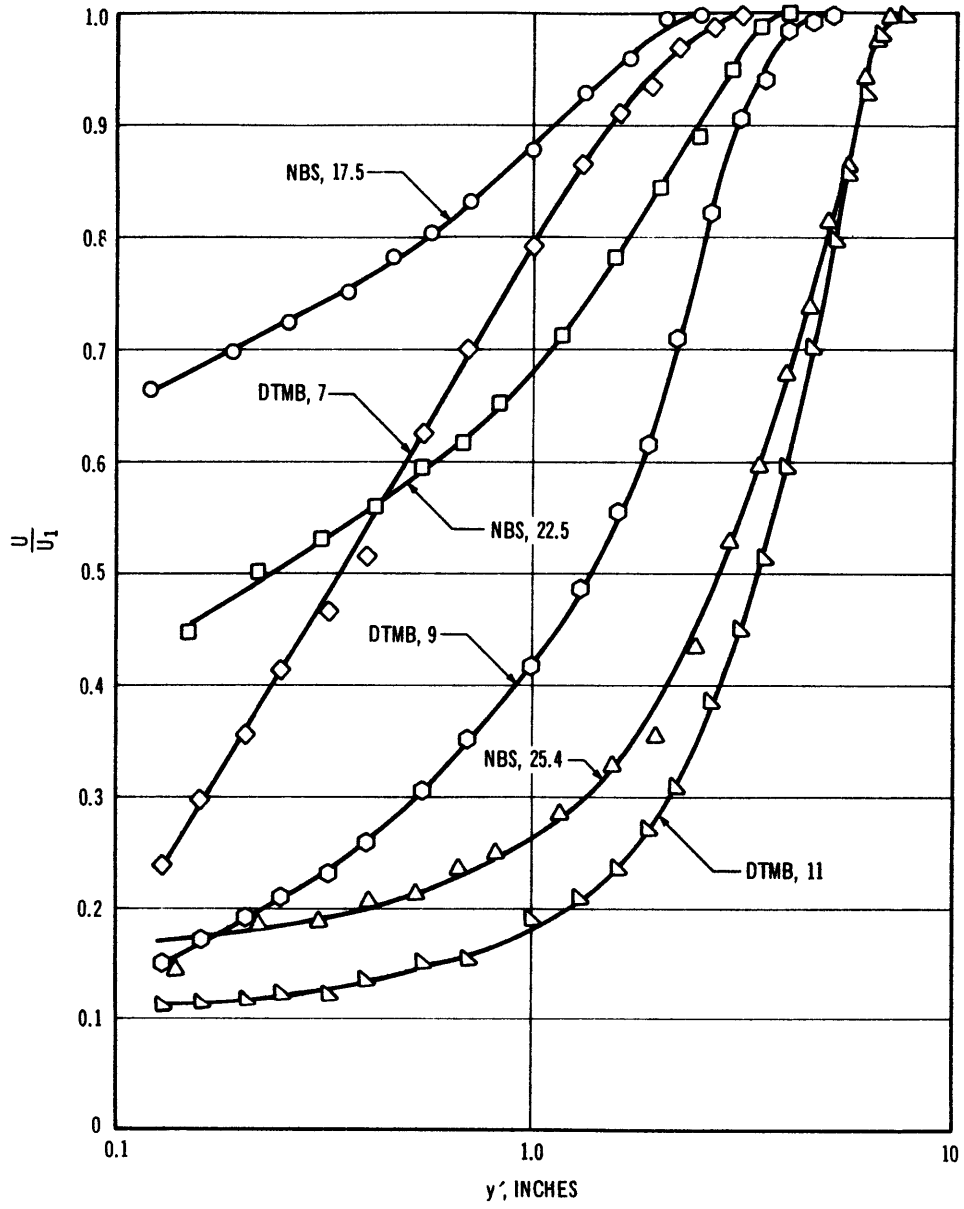


FIGURE 30—Comparison of Mean Velocities in Flows Approaching Separation
 NBS, Smooth Wall
 DTMB, Rough Wall

of the boundary layer thickness, some 85 to 90 percent, that is occupied by the wake region even where the pressure is constant. The logarithmic part of the boundary layer must necessarily be confined to less than 20 percent of the region adjacent to the wall, and the wall roughnesses reduce this region still further.

This reduction in the case of the rough boundary for that part of the boundary layer thickness which follows an essentially linear logarithmic relationship may account for one of the essential differences between the smooth and rough wall behaviors. That is, the source of the turbulence generation at the wall is proportionately much closer to the wake region for the rough wall case and a much greater part of the entire boundary layer exists in the form of a wake region over the entire length of the boundary. The whole question of much more rapid thickening of the boundary layer over rough walls may be related to this difference in behavior.

TURBULENCE INTENSITIES

The relative turbulence intensities are shown in Figures 31 and 32. Apparently, three distinct factors come into play here:

- a. The wall shear stress. High turbulence intensity near the wall is associated with stress due to roughness.

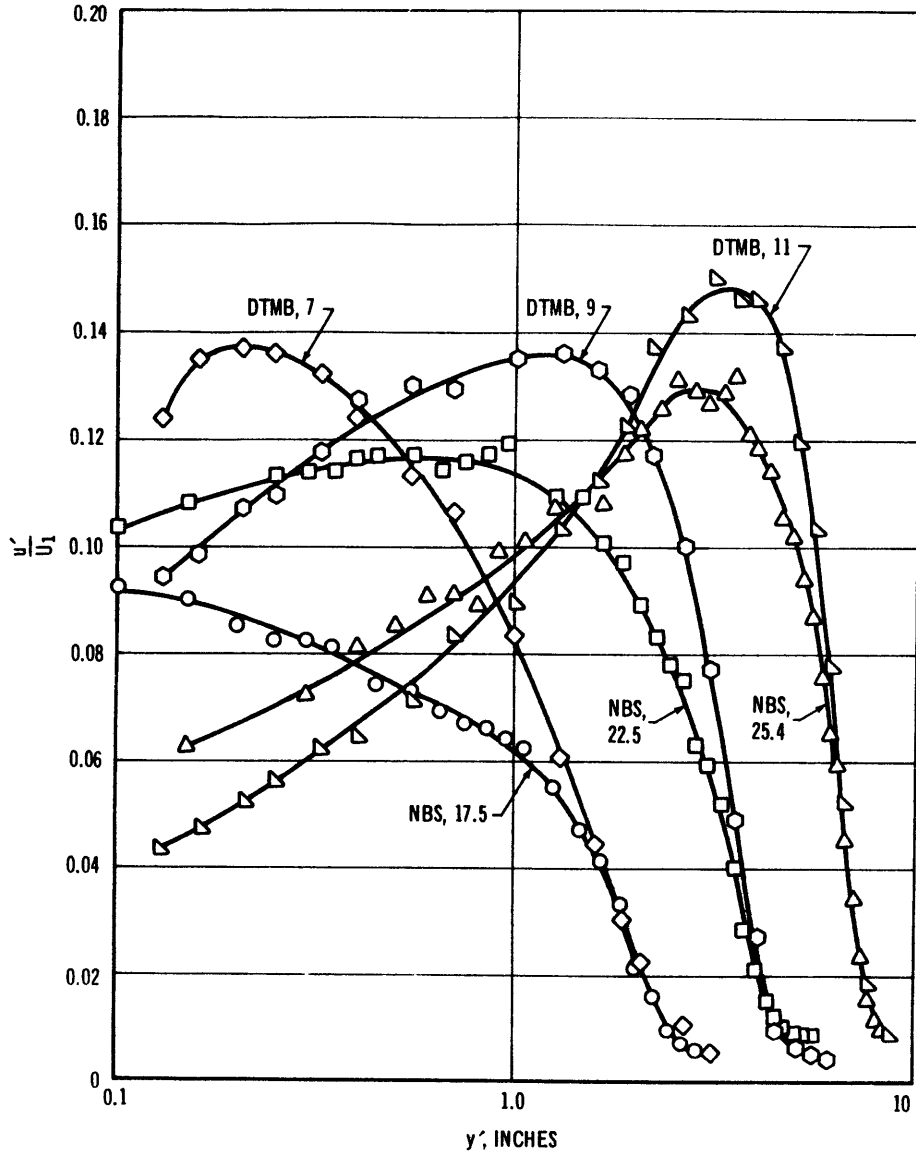


FIGURE 31—Comparison of Turbulent Intensities in Flows Approaching Separation
NBS, Smooth Wall
DTMB, Rough Wall

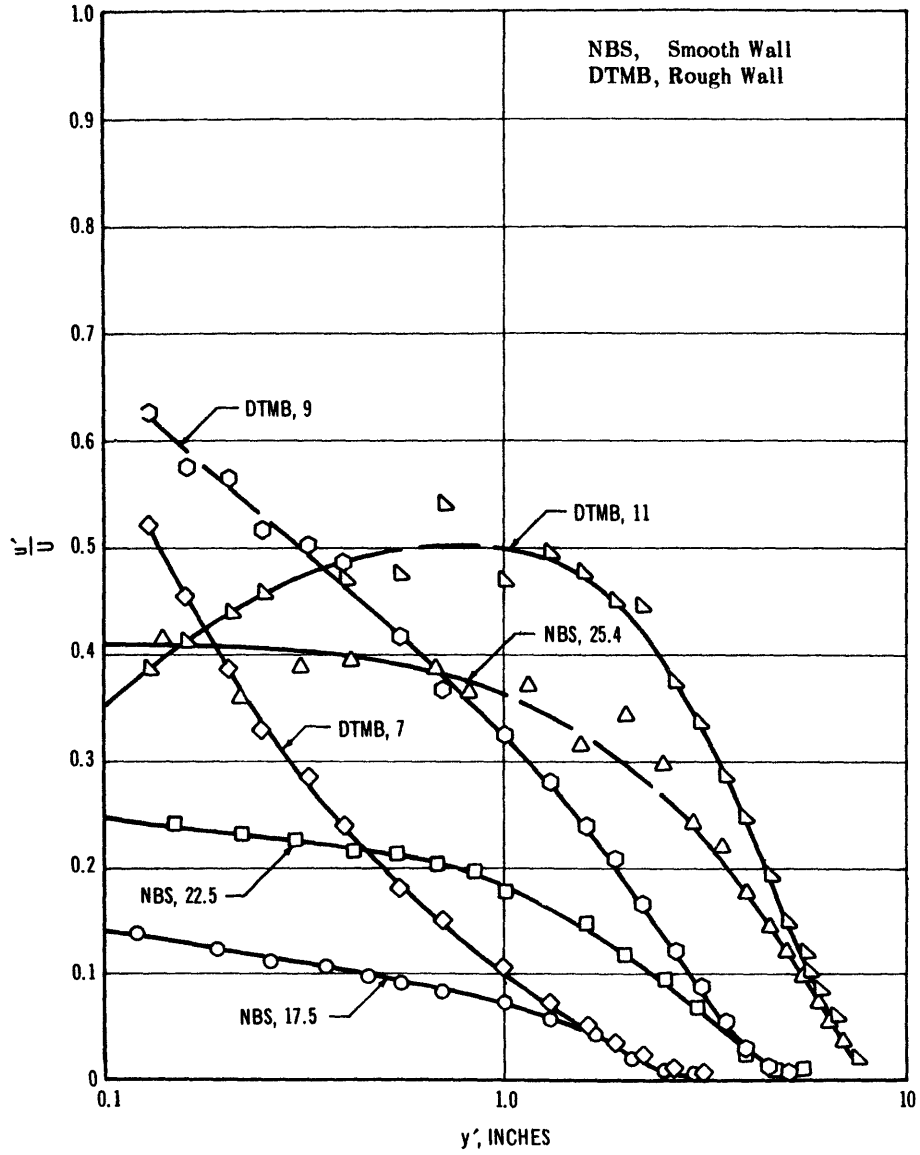


FIGURE 32—Comparison of Turbulent Intensities Based on Local Mean Velocities in Flows Approaching Separation

Reduction in wall shear stress independently of pressure gradients should produce a reduction in turbulence level.

b. Pressure gradient. A sudden application of an adverse pressure gradient will cause a general increase in the turbulence level in the whole region. This effect has been measured in a closed two-dimensional channel by Ruetenik and Corrsin¹⁷ (1954) and it appears to override other effects such as wall shear stress variation.

c. Migration of turbulence levels along streamlines. This appears to dominate the outer law or wake region away from the wall and is observable in the high levels of turbulence which appear well out from the wall near separation. It is reasonable to believe that this is a region of turbulence which has been generated in part upstream closer to the wall and is simply migrating to the outer part of the boundary layer along the streamlines of the flow.

All three effects are observable in both the TMB and NBS data shown in Figures 31 and 32. Since the pressure gradient is quite steep and the wall shear stress is fairly low and changing slowly there is a tendency for the intensity levels at the first two NBS Stations 17.5 and 22.5 to rise rather sharply at first. Then at Station 25.4 the value of c_f drops sharply towards zero reducing the relative turbulent intensity near the wall, but the influence of continued

pressure rise and upstream generated turbulence produces a maximum intensity well out from the wall. The data from TMB Stations 7 and 9 exhibit something of a reversal of intensity levels compared to the NBS data but it must be noted that the initial c_f is extremely high and then drops rapidly to produce the observed trend. The outward movement of wall-generated turbulence supplemented by pressure gradient effect is particularly noticeable in the TMB data. The method of plotting intensity curves ($\frac{u'}{U_1}$ versus y' instead of $\frac{u'}{U_1}$ versus y) has the effect of disguising the importance of the shear stress on the intensity at TMB Station 7 to some extent.

8.2 Moses²³ by the variety of his experiments has provided us with some interesting comparisons for the smooth wall case. In particular, these give a picture of the influence of initial value of θ or δ^* and of pressure gradient. While Moses has used θ as a reference value, it appears more probable that δ^* is the appropriate variable to describe thickening of the boundary layer. For the constant pressure case or with mildly adverse pressure gradients, $H = \delta^*/\theta$ remains substantially constant along the wall so that either δ^* or θ may be used as a reference thickness. However, when the adverse pressure gradient is large enough to produce separation, it is the δ^* which changes

rapidly.

If one compares gradients (2) and (4) in Figure 10 of Reference 23, it is apparent that a steeper adverse pressure gradient will separate at a higher value of U_1/U_0 or with a smaller pressure rise when the initial values of δ^* and θ are the same for both gradients.

A comparison of gradients (1) and (4) in Figures 9 and 10 of the same reference gives the case for large differences in the initial values of δ^* and θ . Pressure gradient (1) has a considerably larger initial value of δ^* and θ at the point of application of the steeply adverse pressure gradient and separates at a higher value of U_1/U_0 or with a smaller pressure rise than gradient (4). Condition (1) does have a somewhat flatter adverse pressure gradient than condition (4) so that the two conditions are not exactly comparable. However, this comparison does serve to emphasize the role played by the initial boundary layer thickness.

8.3 The approach taken in the present tests has been to try to match the pressure gradients for the strongly adverse pressure gradient using both smooth and rough boundaries. This represents a very practical case as it is like the situation in which a given boundary simply becomes rough with time. The effect on the flow will be to produce marked

changes in the various thicknesses and in the wall shear stress. If the hypothesis about boundary layer thickness having a controlling influence on separation, for identical pressure gradients, is correct, one would expect the rough boundary to approach separation more rapidly. This is indeed the case.

Figure 33 shows a comparison of the pressure gradient parameters, $\beta = \delta^* dp/dx/\tau_0$. The displacement thickness δ^* , the shape parameter H , the free stream velocity ratios, and the wall shear coefficients are shown in Figures 23 and 25.

8.4 Discussion

The key factor here would appear to be the existence of a dual mechanism involving boundary layer growth as one part and effective mixing of outer and inner regions as the other. If the mixing process is highly efficient, as in the case of the vortex generators which exhibit low drag while introducing strong longitudinal vorticity, we find that separation is delayed. On the other hand, if the local roughnesses are producing high drag and strong transverse vorticity, the boundary layer will thicken rapidly without benefitting from the improved mixing rate.

This is obviously an extremely complex problem for which the pressure gradient parameter, $\beta = \delta^* dp/dx/\tau_0$,

may be used as an index of local conditions in a mathematical sense, but leaves much to be desired in terms of physical explanation. The rate of change of β with x , the longitudinal coordinate, would seem to be more important than β itself. The examples cited from Moses for smooth boundaries show this effect in a qualitative way. The first example considers a more rapid change in dp/dx . Of additional importance is the fact that the wall shear stress is partly dependent on the pressure gradient and tends to steepen the rise in β . In the second example, the initially thicker boundary layer provides weaker mixing and a more rapid decrease in τ_0 so that β will increase more rapidly as a result. In both instances it appears to be the rate of increase in β which controls the final pressure at which separation occurs.

The present experiments provide a comparison of boundary layer flows over smooth and rough boundaries in pressure fields which are nearly identical. No attempt has been made to produce identical variation in β , although the values are of the same order for the first three stations (6, 7, and 8) as shown in Figure 33. Beyond Station 8 the larger value of δ^* and rapid decrease in τ_0 for the rough boundary serve to drive the value of β up very rapidly. Presumably, this same situation would exist for

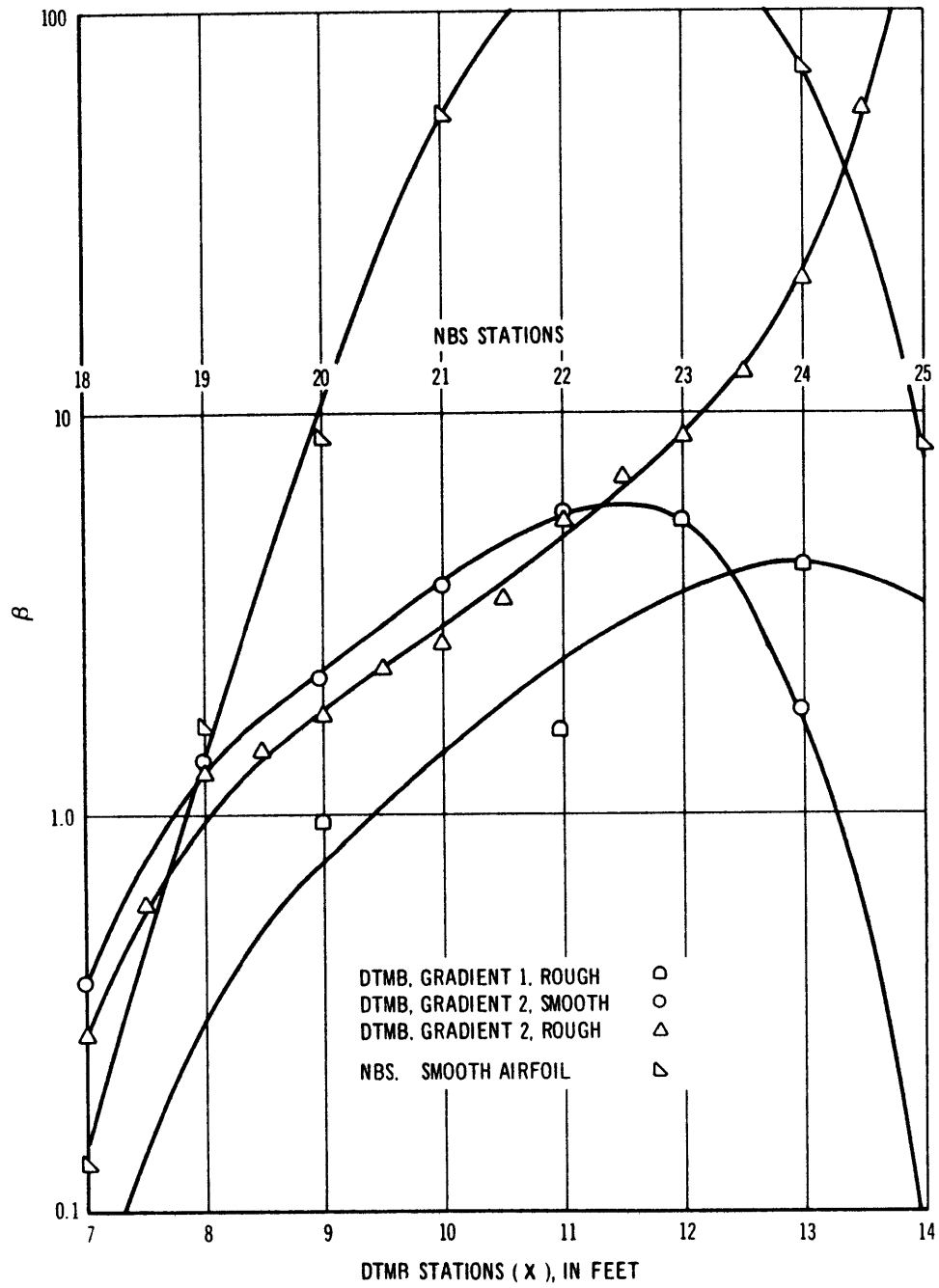


FIGURE 33—Variation of Parameter, β

any rough boundary not specifically designed for efficient mixing and it may be reasonably concluded that free stream flows over a rough boundary will separate more readily than similar flows over a smooth boundary.

Newman²⁹ has suggested that an instability mechanism is involved in the actual occurrence of separation. The NBS data in Figure 33 for the smooth wall with a separated flow seem to support this point of view. The values of β change very rapidly as separation is approached. The use of a logarithmic scale for β tends to understate the case. On the other hand, the TMB rough wall with pressure gradient 2, appears to drive the value of $\beta(x)$ up quite steadily with a nearly constant exponent until the pressure gradient weakens near Station 10. Newman's comment that a small but finite quantity of kinetic energy persists in the mean flow in the boundary layer close to the wall just prior to separation seems to fit both the TMB and NBS data shown in Figure 29.

9. CONCLUSIONS

9.1 In 1954 Clauser¹¹ (p. 102) indicated that it was reasonable to believe that a linear portion in the semilogarithmic plot of U/U_1 versus y' must exist for a rough surface even in an adverse pressure gradient. This conclusion has had ample support both in these experiments and those of Perry and Joubert²⁵, provided the pressure gradient is moderate in character. However, where the adverse pressure gradient is sustained up to the point of separation with wall shear stress approaching zero, the linear portion of the curve gradually disappears. This latter conclusion was first shown by Coles¹⁹ and Stratford^{21,22} and more recently by Mellor and Gibson¹² and Moses²³ for the smooth wall case.

9.2 When the wall is rough, the logarithmic relationship for the inner region exists, but is considerably fore-shortened because of the influence of the roughness elements at the lower values of y' (see Figure 30) as has been noted previously in the discussion of the velocity profiles.

9.3 The general character of velocity distribution at separation for a rough wall is like that predicted by Stratford²¹ and Coles¹⁹ for the smooth wall. It has been noted in article 7.2 that at separation a boundary layer becomes essentially a "wake" flow for either a rough or

smooth wall as the wall shear stress goes to zero. The Stratford solution is a very special case in that τ_0 is kept close to zero over a sizeable distance in a manner quite unlike the usual approach to separation. The evidence in these experiments clearly favors the Coles formulation, which is to be expected since this relationship was derived from other experimental data for flows in which β progresses rapidly from low values to infinity.

9.4 In spite of the rather poor comparisons between the experimental data of these tests and the Coles¹⁹ formulation as shown in Figures 27 and 28, it is believed that the Coles approach is reasonable even for rough walls. In these present tests the pressure gradients are applied rather abruptly and the free streamlines have some curvature at the beginning of the adverse pressure gradient. Thus, the conditions along the flow are changing more rapidly than they would in leaving an exactly parallel or constant pressure flow.

9.5 The limiting condition for separation where the shape parameter H is approximately 3 seems to hold for the rough wall boundary layer (Figure 24b). Tentative experimental studies in which separation was induced near Station 11 with the wall configuration as in Figure 23b tend to confirm this value. This seems to point out a difference between the boundary layer with a free stream and the boundary layer in

a diffuser as presented by Persh and Bailey²⁴. The latter concluded that separation could be delayed or prevented by using coarse roughness to increase the mixing rate of the turbulent layer. In a closed system, the whole character of the flow is changed by introducing roughness in the sense that new velocity distributions and a new streamwise pressure distribution will appear. The free stream and closed system cases are therefore not really comparable.

9.6 When an adverse pressure gradient exists along a rough wall, the magnitude of the wall shear stress must vary through a much greater range than that for the smooth wall case. In both cases the shear stress will start at values close to that for parallel flow and then drop monotonically to zero at separation. This produces a marked difference in the way in which the longitudinal turbulence intensity close to the wall varies with distance along the wall for the two cases. Figures 31 and 32 indicate this strong dominance of turbulence intensity near the wall by the wall shear stress in the rough wall case. It may be seen that this intensity drops continuously in the direction of flow for small values of y' once the boundary layer has thickened appreciably downstream of Station 9.

9.7 The slope method of evaluating c_f provides a workable approximation in spite of difficulty in setting the

exact slope for the rough wall case. For example, this method was used to check out the results given in Figure 17 of Reference 14 (Schubauer and Klebanoff). This resulted in a curve having the same shape as their experimental curve but having values about 30 percent lower. Subsequent reevaluation¹⁹ of the data in Reference 14 indicates that our estimates of c_f are reasonably correct.

9.8 Probably the most interesting "side-effect" to come out of this research is the set of conclusions reached in Chapter 4 regarding the corrections to be applied to pitot tubes and hot-wire anemometers. The extremely high level turbulence intensities shown in Figure 32 coupled with the simultaneous hot-wire and pitot tube measurements provided an unusual set of experimental observations.

Since the hot-wire anemometer corrections for the components of turbulent intensity have been carefully studied by Corrsin⁴⁰, Parthasarathy and Tritton³⁵, and Rose⁴¹, the effect of v' on the readings was easily evaluated. However, the influence of high level intensity has been studied only by Siao⁴³ so that this writer believed that careful reworking of this question was in order. The conclusion reached is that the first-order correction for v' obtained by Rose and the corrections obtained by Siao for instantaneous velocity reversal constitute the best

available hot-wire data.

The pitot tube corrections turned out to be more difficult to evaluate principally because of the large discrepancies in both the physical model and the theory of behavior. A solution which appears reasonable to this writer combined the theories of Hinze⁴² and Toomre⁴⁷ in a fairly complicated algebraic form. Strasberg's⁴⁴ experiments serve to check the magnitude of Toomre's correction for static pressure probes, but did not attempt to establish the algebraic sign. The present experiments indicate that Toomre's algebraic sign for small probes is also reasonable. It is thus concluded that Equation 55 of Article 4.10 constitutes the best available correction for pitot tube measurements of mean velocity in regions of high turbulence intensity.

10. RECOMMENDATIONS

Clearly, more work needs to be done on this problem. The generally unsatisfactory state of the art regarding the measurement and prediction of shear stress, particularly in adverse pressure gradients and with high turbulence, leaves much to be desired. Attempts were made to measure shear stress directly with most unsatisfactory results. Parthasarathy and Tritton³⁵ had predicted extremely large errors for this type of measurement with constant temperature hot-wire equipment. There is little satisfaction to be gained by the knowledge that other experimenters are experiencing the same difficulties.

Two directly pursuable sets of experiments are of interest to this writer. The first of these would look at finer wall roughnesses in strongly adverse pressure gradients. The second would examine an improved entrance into the adverse pressure gradient in order to check the applicability of the Coles wake function to rough walls under a more natural set of conditions.

It is also believed desirable to continue a variety of experiments with pitot tubes and similar probes. These are the most widely used devices for flow measurement, and it is now obvious that under certain turbulence conditions they are subject to extremely large errors.

BIBLIOGRAPHY

1. Hama, F. R., "Boundary-Layer Characteristics for Smooth and Rough Surfaces", Transactions of the Society of Naval Architects and Marine Engineers, Vol. 62, (1954), p. 333.
2. Schoenherr, K.E., "Resistance of Flat Surfaces moving through a Fluid", Transactions of the Society of Naval Architects and Marine Engineers, Vol. 40, (1932), p. 279.
3. Schultz-Grunow, F., "New Frictional Resistance Law for Smooth Plates", National Advisory Committee for Aeronautics Technical Memorandum 986 (1941), (Translation from Luftfahrtforschung, 1940).
4. Hughes, G., "Friction and Form Resistance in Turbulent Flow, and a Proposed Formulation for Use in Model and Ship Correlation", Institution of Naval Architects, London (1954).
5. Granville, P.S., "The Viscous Resistance of Surface Vessels and the Skin Friction of Flat Plates", Transactions of the Society of Naval Architects and Marine Engineers, Vol. 64, (1956).
6. Rotta, J. C., "Turbulent Boundary Layers in Incompressible Flow", Progress in the Aeronautical Sciences,

Vol. 2, Pergammon (1962).

7. Moore, W.L., "An Experimental Investigation of the Boundary-Layer Development along a Rough Surface", Ph.D. Dissertation, State University of Iowa, (Aug. 1951).

8. Prandtl, L., and Schlichting, H., "The Resistance Law for Rough Plates", David Taylor Model Basin Translation 258 (Sep. 1955), (translation from Werft-Reederei-Hafen, Jan. 1934).

9. Granville, P. S., "The Frictional Resistance and Turbulent Boundary Layer of Rough Surfaces", David Taylor Model Basin Report 1024 (Jun. 1958).

10. Corrsin, S., and Kistler, A. L., "The Free-Stream Boundaries of Turbulent Flows", National Advisory Committee for Aeronautics Report 1244 (1955).

11. Clauser, F. H., "Turbulent Boundary Layers in Adverse Pressure Gradients", Journal of the Aeronautical Sciences, Vol. 21, No. 2 (Feb. 1954).

12. Mellor, G. L., and Gibson, D. M., "Equilibrium Turbulent Boundary Layers", Journal of Fluid Mechanics, Vol. 24, Part 2, (Feb. 1966), 225-254.

13. Kehl, A., "Investigations on Convergent and Divergent Turbulent Boundary Layers", British Ministry of Supply R.T.P. No. 2035 (1946), (translated from Ing. Arch., Vol. 13, 1943).
14. Schubauer, G. B., and Klebanoff, P. S., "Investigation of Separation of the Turbulent Boundary Layer", National Advisory Committee For Aeronautics Report 1030 (1951).
15. Ludwig, H., Tillmann, W., "Investigations of the Wall Shearing Stress in Turbulent Boundary Layers", National Advisory Committee for Aeronautics Technical Memorandum 1285 (1950) (translated from Ing. Archiv., Vol. 17, No. 4, 1949).
16. Granville, P. S., "A Method for the Calculation of the Turbulent Boundary Layer in a Pressure Gradient", David Taylor Model Basin Report 752 (May 1951).
17. Ruetenik, J. R., and Corrsin, S., "Equilibrium Flow in a Slightly Divergent Channel", 50 Jahre Grenzschichtforschung, F. Vieweg and Sohn, Braunschweig, (1954).
18. Coles, D., "The Law of the Wall in Turbulent Shear Flow", 50 Jahre Grenzschichtforschung, F. Vieweg and Sohn, Braunschweig, (1954).

19. Coles, D., "The Law of the Wake in the Turbulent Boundary Layer", Journal of Fluid Mechanics, Vol. 1, (1956), 191-226.
20. Clauser, F. H., "The Turbulent Boundary Layer", Advances in Applied Mechanics, Vol. 4 (1956).
21. Stratford, B. S., "The Prediction of Separation of the Turbulent Boundary Layer", Journal of Fluid Mechanics, Vol. 5, Part 1 (Jan. 1959).
22. Stratford, B. S., "An Experimental Flow with Zero Skin Friction throughout its region of Pressure Rise", Journal of Fluid Mechanics, Vol. 5, Part 1, (Jan. 1959).
23. Moses, Hal L., "The Behavior of Turbulent Boundary Layers in Adverse Pressure Gradients", Gas Turbine Laboratory, Massachusetts Institute of Technology, Report No. 73, (Jan. 1964). See also D. Sc. Dissertation M.I.T. (Jan. 1964).
24. Persh, J., and Bailey, B. M., "Effect of Surface Roughness over the Downstream Region of a 23° Conical Diffuser", National Advisory Committee for Aeronautics Technical Note 3066, (Jan. 1954).
25. Perry, A. E., and Joubert, P. N., "Rough-Wall Boundary Layers in Adverse Pressure Gradients", Journal of

Fluid Mechanics, Vol. 17, Part 2, (Oct. 1963).

26. Smith, D. W., and Walker, J. H., "Skin-Friction Measurements in Incompressible Flow", National Advisory Committee for Aeronautics Technical Note 4231, (Mar. 1958).

27. Granville, P. S., "The Determination of the Local Skin Friction and the Thickness of Turbulent Boundary Layers from the Velocity Similarity Laws", David Taylor Model Basin Report 1340, (Oct. 1959).

28. Hsu, E. Y., "The Measurement of Local Turbulent Skin Friction by Means of Surface Pitot Tubes", David Taylor Model Basin Report 957, (Aug. 1955).

29. Newman, B. G., "Some Contributions to the Study of Turbulent Boundary Layers Near Separation", Department of Supply, Aeronautical Research Consultative Committee, Australia, Report ACA 53, (Mar. 1951).

30. Wieghardt, K., and Tillmann, W., "On the Turbulent Friction for Rising Pressure", National Advisory Committee for Aeronautics Technical Memorandum 1314 (Oct. 1951), (translated from: "Zur Turbulenten Reibungsschicht bei Druckanstieg", Z.W.B., K.W.I., Goettingen, U. & M. 6617, 1944).

31. Klebanoff, P. S., "Characteristics of Turbulence

in a Boundary Layer with Zero Pressure Gradient", National Advisory Committee for Aeronautics Report 1247, (1955).

32. Scottron, V., and Shaffer, D., "The Low Turbulence Wind Tunnel of the David Taylor Model Basin", David Taylor Model Basin Report 2116, (Dec. 1965).

33. Hubbard, P. G., "Operating Manual for the IIHR Hot Wire and Hot Film Anemometers", Bult. 37, Iowa Institute of Hydraulic Research, (1958).

34. Smith, A.M.O., and Murphy, J. S., "Micromanometer for Measuring Boundary Layer Profiles", The Review of Scientific Instruments Vol. 26, No. 8, (Aug. 1955).

35. Parthasarathy, S. P., and Tritton, D. J., "Impossibility of Linearizing a Hot-Wire Anemometer for Measurements in Turbulent Flows", American Institute of Aeronautics and Astronautics Journal, Vol. 1, No. 5, (May 1963), p. 1210.

36. Laufer, J., "The Structure of Turbulence in Fully Developed Pipe Flow", National Advisory Committee for Aeronautics Technical Note 2954, (Jun. 1953).

37. Laufer, J., "Investigation of Turbulent Flow in a Two-Dimensional Channel", National Advisory Committee for Aeronautics Technical Note 2123, (Jul. 1950).

38. Burkhart, T. H., "Turbulent Flow in an Artificially Roughened Pipe", University of Illinois, T. & A. M. Report No. 616,(Jan. 1962).
39. Batchelor, G. K., "The Theory of Homogeneous Turbulence", Cambridge University Press, (1953).
40. Corrsin, S., "Investigation of Flow in an Axially Symmetrical Heated Jet of Air", National Advisory Committee for Aeronautics Wartime Report ACR 3L23, (WR W-94), (Dec. 1943).
41. Rose, W. G., "Some Corrections to the Linearized Response of a Constant-Temperature Hot-Wire Anemometer Operated in a Low-Speed Flow", American Society of Mechanical Engineers, Journal of Applied Mechanics, Vol. 29, (Nov. 1962), p. 554.
42. Hinze, J. O., "Turbulence", McGraw-Hill Book Co., (1959).
43. Siao, T-T., "Corrections for Mean-Velocity and Turbulence Measurements for High Turbulence Levels", Scientia Sinica, Vol. VIII, No. 12, (1959), p. 1558.
44. Strasberg, M., "Measurements of the Fluctuating Static and Total-Head Pressures in a Turbulent Wake", David Taylor Model Basin Report 1779 (Dec. 1963).

45. Goldstein, S., "A Note on the Measurement of Total-Head and Static Pressure in a Turbulent Stream", Proceedings of the Royal Society, London, A Vol. CLV (1936), p. 570.

46. Fage, A., "On the Static Pressure in a Fully-Developed Turbulent Flow", Proceedings of the Royal Society, London, A Vol. CLV (1936), p. 576.

47. Toomre, A., "The Effect of Turbulence on Static Pressure Measurements", Aeronautical Research Council, England, F. M. 2972, (Jun. 1960).

48. Corrsin, S., "Turbulence: Experimental Methods", Handbuch der Physik, Vol. VIII/2, Springer-Verlag, Berlin, (1963).

49. Davies, P.O.A.L., "The Behavior of a Pitot Tube in Transverse Shear", Journal of Fluid Mechanics, Vol. 3, Part 5 (Feb. 1958), p. 441.

50. MacMillan, F. A., "Viscous Effects on Pitot Tubes at Low Speeds", Journal of the Royal Aeronautical Society, London, Vol. 58, (1954), p. 570.

51. Dhawan, S., and Vasudeva, B. R., "The Pitot Tube Displacement Effect in Boundary Flows", Journal of the

Aeronautical Society of India, Vol. 11, No. 1 (Feb. 1959),
p. 1.

52. MacMillan, F. A., "Experiments on Pitot-Tubes in Shear Flow", Aeronautical Research Committee Reports and Memoranda No. 3028 (Feb. 1956).

53. Daily, J. W., and Hardison, R. L., "A Review of Literature Concerning Impact Probes Used in Steady Flows", Massachusetts Institute of Technology Hydrodynamics Laboratory Report No. 67 (Apr. 1964), Appendix I.

54. Townsend, A. A., "The Structure of Turbulent Shear Flow", Cambridge University Press (1956).

55. Rouse, H. (Editor), "Advanced Mechanics of Fluids", John Wiley and Sons, N. Y. (1959).

56. Sandborn, V. A., and Slogar, R. J., "Study of the Momentum Distribution of Turbulent Boundary Layers in Adverse Pressure Gradients", National Advisory Committee for Aeronautics, Technical Note 3264 (Jan. 1955).

57. Mellor, G. L., "The Effects of Pressure Gradients on Turbulent Flow near a Smooth Wall", Journal of Fluid Mechanics, Vol. 24, Part 2, (Feb. 1966), 255-274.

INITIAL DISTRIBUTION

Copies		Copies	
7	NAVSHIPSYSKOM	1	DIR, BuStand
	2 Tech Lib (Ships 2052)		Attn: Dr. G.B. Schubauer
	1 Chief Sci for R&D	1	Library of Congress
	(Ships 031)		(Sci & Technology Div)
	1 Ships Research Br	1	MARAD
	(Ships 03412)		Attn: Div of Ship
	1 Ships Materials & Struc Br		Design & Dev
	(Ships 03412)		
	2 Ship Sil Br (Ships 03432)	1	CO, U.S. Army Trans Res
1	DSSPO (PM 1100)		& Dev Command, Fort
			Eustis, Va.
4	NAVSEC		Attn: Marine Transport Div
	1 Materials Devl and Appli	2	NASA Headquarters
	Office (Sec 6101)		Fluid Physics Br
	1 Ship Con Des Div (Sec 6360)		(Code RRF), J.T. Howe
	1 Ship Control & Fluid Dyn	1	Director, Eng Sci Div
	Br (Sec 6136)		National Science
20	CDR, DDC		Foundation, Wash., D.C.
4	CHONR	1	SNAME
	3 Fluid Dyn (Code 438)		74 Trinity Place
	1 Air Programs (Code 461)		New York, New York
1	ONR, Boston	2	Supt USNA, Annapolis
1	ONR, New York		1 Prof. B. Johnson,
1	ONR, Pasadena		Eng Dept
1	ONR, San Francisco	1	USMMA
25	ONR, London	1	Webb Inst of Naval Arch
			Crecent Beach Rd.
			Glen Cove, L.I., N.Y.
3	NAVORDSYSKOM	2	Davidson Lab, SIT
	1 Undersea Warfare Sys	2	ORL, Penn State Univ
	Direct		1 Dr. G.F. Wislicenus
	1 Torpedo Div (Code 054131)		1 Dr. J.L. Lumley
2	NAVAIRSYSKOM	2	Univ of Mich, Ann Arbor,
	1 Aero & Hydro Br (Code 5301)		Dept of Nav Arch
1	CO & DIR, USNUSL	2	MIT, Dept of Naval Arch
1	CO & DIR, USNEL	2	Alden Hydraulic Lab,
3	CO & DIR, USNOL		Worchester, Mass
	1 Dr. A. May		1 Dr. L. J. Hooper
	1 N. Tetervin		1 L.C. Neale

Copies

6 DIR, USNRL, Tech Info Div
1 Dr. C. R. Singleterry

3 CDR, USUWC (Pasadena)
1 Dr. J.W. Hoyt
1 Dr. A.G. Fabula

2 CDR, USNWC (China Lake)
1 Dr. H. Kelly

2 CO, USNAVUWRES
1 R.J. Grady

1 Prof. L. Landweber, Iowa
Inst of Hydraulic Research
State Univ of Iowa,
Iowa City, Iowa

1 Prof E.Y. Hsu, Dept of Civil
Engineering, Stanford Univ
Stanford, Calif

3 Hydronautics, Inc. Laurel, Md.
1 Dr. B.L. Silverstein
1 M.P. Tulin

1 Prof C.E. Carver, Jr., Dept
of Civil Engineering, Univ
of Mass, Amherst, Mass

1 Prof A.J. Acosta, Hydro-
dynamics Lab, CIT,
Pasadena, Calif

2 California Inst of Tech.,
Hydraulics Lab,
Pasadena, Calif

1 Director, Inst of Eng Res
Univ of Calif

2 Director, Hydraulics Lab
Colorado State Univ

1 Dr. J. M. Robertson, Dept
Theo & Applied Mechanics
Univ of Ill,
Urbana, Ill.

Copies

1 Director, Inst for Fluid Dyn
& Applied Math, Univ of Md.

2 Director, Jet Propulsion Lab
Calif Inst of Tech,
Pasadena, Calif.
1 Dr. F.R. Hama

1 Director, St. Anthony Falls
Hydraulic Lab, Univ of Minn

1 Director, Robinson Model Basin,
Webb Inst of Naval Arch,
Glen Cove

1 SWRI, San Antonio, Texas

1 Hydronautics, Inc.
Rockville, Md.
1 Dr. M.P. Tulin

1 Editor, Engineering Index,
New York

1 Mr. A.M.O. Smith,
Douglas Aircraft Co.
El Legends

1 Dr. Joseph Kestin, Eng Div
Brown Univ,
Providence, R.I.

1 Dr. T.J. Carmody, Civil Eng
Dept. Univ of Arizona
Tucson, Arizona

2 Director, Gas Turbine Lab,
Mass Inst Tech,
Cambridge, Mass

1 Dr. G.L. Mellor, Dept of Aero.
& Mech., Princeton Univ.,
Princeton, N.J.

1 Dr. D. Coles, Calif Inst of
Tech., Pasadena

DOCUMENT CONTROL DATA - R & D

(Security classification of title, body of abstract and indexing annotation must be entered when the overall report is classified)

1 ORIGINATING ACTIVITY (Corporate author) Naval Ship Research and Development Center Washington, D.C. 20007		2a. REPORT SECURITY CLASSIFICATION UNCLASSIFIED	
		2b. GROUP	
3 REPORT TITLE TURBULENT BOUNDARY LAYER CHARACTERISTICS OVER A ROUGH SURFACE IN AN ADVERSE PRESSURE GRADIENT			
4 DESCRIPTIVE NOTES (Type of report and inclusive dates) Final			
5 AUTHOR(S) (First name, middle initial, last name) Victor E. Scottron			
6 REPORT DATE September 1967		7a. TOTAL NO OF PAGES 154	7b. NO OF REFS 57
8a. CONTRACT OR GRANT NO. S-R 009 01 01		9a. ORIGINATOR'S REPORT NUMBER(S) 2659	
b. PROJECT NO. Task 0104		9b. OTHER REPORT NO(S) (Any other numbers that may be assigned this report) AD 669 486	
c.			
d.			
10 DISTRIBUTION STATEMENT Distribution of this document is unlimited.			
11. SUPPLEMENTARY NOTES		12. SPONSORING MILITARY ACTIVITY Naval Ship Systems Command Washington, D.C.	
13 ABSTRACT <p>The boundary layers produced on rough surfaces in adverse pressure gradients have been investigated. Experimental data on two pressure gradients are studied and compared with flow over a smooth surface. Experimental data obtained with both pitot tubes and hot wires are carefully analyzed and corrected for the effects of high level turbulence. An improved pitot tube correction is proposed. It is shown that a boundary layer on a rough wall will separate more readily than on a smooth wall.</p>			

14 KEY WORDS	LINK A		LINK B		LINK C	
	ROLE	WT	ROLE	WT	ROLE	WT
Wind tunnel tests Adverse pressure gradients Wall roughness Boundary layers High level turbulence Separation Skin friction Hot-wire anemometers Pitot tube correction						

Naval Ship R&D Center. Report 2659.

TURBULENT BOUNDARY LAYER CHARACTERISTICS OVER A ROUGH SURFACE IN AN ADVERSE PRESSURE GRADIENT, by Victor E. Scottron. Sep 1967. v, 167p. illus., diags., graphs, UNCLASSIFIED

The boundary layers produced on rough surfaces in adverse pressure gradients have been investigated. Experimental data on two pressure gradients are studied and compared with flow over a smooth surface. Experimental data obtained with both pitot tubes and hot wires are carefully analyzed and corrected for the effects of high level turbulence. An improved pitot tube correction is proposed. It is shown that a boundary layer on a rough wall will separate more readily than on a smooth wall.

1. Turbulent boundary layer--Pressure distribution--Wind tunnel tests
 2. Surface conditions--Boundary layer effects--Wind tunnel tests
 3. Skin friction--Measurement--Instrumentation
 4. Hot wire anemometers--Applications
 5. Pitot tubes--Applications
- I. Scottron, Victor E.

Naval Ship R&D Center. Report 2659.

TURBULENT BOUNDARY LAYER CHARACTERISTICS OVER A ROUGH SURFACE IN AN ADVERSE PRESSURE GRADIENT, by Victor E. Scottron. Sep 1967. v, 167p. illus., diags., graphs, UNCLASSIFIED

The boundary layers produced on rough surfaces in adverse pressure gradients have been investigated. Experimental data on two pressure gradients are studied and compared with flow over a smooth surface. Experimental data obtained with both pitot tubes and hot wires are carefully analyzed and corrected for the effects of high level turbulence. An improved pitot tube correction is proposed. It is shown that a boundary layer on a rough wall will separate more readily than on a smooth wall.

1. Turbulent boundary layer--Pressure distribution--Wind tunnel tests
 2. Surface conditions--Boundary layer effects--Wind tunnel tests
 3. Skin friction--Measurement--Instrumentation
 4. Hot wire anemometers--Applications
 5. Pitot tubes--Applications
- I. Scottron, Victor E.

Naval Ship R&D Center. Report 2659.

TURBULENT BOUNDARY LAYER CHARACTERISTICS OVER A ROUGH SURFACE IN AN ADVERSE PRESSURE GRADIENT, by Victor E. Scottron. Sep 1967. v, 167p. illus., diags., graphs, UNCLASSIFIED

The boundary layers produced on rough surfaces in adverse pressure gradients have been investigated. Experimental data on two pressure gradients are studied and compared with flow over a smooth surface. Experimental data obtained with both pitot tubes and hot wires are carefully analyzed and corrected for the effects of high level turbulence. An improved pitot tube correction is proposed. It is shown that a boundary layer on a rough wall will separate more readily than on a smooth wall.

1. Turbulent boundary layer--Pressure distribution--Wind tunnel tests
 2. Surface conditions--Boundary layer effects--Wind tunnel tests
 3. Skin friction--Measurement--Instrumentation
 4. Hot wire anemometers--Applications
 5. Pitot tubes--Applications
- I. Scottron, Victor E.

Naval Ship R&D Center. Report 2659.

TURBULENT BOUNDARY LAYER CHARACTERISTICS OVER A ROUGH SURFACE IN AN ADVERSE PRESSURE GRADIENT, by Victor E. Scottron. Sep 1967. v, 167p. illus., diags., graphs, UNCLASSIFIED

The boundary layers produced on rough surfaces in adverse pressure gradients have been investigated. Experimental data on two pressure gradients are studied and compared with flow over a smooth surface. Experimental data obtained with both pitot tubes and hot wires are carefully analyzed and corrected for the effects of high level turbulence. An improved pitot tube correction is proposed. It is shown that a boundary layer on a rough wall will separate more readily than on a smooth wall.

1. Turbulent boundary layer--Pressure distribution--Wind tunnel tests
 2. Surface conditions--Boundary layer effects--Wind tunnel tests
 3. Skin friction--Measurement--Instrumentation
 4. Hot wire anemometers--Applications
 5. Pitot tubes--Applications
- I. Scottron, Victor E.

Naval Ship R&D Center. Report 2659.
TURBULENT BOUNDARY LAYER CHARACTERISTICS OVER A ROUGH SURFACE IN AN ADVERSE PRESSURE GRADIENT,
by Victor E. Scottron. Sep 1967. v, 167p. illus., diags., graphs, UNCLASSIFIED refs.

The boundary layers produced on rough surfaces in adverse pressure gradients have been investigated. Experimental data on two pressure gradients are studied and compared with flow over a smooth surface. Experimental data obtained with both pitot tubes and hot wires are carefully analyzed and corrected for the effects of high level turbulence. An improved pitot tube correction is proposed. It is shown that a boundary layer on a rough wall will separate more readily than on a smooth wall.

1. Turbulent boundary layer--Pressure distribution--Wind tunnel tests
 2. Surface conditions--Boundary layer effects--Wind tunnel tests
 3. Skin friction--Measurement--Instrumentation
 4. Hot wire anemometers--Applications
 5. Pitot tubes--Applications
- I. Scottron, Victor E.

Naval Ship R&D Center. Report 2659.
TURBULENT BOUNDARY LAYER CHARACTERISTICS OVER A ROUGH SURFACE IN AN ADVERSE PRESSURE GRADIENT,
by Victor E. Scottron. Sep 1967. v, 167p. illus., diags., graphs, UNCLASSIFIED

The boundary layers produced on rough surfaces in adverse pressure gradients have been investigated. Experimental data on two pressure gradients are studied and compared with flow over a smooth surface. Experimental data obtained with both pitot tubes and hot wires are carefully analyzed and corrected for the effects of high level turbulence. An improved pitot tube correction is proposed. It is shown that a boundary layer on a rough wall will separate more readily than on a smooth wall.

1. Turbulent boundary layer--Pressure distribution--Wind tunnel tests
 2. Surface conditions--Boundary layer effects--Wind tunnel tests
 3. Skin friction--Measurement--Instrumentation
 4. Hot wire anemometers--Applications
 5. Pitot tubes--Applications
- I. Scottron, Victor E.

Naval Ship R&D Center. Report 2659.
TURBULENT BOUNDARY LAYER CHARACTERISTICS OVER A ROUGH SURFACE IN AN ADVERSE PRESSURE GRADIENT,
by Victor E. Scottron. Sep 1967. v, 167p. illus., diags., graphs, UNCLASSIFIED

The boundary layers produced on rough surfaces in adverse pressure gradients have been investigated. Experimental data on two pressure gradients are studied and compared with flow over a smooth surface. Experimental data obtained with both pitot tubes and hot wires are carefully analyzed and corrected for the effects of high level turbulence. An improved pitot tube correction is proposed. It is shown that a boundary layer on a rough wall will separate more readily than on a smooth wall.

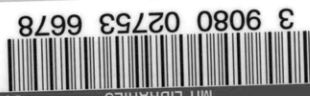
1. Turbulent boundary layer--Pressure distribution--Wind tunnel tests
 2. Surface conditions--Boundary layer effects--Wind tunnel tests
 3. Skin friction--Measurement--Instrumentation
 4. Hot wire anemometers--Applications
 5. Pitot tubes--Applications
- I. Scottron, Victor E.

Naval Ship R&D Center. Report 2659.
TURBULENT BOUNDARY LAYER CHARACTERISTICS OVER A ROUGH SURFACE IN AN ADVERSE PRESSURE GRADIENT,
by Victor E. Scottron. Sep 1967. v, 167p. illus., diags., graphs, UNCLASSIFIED

The boundary layers produced on rough surfaces in adverse pressure gradients have been investigated. Experimental data on two pressure gradients are studied and compared with flow over a smooth surface. Experimental data obtained with both pitot tubes and hot wires are carefully analyzed and corrected for the effects of high level turbulence. An improved pitot tube correction is proposed. It is shown that a boundary layer on a rough wall will separate more readily than on a smooth wall.

1. Turbulent boundary layer--Pressure distribution--Wind tunnel tests
 2. Surface conditions--Boundary layer effects--Wind tunnel tests
 3. Skin friction--Measurement--Instrumentation
 4. Hot wire anemometers--Applications
 5. Pitot tubes--Applications
- I. Scottron, Victor E.

MIT LIBRARIES
DUPL



3 9080 02753 6678

